
Electronic Thesis and Dissertation Repository

June 2017

Molecular and Polymeric Materials Based On Asymmetrically Substituted BF₂ 3-Cyanoformazanates

Samantha Novoa

The University of Western Ontario

Supervisor

Dr. Joe Gilroy

The University of Western Ontario

Graduate Program in Chemistry

A thesis submitted in partial fulfillment of the requirements for the degree in Master of Science

© Samantha Novoa 2017

Follow this and additional works at: <https://ir.lib.uwo.ca/etd>

 Part of the [Polymer Chemistry Commons](#)

Recommended Citation

Novoa, Samantha, "Molecular and Polymeric Materials Based On Asymmetrically Substituted BF₂ 3-Cyanoformazanates" (2017).
Electronic Thesis and Dissertation Repository. 4585.
<https://ir.lib.uwo.ca/etd/4585>

This Dissertation/Thesis is brought to you for free and open access by Scholarship@Western. It has been accepted for inclusion in Electronic Thesis and Dissertation Repository by an authorized administrator of Scholarship@Western. For more information, please contact tadam@uwo.ca, wlsadmin@uwo.ca.

Abstract

This thesis outlines the synthesis and characterization of asymmetric and symmetric 3-cyanoformazanate BF_2 complexes and their incorporation into polymers. CuAAC chemistry was used to synthesize two additional asymmetric BF_2 complexes and a side product that was identified as a symmetric dimer. Spectroscopic and electrochemical properties of these compounds are described.

Incorporation of an asymmetric 3-cyanoformazante BF_2 complex into polymers was done by ROMP. This reaction was used to make homo, block, and random copolymers, where the comonomer was an organic norbornene derivative. Spectroscopic studies of these polymers revealed that, as the mole fraction of BF_2 (f_{BF_2}) in random copolymers decreased, the quantum yield of fluorescence increased; this was due to less quenching/self-absorption from nearby chromophores. Thermal and electrochemical properties of all polymers are described.

Keywords

Formazanate ligands, Copper (I)-assisted alkyne-azide cycloaddition, Ring-Opening Metathesis Polymerization, Absorption/Emission Spectroscopy, Redox-active polymers.

Co-Authorship Statement

The work described in this thesis contains contributions from the author as well as my co-worker Stephanie Barbon and my supervisor Prof. Joe B. Gilroy. The contributions of each are described below.

Chapter 1 was written by the author and edited by Prof. Gilroy.

Chapter 2 describes various small molecule syntheses that were completed by the author. All X-ray crystallographic studies described were done by Stephanie Barbon. The chapter was written by the author and edited by Prof. Gilroy.

Chapter 3 describes a project where all the experimental work and characterization was performed by the author. The chapter was written by the author and edited by Prof. Gilroy.

Chapter 4 was written by the author and edited by Prof. Gilroy.

Acknowledgments

First and foremost, I would like to thank Professor Joe Gilroy for his immeasurable mentorship and support; thank you for giving me the opportunity to work in your group and for always pushing me to do my best. I can say that, through your guidance, I have become a better chemist, presenter, mentor, and an overall professional that is ready for the real world. Your dedication to all your students is admirable and has been an essential part of the completion of my degree. Thank you.

I would also like to thank my amazing lab mates for always lending a helping hand and for being the kindest people I could have asked to work with. More specifically, I would like to thank Dr. Rabiee Kenaree for always being available for real life-talk and venting; I'm also glad you can use Snapchat now. Dr. Paquette, thank you for all the laughs, jokes, and for providing me with great interview question examples— you're the best. Ryan Maar, thanks for being my competitive twin; your passion and dedication for research really pushed me to put in 110%. Alex Van Belois, thanks for teaching me how to play squash and for laughing at my jokes. And last, but certainly not least, Stephanie Barbon; you started off as a mentor and have become a close friend. Thank you for always being there whether it was to joke around or to discuss research, grad school would not have been the same without you! I would also like to thank the rest of the graduate students I have had the pleasure of working with and meeting specifically all the members of the baseball, soccer, and ultimate Frisbee teams, it was super fun getting to know you all!

The Department of Chemistry has been essential in the completion of this degree, and I would also like to express my gratitude. Thank you to Aneta Borecki for running all of my GPC samples, Mat Willans for his advice and support in the NMR spectroscopy field, Doug Harsine for running mass spectrometry experiments, and Steph for crystallography studies. I would also like to thank the office staff, especially Darlene who was always available to answer my questions and help with all the paperwork needed to graduate. Also, thank you to ChemBio Stores for all your help throughout the years.

Finally, I would like to thank my family and friends. To my parents, Pedro and Nubia, I want to thank you for always supporting me in everything that I do. Thank you for sacrificing so

much for my sister and me; your immense courage and perseverance have founded my core. I would not be the same person without you, I love you both immensely. To my sister, Stefania, I want to tell you that I thank God every day for providing me with my best friend. Thank you for always being with me through thick and thin, I love you so much, and I'm so excited to see where life will take us. To all my friends and family, you know who you are, I just want to say thank you for your support and friendship throughout my life. I love you all.

Table of Contents

Abstract	i
Co-Authorship Statement.....	ii
Acknowledgments.....	iii
Table of Contents	v
List of Tables.....	viii
List of Figures	ix
List of Schemes	xiii
List of Appendices	xv
List of Abbreviations.....	xvi
Chapter 1	1
1 Introduction.....	1
1.1 Polymers Containing Quinoline Derivatives	1
1.2 Polymers Containing Naphthalene and Anthracene Derivatives.....	5
1.3 Polymers Containing Fluorene Derivatives	10
1.4 Boron Containing Fluorophores and Polymers	14
1.5 Scope of Thesis.....	19
1.6 References.....	20
Chapter 2	25
2 Asymmetric 3-Cyanoformazanate BF ₂ Complexes.....	25
2.1 Introduction.....	25
2.2 Results and Discussion	27
2.2.1 Synthesis of Asymmetric 3-Cyanoformazans.....	27
2.2.2 Synthesis of BF ₂ 3-Cyanoformazanate Complexes	28
2.2.3 X-ray Crystallography	32

2.2.4	Absorption/Emission Properties of BF ₂ 3-Cyanoformazanate Complexes	35
2.2.5	Electrochemical Properties of BF ₂ 3-Cyanoformazanate Complexes	37
2.3	Conclusion	38
2.4	Experimental	39
2.4.1	General Considerations	39
2.4.2	X-ray Crystallography Methods	40
2.4.3	Electrochemical Methods	41
2.4.4	Synthetic Procedures	42
2.5	References	46
Chapter 3		49
3	Fluorescent BF ₂ 3-Cyanoformazanate Polymers	49
3.1	Introduction	49
3.2	Results and Discussion	50
3.2.1	Synthesis of Side-Chain Polymers	50
3.2.2	Synthesis of Block Copolymers Containing BF ₂ Complexes	56
3.2.3	Synthesis of Random Copolymers Containing BF ₂ Complexes	61
3.2.4	Thermal Properties	64
3.2.5	Spectroscopic Properties	67
3.3	Conclusions	69
3.4	Experimental	70
3.4.1	General Considerations	70
3.4.2	Electrochemical Methods	71
3.4.3	Gel Permeation Chromatography	71
3.4.4	Thermal Analysis	71
3.4.5	Synthetic Procedures	72

3.5 References.....	78
Chapter 4.....	81
4 Conclusions and Future Work.....	81
4.1 Conclusions.....	81
4.2 Future Work.....	84
4.3 References.....	85
Appendices.....	86
Appendix 1 – Supporting Information for Chapter 2.....	86
Appendix 2 – Supporting Information for Chapter 3.....	97
Curriculum Vitae.....	106

List of Tables

Table 2.1 Experimental yields for asymmetric syntheses	28
Table 2.2. Selected bond lengths (Å) and angles (degrees) for 2.13 BF ₂ complex.....	33
Table 2.3. Selected bond lengths (Å) and angles (degrees) for 2.18 BF ₂ complex.....	34
Table 2.4. Spectroscopic properties of BF ₂ complex 2.13 , benzyl-substituted BF ₂ complex 2.14 , monomer 2.17 , and dimer 2.18	36
Table 2.5. Electrochemical properties of BF ₂ complex 2.13 , benzyl-substituted BF ₂ complex 2.14 , monomer 2.17 , and dimer 2.18	38
Table 2.6 Crystallographic data for compounds 2.13 and 2.18	41
Table 3.1. Summary of molecular weight data determined by GPC for PBF₂N polymers ...	52
Table 3.2. Summary of molecular weight data determined by GPC for PDND	56
Table 3.3. Summary of molecular weight data determined for the first block and diblock copolymers (PDND) ₂₇₆ - b -(PBF₂N) ₂₅₅ ($f_{\text{BF}_2} = 0.48$), (PDND) ₃₅₅ - b -(PBF₂N) ₅₃ ($f_{\text{BF}_2} = 0.13$) and (PDND) ₂₆₆ - b -(PBF₂N) ₂₀ ($f_{\text{BF}_2} = 0.07$)	61
Table 3.4. Summary of molecular weight data for random copolymers (PDND) ₃₁₆ - r -(PBF₂) ₃₁₆ ($f_{\text{BF}_2} = 0.50$), (PDND) ₂₉₂ - r -(PBF₂N) ₅₂ ($f_{\text{BF}_2} = 0.15$) and (PDND) ₂₉₈ - r -(PBF₂N) ₂₆ ($f_{\text{BF}_2} = 0.08$)	63
Table 3.5. Spectroscopic properties of BF₂N , PBF₂N , and all block copolymers (PDND) _m - b -(PBF₂N) _n and random copolymers (PDND) _m - r -(PBF₂N) _n	67

List of Figures

- Figure 2.1.** Overlay of ^1H NMR spectra of compounds **2.13** (red) and **2.14** (black) in CDCl_3 . The triangle represents the $\equiv\text{CH}$ proton and the circle represents $=\text{CH}$ peak of the triazole ring.
..... 30
- Figure 2.2.** Solid-state structure of BF_2 complex **2.13** (top and side views). Hydrogen atoms have been omitted for clarity. Thermal displacement ellipsoids are shown at 50% probability
..... 32
- Figure 2.3.** Solid-state structure of dimer **2.18** (top and side views). Hydrogen atoms have been omitted for clarity. Thermal displacement ellipsoids are shown at 50% probability..... 34
- Figure 2.4.** Normalized absorption (a) and emission (b) spectra for BF_2 complex **2.13** (black), benzyl-substituted BF_2 complex **2.14** (blue), monomer **2.17** (green), and dimer **2.18** (red) recorded in CH_2Cl_2 35
- Figure 2.5.** Normalized absorption (solid line) and emission (dashed line) spectra for monomer **2.17** recorded in CH_2Cl_2 35
- Figure 2.6.** Cyclic voltammograms for BF_2 complex **2.13** (black), benzyl-substituted BF_2 complex **2.14** (blue), monomer **2.17** (green), and dimer **2.18** (red), were recorded at a scan rate of 250 mV s^{-1} for 1 mM analyte solutions in CH_2Cl_2 containing 0.1 M $[\text{nBu}_4\text{N}][\text{PF}_6]$ as the supporting electrolyte. All voltammograms were referenced internally against the ferrocene/ferrocenium redox couple 38
- Figure 3.1.** Overlay of the ^1H NMR spectra for BF_2N monomer (red) and PBF_2N (black) in CDCl_3 . The triangles represent the norbornene alkene protons on BF_2N and the circles represents the new alkene protons found in the backbone of PBF_2N 51
- Figure 3.2.** Relationship between M_n of PBF_2N as a function of time (a), and corresponding GPC traces (b). Dark blue dot at zero 0 min in (a) represents the M_n value determined for the BF_2N monomer. GPC traces in (b) are colour coded: 1 min (light blue), 3 min (red), 5 min (black), 10 min (dark yellow), 20 min (green), 30 min (purple), 60 min (grey) 52

Figure 3.3. Overlay of the ^1H NMR spectra of compound **DND** (red) and **PDND** (black) in CDCl_3 . The triangle represents the norbornene alkene protons and the circles represent the new alkene protons found in the backbone of **PDND** 55

Figure 3.4. Relationship between the M_n of **PDND** as a function of time (a), and corresponding GPC traces (b). GPC traces in (b) are colour coded: 0.5 min (light blue), 1 min (red), 3 min (black), 5 min (dark yellow), 7 min (green), 9 min (purple) 56

Figure 3.5. GPC traces (in DMF) of polymer **PDND** ($f_{\text{BF}_2} = 0.0$, dark yellow) and block copolymers **(PDND)_{276-b-(PBF₂N)₂₅₅}** ($f_{\text{BF}_2} = 0.48$, blue), **(PDND)_{355-b-(PBF₂N)₅₃}** ($f_{\text{BF}_2} = 0.13$, purple) and **(PDND)_{266-b-(PBF₂N)₂₀}** ($f_{\text{BF}_2} = 0.07$, red) 58

Figure 3.6. Overlay of ^1H NMR spectra of compound **PDND** (green), **PBF₂N** (red) and polymer **(PDND)_{276-b-(PBF₂N)₂₅₅}** (black) in CDCl_3 . The circles represent the new alkene protons found in the backbone of **(PDND)_{276-b-(PBF₂N)₂₅₅}**, the triangle represents the protons on the methoxy substituent of **PBF₂N**, the square represents the methyl groups on **PDND**, and the star represents two aryl protons on the **PBF₂N** subunit 59

Figure 3.7. ^1H NMR spectra of **(PDND)_{316-r-(PBF₂N)₃₁₆}** in CDCl_3 . The circles represent the alkene protons found in the backbone of the polymer, the triangle represents the protons on the methoxy group on the **PBF₂N** subunit, and the square represents the methyl groups on the **DND** subunit. The star represents two aryl protons on the **PBF₂N** subunit 63

Figure 3.8. GPC traces (in DMF) of polymer **PDND** ($f_{\text{BF}_2} = 0.0$, dark yellow) and random copolymers **(PDND)_{316-r-(PBF₂N)₃₁₆}** ($f_{\text{BF}_2} = 0.50$), **(PDND)_{292-r-(PBF₂N)₅₂}** ($f_{\text{BF}_2} = 0.15$) and **(PDND)_{298-r-(PBF₂N)₂₆}** ($f_{\text{BF}_2} = 0.08$) 64

Figure 3.9. TGA graphs of **PBF₂N** ($f_{\text{BF}_2} = 1.0$, black), **(PDND)_{276-b-(PBF₂N)₂₅₅}** ($f_{\text{BF}_2} = 0.48$, blue), **(PDND)_{355-b-(PBF₂N)₅₃}** ($f_{\text{BF}_2} = 0.13$, purple), **(PDND)_{266-b-(PBF₂N)₂₀}** ($f_{\text{BF}_2} = 0.07$, red), and **PDND** ($f_{\text{BF}_2} = 0.0$, dark yellow) 65

Figure 3.10. TGA graphs of **PBF₂N** ($f_{\text{BF}_2} = 1.0$, black), **(PDND)_{316-r-(PBF₂N)₃₁₆}** ($f_{\text{BF}_2} = 0.50$, blue), **(PDND)_{292-r-(PBF₂N)₅₂}** ($f_{\text{BF}_2} = 0.15$, purple), **(PDND)_{298-r-(PBF₂N)₂₆}** ($f_{\text{BF}_2} = 0.08$, red), and **PDND** ($f_{\text{BF}_2} = 0.0$, dark yellow) 65

Figure 3.11. DSC traces (a) and first derivative traces (b) for polymer **PDND** ($f_{\text{BF}_2} = 0.0$, dark yellow), **PBF₂N** ($f_{\text{BF}_2} = 1.0$, black), and block copolymers **(PDND)_{276-b}-(PBF₂N)₂₅₅** ($f_{\text{BF}_2} = 0.48$, blue), **(PDND)_{355-b}-(PBF₂N)₅₃** ($f_{\text{BF}_2} = 0.13$, purple) and **(PDND)_{266-b}-(PBF₂N)₂₀** ($f_{\text{BF}_2} = 0.07$, red). Decomposition point of **PDND** was lower than the other polymers, and thus DSC could only be done up to 130 °C..... 66

Figure 3.12. DSC traces (a) and first derivative traces (b) for polymer **PDND** ($f_{\text{BF}_2} = 0.0$, dark yellow), **PBF₂N** ($f_{\text{BF}_2} = 1.0$, black), and random copolymers **(PDND)_{316-r}-(PBF₂N)₃₁₆** ($f_{\text{BF}_2} = 0.50$, blue), **(PDND)_{292-r}-(PBF₂N)₅₂** ($f_{\text{BF}_2} = 0.15$, purple) and **(PDND)_{298-r}-(PBF₂N)₂₆** ($f_{\text{BF}_2} = 0.08$, red)..... 66

Figure 3.13. UV-vis absorption spectra of **BF₂N** (dark yellow) and **PBF₂N** ($f_{\text{BF}_2} = 1.0$, black) (a, b), and block copolymers **(PDND)_{m-b}-(PBF₂N)_n** (a), and random copolymers **(PDND)_{m-r}-(PBF₂N)_n** (b). All spectra were recorded in CH₂Cl₂ using 0.00005 g mL⁻¹ solutions 67

Figure 3.14. Emission spectra for **BF₂N** (dark yellow), **PBF₂N** ($f_{\text{BF}_2} = 1.0$, black) and random copolymers **(PDND)_{316-r}-(PBF₂N)₃₁₆** ($f_{\text{BF}_2} = 0.50$, blue), **(PDND)_{292-r}-(PBF₂N)₅₂** ($f_{\text{BF}_2} = 0.15$, purple) and **(PDND)_{298-r}-(PBF₂N)₂₆** ($f_{\text{BF}_2} = 0.08$, red) (b). All spectra were recorded in CH₂Cl₂ and their absorbance in the UV-vis region was approximately 0.1 68

Figure 3.15. Summary of the quantum yields of fluorescence (red dots) for the random copolymers **(PDND)_{m-r}-(PBF₂N)_n**, as well as for **BF₂N** (defined as $f_{\text{BF}_2} = 1.0$), and **PBF₂N** ($f_{\text{BF}_2} = 1.0$). Errors bars associated with the quantum yields calculated were placed by using the standard deviation for three repeated experiments of each. Spectra were recorded in CH₂Cl₂ and their maximum absorbance in solution was approximately 0.1 68

Figure 4.1. BF₂ complexes studied in Chapter 2..... 82

Figure 4.2. Block and random copolymers of **PBF₂N** and **PDND** studied in Chapter 3..... 83

Figure 4.3. Block copolymers **4.1** and **4.2**. The cartoon is a representation of the block copolymer where the blue represents the first block (BF₂ containing random copolymer) and the black represents the non-fluorescent organic block..... 84

Figure 4.4. Visual representation of micelle formation of block copolymers **4.1** and **4.2**.
Yellow cartoon around the micelle on the right represents fluorescence 85

List of Schemes

Scheme 1.1. Synthesis of quinoline containing monomer 1.3 and polymer 1.4	2
Scheme 1.2. Synthesis of monomer 1.12 and 1.13 for subsequent Suzuki coupling to afford polymers 1.14	4
Scheme 1.3. Free radical copolymerization of 1.15 and 1.16 for the synthesis of 1.17	5
Scheme 1.4. Synthesis of linear polymer 1.23 and cyclic polymer 1.25	7
Scheme 1.5. Synthesis of monomer 1.28 and polymers 1.31 and 1.32	8
Scheme 1.6. Synthesis of monomer 1.35	9
Scheme 1.7. Synthesis of monomer 1.37	9
Scheme 1.8. Synthesis of polymer 1.39	10
Scheme 1.9. Synthesis of polymer 1.41	10
Scheme 1.10. Synthesis of polymers 1.47 and 1.48	11
Scheme 1.11. Synthesis of polymer 1.51	12
Scheme 1.12. Synthesis of polymer 1.57	13
Scheme 1.13. Isomerization of <i>trans</i> - 1.57 to <i>cis</i> - 1.58 using visible light	14
Scheme 1.14. Synthesis of monomers 1.68–1.70 and polymers 1.72–1.74	17
Scheme 1.15. ROMP of monomer 1.76 to yield homopolymer 1.77	19
Scheme 1.16. ROMP of monomer 1.78 and monomer 1.76 to yield block copolymer 1.79 .	19
Scheme 2.1. Benzoid (2.4) to quinoid (2.5) resonance structures	26
Scheme 2.2. Stolarski synthesis of asymmetric 3-cyanoformazans	27

Scheme 2.3. Elnagdi synthesis for asymmetric 3-cyanoformazans	27
Scheme 2.4. “Statistical” synthesis of asymmetric 3-cyanoformazan 2.12	28
Scheme 2.5. Synthesis of asymmetric BF ₂ formazanate complex 2.13	29
Scheme 2.6. CuAAC reaction for the synthesis of benzyl-substituted BF ₂ complex 2.14	29
Scheme 2.7. DCC coupling for the synthesis of azide-substituted norbornene 2.16	31
Scheme 2.8. Synthesis of monomer 2.17 by CuAAC	31
Scheme 2.9. Redox reactions of a BF ₂ formazanate complex (2.19a) to afford a radical anion (2.19b) and dianion (2.19c)	37
Scheme 3.1. ROMP of BF₂N monomer	51
Scheme 3.2. Synthesis of monomer <i>exo</i> - NDCA	53
Scheme 3.3. Polymerization of monomer <i>exo</i> - NDCA	53
Scheme 3.4. Synthesis of monomer DND	54
Scheme 3.5. ROMP of DND	55
Scheme 3.6. Representative synthesis of (PDND) _m - <i>b</i> -(PBF₂N) _n polymers using ROMP	57
Scheme 3.7. Synthesis for random block copolymers (PDND) _{m-r} -(PBF₂N) _n . m represents the DP _n for the DND subunit, and n represents the DP _n for the BF₂N subunit	62

List of Appendices

Appendix 1 – Supporting Information for Chapter 2.....	86
Appendix 2 – Supporting Information for Chapter 3.....	97

List of Abbreviations

°	degree
°C	degrees Celsius
¹¹ B	boron-eleven
¹³ C	carbon-thirteen
¹ H	proton
¹⁹ F	fluorine-nineteen
+ve	positive
A	absorbance
Å	angstrom
a. u.	arbitrary units
AcOH	acetic acid
AIBN	2,2'-azo-bis(2-methylpropionitrile)
AIE	aggregation-induced emission
ATR	attenuated total reflectance
ATRP	atom transfer radical polymerization
BASi	Bioanalytical Systems Inc.
BOIMPY	boron complexes of iminopyrrolide ligands
BODIPY	boron dipyrromethene
bpy	bispyridine

br	broad
Bu	butyl
CCDC	Cambridge crystallographic data centre
cm	centimeter
Δ	change
cm^{-1}	wavenumber
CMPB	2-(4-chloromethyl-phenyl)-benzoxazole
CuAAC	copper (I)-assisted alkyne-azide cycloaddition
\mathcal{D}	dispersity
d	doublet
DCC	<i>N,N'</i> -dicyclohexylcarbodiimide
DLS	dynamic light scattering
DMA	dimethylacetamide
dd	doublet of doublets
DMAP	dimethylaminopyridine
DMF	dimethylformamide
DMSO	dimethylsulfoxide
DMSO- <i>d</i> 6	deuterated dimethylsulfoxide
DNA	deoxyribonucleic acid
DP_n	degree of polymerization

DSC	differential scanning calorimetry
E	potential
EDX	energy dispersive X-ray
EI	electron-impact ionization
Et	ethyl
Et ₂ O	diethyl ether
Et ₃ N	triethylamine
EtOAc	ethyl acetate
EtOH	ethanol
FT-IR	Fourier transform infra-red spectroscopy
f_{BF_2}	mole fraction of BF ₂ N
g	gram
GIII	3-bromo pyridine derivative of Grubb's third generation catalyst
GPC	gel permeation chromatography
GOF	goodness of fit
h	hours
hex	hexanes
Hz	hertz
IR	infrared
J	<i>NMR coupling constant</i>

K	Kelvin
LED	light emitting diode
$[M]_0$	initial monomer concentration
$[M]$	monomer concentration
M	molar
μM	micromolar
m	multiplet
mA	milliamps
max	maximum
Me	methyl
MeOH	methanol
mg	milligram
MHz	megahertz
min	minute/minutes
mL	milliliter
mm	millimeter
mM	millimolar
mmol	millimoles
M_n	number average molecular weight
mol	moles

mV	millivolts
MW	molecular weight
M_w	weight average molecular weight
nm	nanometers
NMP	1-methyl-2-pyrrolidinone
NMR	nuclear magnetic resonance
O. D.	onset of decomposition
OAc	acetate
OLED	organic light-emitting diode
<i>p</i>	para
PBB	propargyl-2-bromoisobutyrate
Pd(dppf)Cl ₂	[1,1'-Bis(diphenylphosphino)ferrocene]dichloropalladium(II)
PLA	polylactic acid
Ph	phenyl
PMDETA	<i>N,N,N',N'',N''</i> -pentamethyldiethylenetriamine
ppm	parts per million
π	pi
py	pyridine
ppm	parts per million
Φ_F	fluorescence quantum yield

q	quartet
R ₁	residual factor
r.t.	room temperature
RI	refractive index
RAFT	reversible addition-fragmentation chain transfer
ROMP	ring-opening metathesis polymerization
s	singlet
t	triplet
<i>t</i> -BuOK	potassium <i>tert</i> -butoxide
T _g	glass transition temperature
TGA	thermal gravimetric analysis
THF	tetrahydrofuran
TBAI	tetrabutylammonium iodide
UV	ultraviolet
UV-vis	ultraviolet-visible
v/v	volume to volume ratio
w	weak
vs.	versus
<i>x</i>	Cartesian axis
XRD	X-ray diffraction

y	Cartesian axis
z	Cartesian axis
α	crystallographic lattice constant, torsional angle
β	crystallographic lattice constant, torsional angle
γ	crystallographic lattice constant, torsional angle
δ	chemical shift, partial charge
ε	molar absorptivity
ν_{ST}	Stoke's shift
θ	theta (range for crystallographic data collection)
λ	wavelength
λ_{max}	wavelength of maximum absorption
λ_{em}	wavelength of maximum emission

Chapter 1

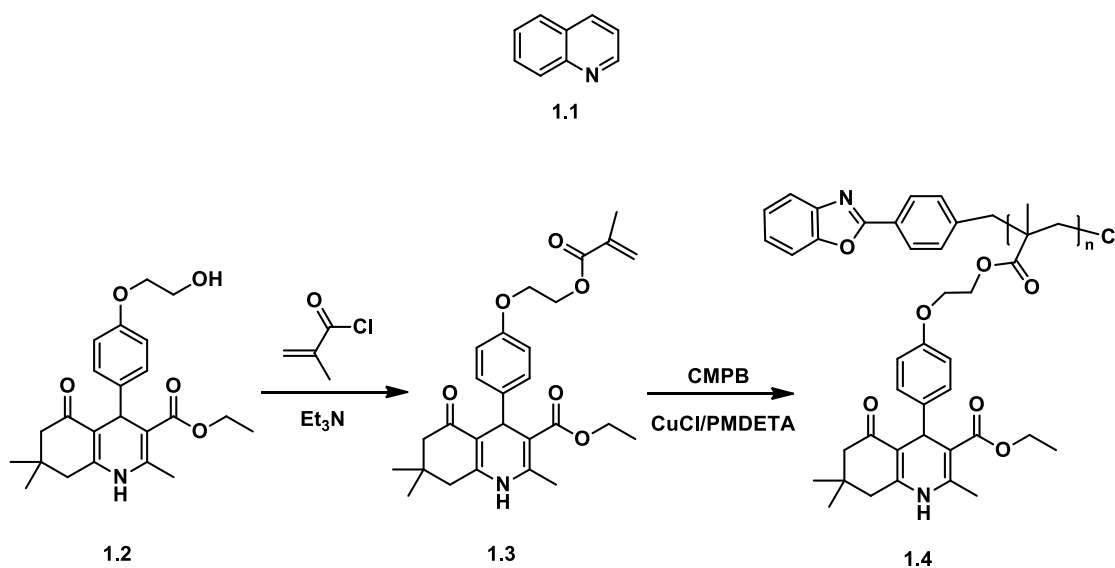
1 Introduction

Polymers have been synthesized for over 100 years due to the observation that molecular properties change dramatically once molecules are incorporated into long chains. Polymers are essential on a day to day basis whether they are found in plastic containers (polystyrene), batteries (polyethylene and polypropylene), or as the genetic code needed for human function and growth (DNA). Furthermore, π -conjugated polymers that have luminescent properties have been researched for their potential use in biological sensors, semiconductors and LED applications.¹⁻² Below, several classes of emissive polymers are highlighted.

1.1 Polymers Containing Quinoline Derivatives

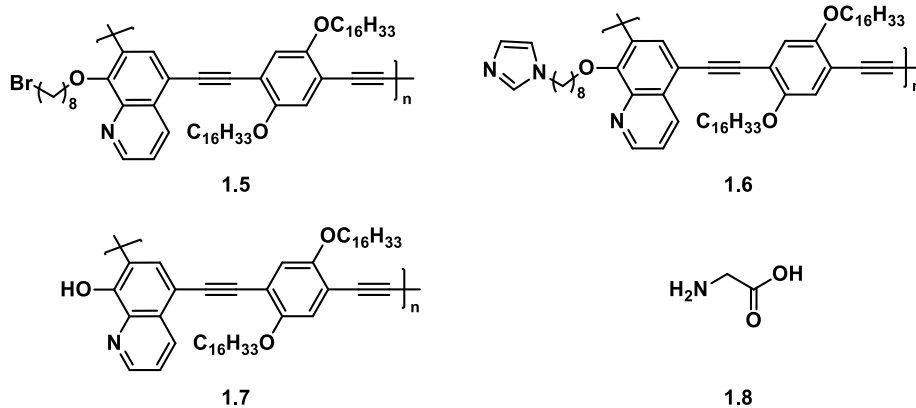
Polymers containing quinoline chromophores (**1.1**) (or derivatives of) have been studied for their use in applications such as LEDs,^{3,4,5} electronic optical materials,^{6,7} and optical sensors.^{8,9} These polymers can be synthesized in different ways so that the quinoline chromophores appear in the side- or main-chain of polymers. For example, Wen and co-workers synthesized a novel polymer that contained a quinoline derivative in the side-chain (**1.4**) (Scheme 1.1). The synthesis of monomer **1.3** was carried out by dissolving previously synthesized molecule **1.2**¹⁰ in THF and Et₃N, cooling the solution down, and then adding methacryloyl chloride. Monomer **1.3** was then polymerized by using atom transfer radical polymerization (ATRP) where CMPB was used as the initiator, and CuCl/PMDETA as the catalyst/ligand system. A plot of $\ln([M]_0/[M])$ vs. time was plotted where $[M]_0$ corresponds to the initial monomer concentration, and $[M]$ corresponds to the monomer concentration at a certain time interval. This relationship was found to be linear, which showed the controlled polymerization of monomer **1.3**, along with the fact that the polymers had low dispersity (D) values. The spectroscopic properties of monomer **1.3** and polymer **1.4** were studied, and it was found that the emission of the polymer was significantly higher than that of the monomer. This was attributed to a phenomenon known as “fluorescence structural self-quenching”¹¹ whereby intra- or intermolecular excimer formation occurs. In this case, the alkene of the methacrylate group on monomer **1.3** is electron-accepting and will quench fluorescence from the quinoline portion of the monomer (excimer formation). However, the absence of alkene group in polymer

1.4 allows for emission from the chromophore without quenching. These polymers emitted at 424 nm in the solution state (DMF) and 432 nm in the solid state.

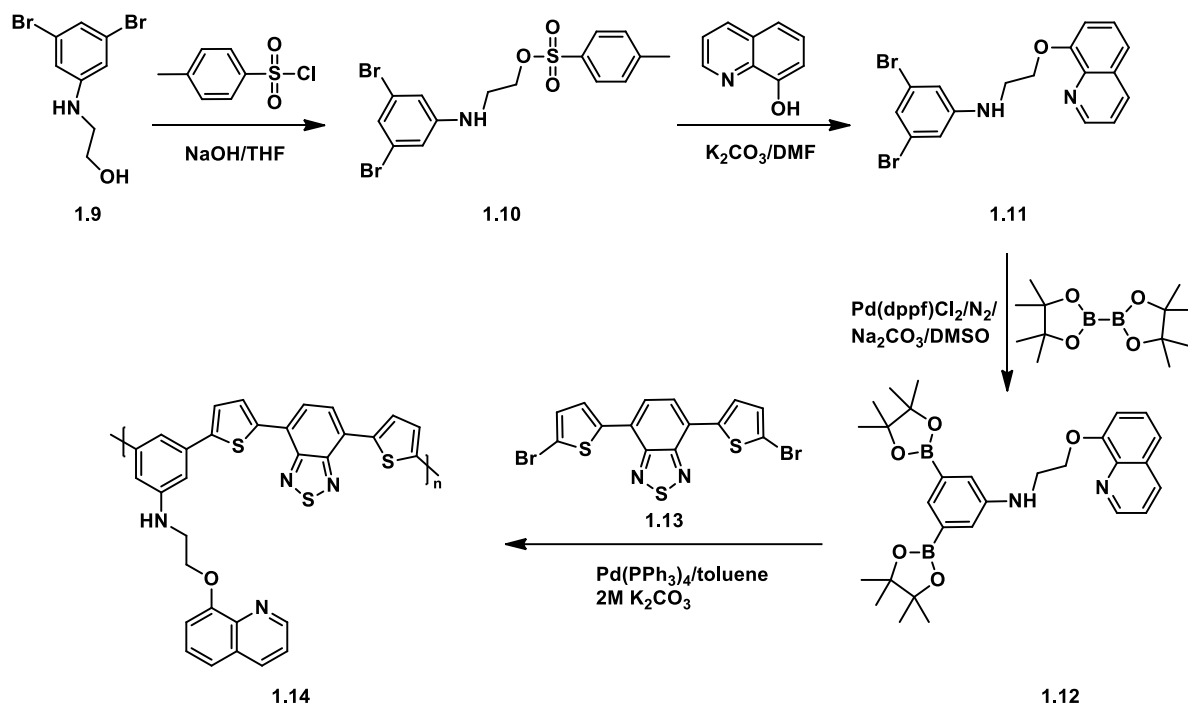


Scheme 1.1. Synthesis of quinoline containing monomer **1.3** and polymer **1.4**.

The effect of quenching or enhancing the fluorescence of quinoline based polymers due to the presence of other molecules in the structure or in solution has been explored as a means of using these molecules in sensing applications. For example, quinoline-containing conjugated polymers **1.5**, **1.6** and **1.7** were studied for their potential use in sensing Cu^{2+} ions and amino acids.¹² It was observed that when **1.6** was dissolved in THF it had a wavelength of maximum absorption (λ_{max}) of 410 nm, and a wavelength of maximum emission (λ_{em}) of 460 nm. This emission was quenched to 10% of its initial value when 1.6 μM concentrations of Cu^{2+} were added. The same response was observed for **1.7**, but the emission of **1.5** was not affected. This was attributed to the fact that functional groups on **1.5** do not have a specific affinity to Cu^{2+} ions, and thus no quenching was observed. However, **1.6** contains an imidazole functional group and **1.7** contains an 8-hydroxyquinoline group which can chelate Cu^{2+} and result in quenched emission. The emission of **1.6** was recovered by adding amino acid glycine (**1.8**); this was rationalized by the fact that glycine is a stronger chelate to Cu^{2+} than the imidazole functional group on **1.6**. Conversely, no change of the emission of **1.7** was observed upon addition of glycine because 8-hydroxyquinoline is a stronger chelate than glycine.



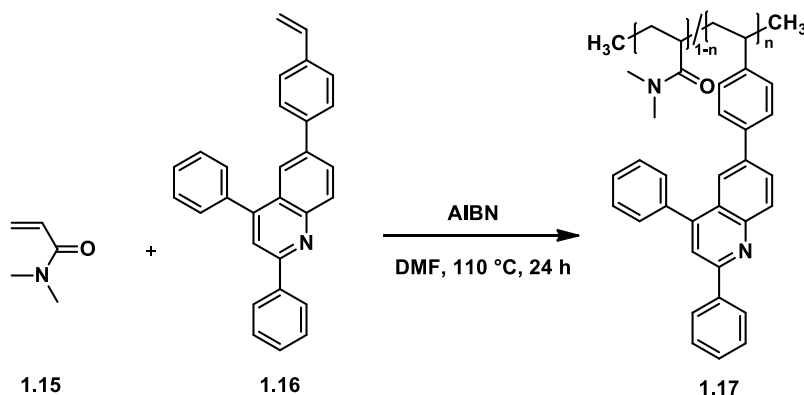
The Liu group synthesized copolymers **1.14** containing derivatives of quinoline, thiophene and benzothiazole and studied their potential use in metal ion sensing.¹³ The synthesis of these copolymers began by the addition of sulfonyl chloride to compound **1.9** in a NaOH/THF solution. This reaction afforded compound **1.10** in 70% yield, which was then reacted with 8-hydroxyquinoline in a K₂CO₃/DMF solution to afford **1.11** in 66% yield (Scheme 1.2). Monomer **1.12** was then synthesized by reacting **1.11** with bis(pinacolato)diboron, Pd(dppf)Cl₂ and Na₂CO₃ in DMSO for 12 h at 100 °C. Suzuki coupling was then employed as a means to synthesize polymer **1.14**. First, monomer **1.12** and monomer **1.13** were dissolved in a solution of Na₂CO₃/toluene and then catalyst Pd(PPh₃)₄ was added. The reaction proceeded for 48 h at 110 °C and the polymer was isolated in 65% yield. Spectroscopic studies for the polymer revealed that it had a λ_{max} at 490 nm, and a λ_{em} at 610 nm (in DMSO), although its emission was rather weak. However, a 12 fold enhancement of the emission was observed when a 5.0 x 10⁻⁵ M Hg(II) ion solution was added, along with a 10 nm blue shift in the λ_{max}. Therefore, polymers **1.14** are effective as sensors for Hg(II) ions.



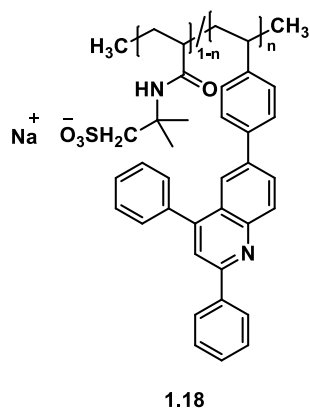
Scheme 1.2. Synthesis of monomer **1.12** and **1.13** for subsequent Suzuki coupling to afford polymers **1.14**.

Water-soluble copolymers containing quinoline units (e.g., **1.17**) have also been synthesized and studied for their pH tunable fluorescence response.¹⁴ These polymers were made by free radical copolymerization of *N,N*-dimethylacrylamide (**1.15**) and quinoline containing monomer **1.16** using AIBN as the free radical initiator (Scheme 1.3).⁹ The resulting polymers contained approximately 3.5 mol % of quinoline units; this was done to avoid excimer formation between quinoline units which would result in the quenching of their emission. The polymers' λ_{em} was observed to shift from 411 nm to 484 nm as the pH of the solution decreased, and its emission intensity changed linearly. This shift in λ_{em} was attributed to the protonation of the quinoline group in the polymer. A second copolymer containing an anionic backbone and quinoline units was synthesized (**1.18**). It was found that this polymer was more readily protonated than neutral polymer **1.17**, due to the electrostatic attraction between the protonated quinoline unit and the negatively charged chain. This phenomenon was demonstrated by looking at the fluorescence quantum yields (Φ_F) at 411 nm (free quinoline) and 485 nm (protonated quinoline). For polymer **1.17**, the Φ_F at pH 7 and pH 2 were 85% and 38%, respectively. Conversely, the Φ_F for polymer **1.18** at pH 7 and pH 2 were 84% and 55%, respectively. This difference in Φ_F at 485 nm was attributed to the shift in equilibrium for the protonation of quinoline whereby polymer **1.18** was more easily protonated due to electrostatic

interactions of the protonated quinoline group with the polymer backbone. These properties highlight the use of these polymers as pH indicators.



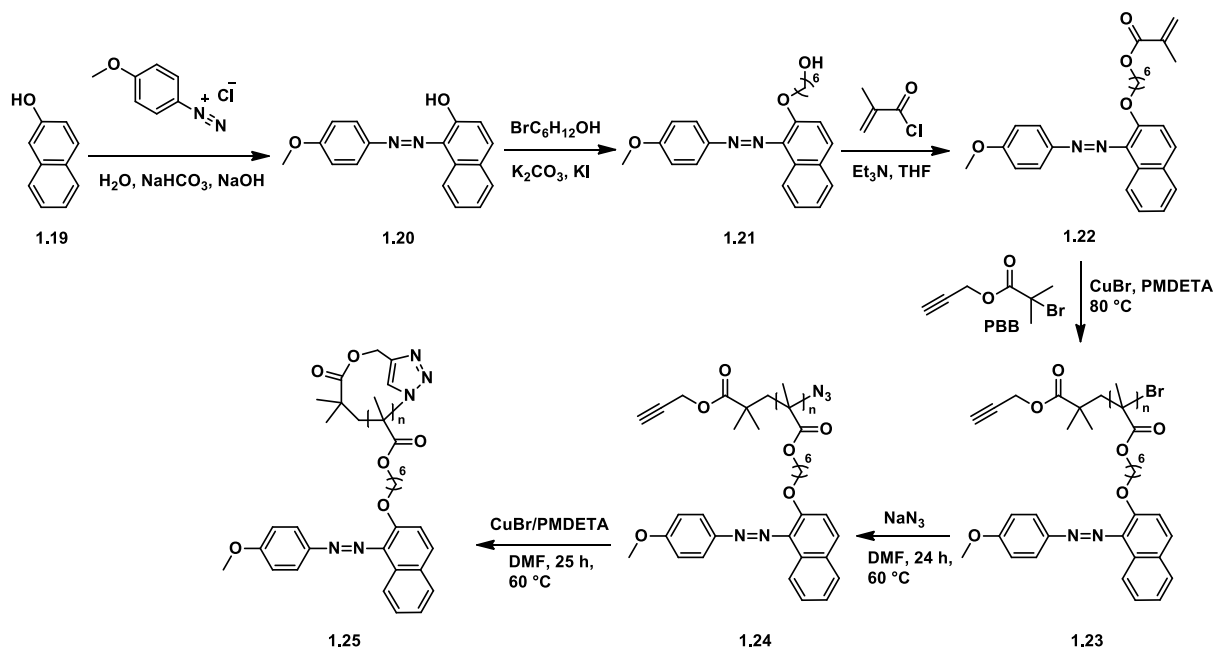
Scheme 1.3. Free radical copolymerization of **1.15** and **1.16** for the synthesis of **1.17**.



1.2 Polymers Containing Naphthalene and Anthracene Derivatives

Naphthalenes have been incorporated into various types of polymers due to their interesting spectroscopic properties. For example, the Zhu group synthesized linear and cyclic side-chain phenylazo naphthalene polymers and studied their photoisomerization as well as their fluorescence.¹⁵ Synthesis of these polymers began by the addition of the diazonium salt of 4-methoxy aniline to a solution of 1-naphthol (**1.19**) in NaHCO_3 and NaOH to afford **1.20** which contains both a naphthalene group and an azo-benzene group (Scheme 1.4).¹⁶ This molecule was then reacted with 6-bromohexanol in a DMF solution containing K_2CO_3 and catalytic amounts of KI to obtain **1.21**. A polymerizable group (methyl methacrylate) was then attached

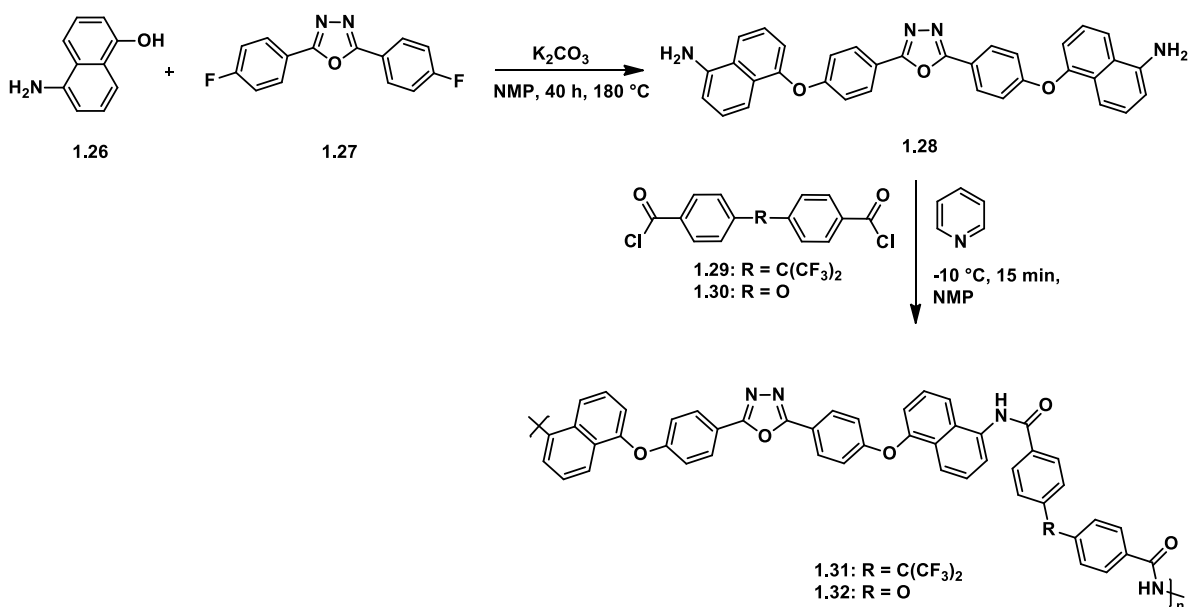
to **1.21** by adding methacryloyl chloride into a solution of **1.21** and Et₃N in THF; this resulted in the synthesis of monomer **1.22**. This monomer was polymerized by using ATRP where propargyl-2-bromoisobutyrate (PBB) was the initiator, and CuBr (with PMDETA as the ligand) was the catalyst. Post-polymerization functionalization of linear polymer **1.23** was then used to attach an azide group at the chain end (**1.24**). CuAAC was employed in order to convert linear polymer **1.24** into cyclic polymer **1.25**. Both linear and cyclic polymer **1.23** and **1.25** have azo-benzene groups as part of their side-chain and thus these polymers could undergo photoisomerization. Studies of the rate of photoisomerization of the azobenzene unit from *trans* to *cis* revealed that cyclic polymers **1.25** had a faster rate of conversion from *trans* to *cis* than that of the linear polymers **1.23**. This was attributed to the fact that there is less resistance upon conversion due to minimal entanglement in the cyclic polymers *vs.* the linear polymers. The naphthalene unit is also found in the side-chain of both the linear (**1.23**) and cyclic (**1.25**) polymers and thus the fluorescence of these polymers was investigated. It was found that the linear polymers exhibited weak fluorescence at 430 nm, but cyclic polymers showed an enhancement in fluorescence intensity, which was more obvious when looking at polymers with lower weight average molecular weights (M_w). Although this phenomenon is not completely understood, it was suggested that there is more rigidity in the cyclic polymers *vs.* the linear ones, reducing both aggregation-caused self-quenching in solution, and vibrational non-radiative relaxation pathways.



Scheme 1.4. Synthesis of linear polymer **1.23** and cyclic polymer **1.25**.

Copolymers containing naphthalene and a second fluorescent molecule known as oxadizole, were synthesized by the Bruma group.¹⁷ Polycondensation was used to synthesize these polymers from monomers **1.29** and **1.30**. Synthesis of monomer **1.28** began by stirring 5-amino-naphthol **1.26** with fluorophenyl-oxadiazole derivative **1.27** in K_2CO_3 and 1-methyl-2-pyrrolidinone (NMP) for 40 h at 180 °C. Polymers **1.31** and **1.32** were prepared through low temperature (−10 °C) polycondensation reaction of monomer **1.28** with diacid chloride monomer **1.29** or **1.30** in NMP and pyridine. After 15 min of stirring, the reaction was warmed to room temperature and stirred for an additional 6 h. Polymer films were made by drop casting solutions (in NMP) of these polymers into glass plates. The spectroscopic properties of the polymers in solution and in the solid state were investigated. It was found that in solution, both polymers absorbed in the UV-vis region at a λ_{max} of 312 nm, however, as films, these absorptions red-shifted to 343–350 nm. This shift in absorbance was attributed to an increase in intermolecular interactions of the bulk polymer, leading to differences in the conformational state of the polymer in the solid state vs. in solution. The polymers were also emissive in solution and in the solid state. In solution, λ_{em} was at 420 nm and in the solid state (films) emission occurred at 413–420 nm and at 445–465 nm. The first peak was concluded to arise from the phenyl-oxadiazole portion of the polymers, whereas the second was due to the naphthalene-containing portion of the polymers. Polymer **1.31** also gave rise to an emission

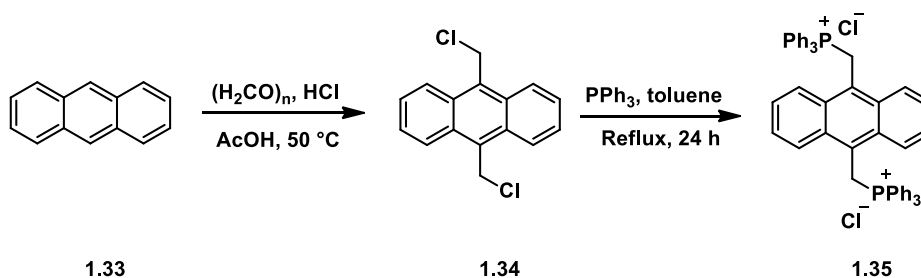
shoulder at 433 nm and polymer **1.32** had an emission shoulder at 498 nm; these emissions were due to aggregation and excimer formation which led to a red-shift in the emission as well as quenching.⁴ It is noteworthy that the emission of these polymers in the solid state were blue-shifted from that in the solution phase. This led to the conclusion that there was no extended π -conjugation in the polymers in the solid state, but rather there is organization of the chains that causes their emission to shift.¹⁸ This makes these polymers excellent candidates for blue light-emitting devices.



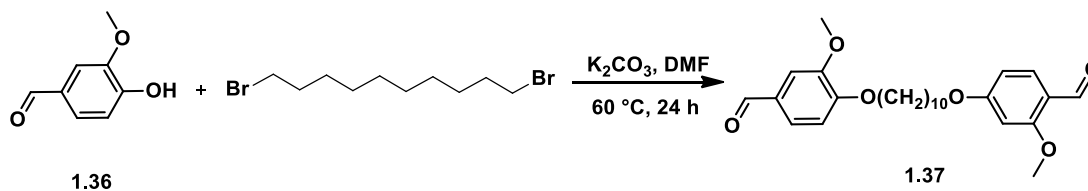
Scheme 1.5. Synthesis of monomer **1.28** and polymers **1.31** and **1.32**.

Anthracenes (**1.33**) are another class of aromatic molecules that have found use as functional materials in organic light-emitting diodes (OLEDs),¹⁹⁻²⁰ transistors²¹ and photovoltaic cells²²; they are fluorescent and have been incorporated into semiconducting polymers.²³⁻²⁴ The Majdoub group synthesized two anthracene containing copolymers (**1.39** and **1.41**) whose properties differed greatly as a result of the nature of the comonomer.²⁵⁻²⁶ Synthesis of polymer **1.39** began by the direct bischloromethylation of anthracene (**1.33**) with paraformaldehyde ((H₂CO)_n) and HCl in acetic acid (AcOH) to afford **1.34**. The next step was the synthesis of comonomer **1.35** which was carried out by reacting **1.34** with PPh₃ in toluene (Scheme 1.6). Dialdehyde **1.37** was then synthesized by reacting vanillin (**1.36**) with K₂CO₃ in DMF and adding dibromodecane dropwise (Scheme 1.7). Once the monomers had been prepared, polymers **1.39** and **1.41** were synthesized by using Wittig polycondensation whereby monomer

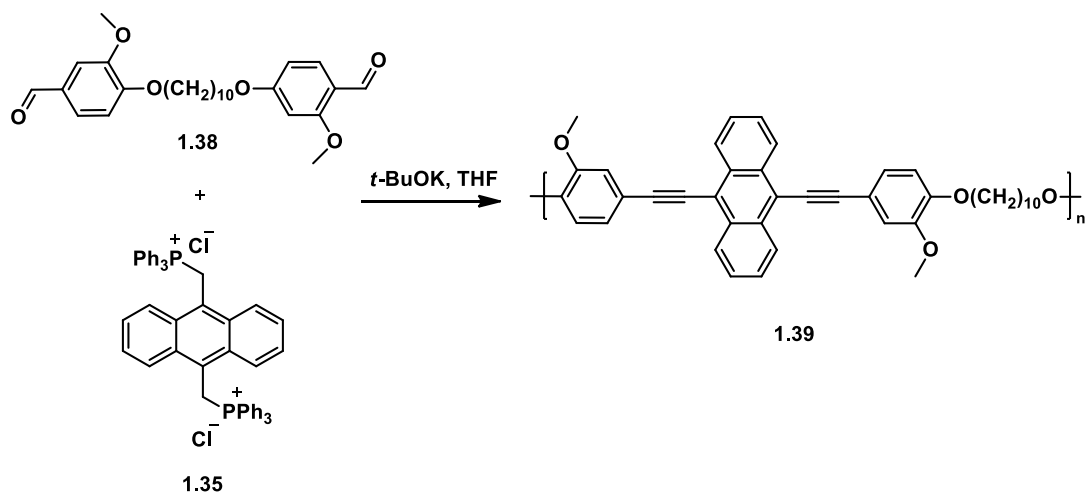
1.37 or **1.39** were stirred with **1.35** in THF and 0.5 M *t*-BuOK solution was added (Scheme 1.8 and 1.9). UV-vis absorption spectra for both polymers revealed three maxima in solution; these maxima were consistent with UV-vis absorptions of anthracene molecules.²⁷ Polymers **1.39** had a λ_{max} at 365, 385, and 408 nm, while polymers **1.41** had a λ_{max} at 357, 383, and 406 nm, pertaining to $\pi \rightarrow \pi^*$ electronic transitions in the anthracene group. Both polymers were fluorescent in solution, **1.39** had λ_{em} at 410, 432, and 458 nm ($\Phi_{\text{F}} = 37\%$), whereas polymer **1.41** had λ_{em} at 420 and 443 nm ($\Phi_{\text{F}} = 72\%$). The difference in Φ_{F} between the two polymers was attributed to the fact that in polymer **1.41** the isosorbide groups (functional group on comonomer **1.40**) increased the rigidity of the polymer, which in turn decreased the vibrational and rotational degrees of freedom of the chain, making vibrational relaxation less likely, and relaxation through emission more likely. Films of both polymers were also made and their λ_{em} were found to be at 570 nm and 562 nm for **1.39** and **1.41**, respectively. The shift of the λ_{em} in the solid state versus that in solution was due to π - π interactions of the conjugated fluorophores which lead to excimer formation.²⁸



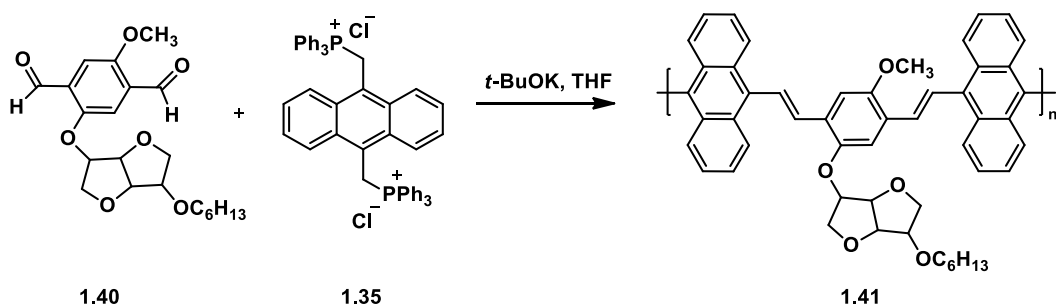
Scheme 1.6. Synthesis of monomer **1.35**.



Scheme 1.7. Synthesis of monomer **1.37**.



Scheme 1.8. Synthesis of polymer **1.39**.

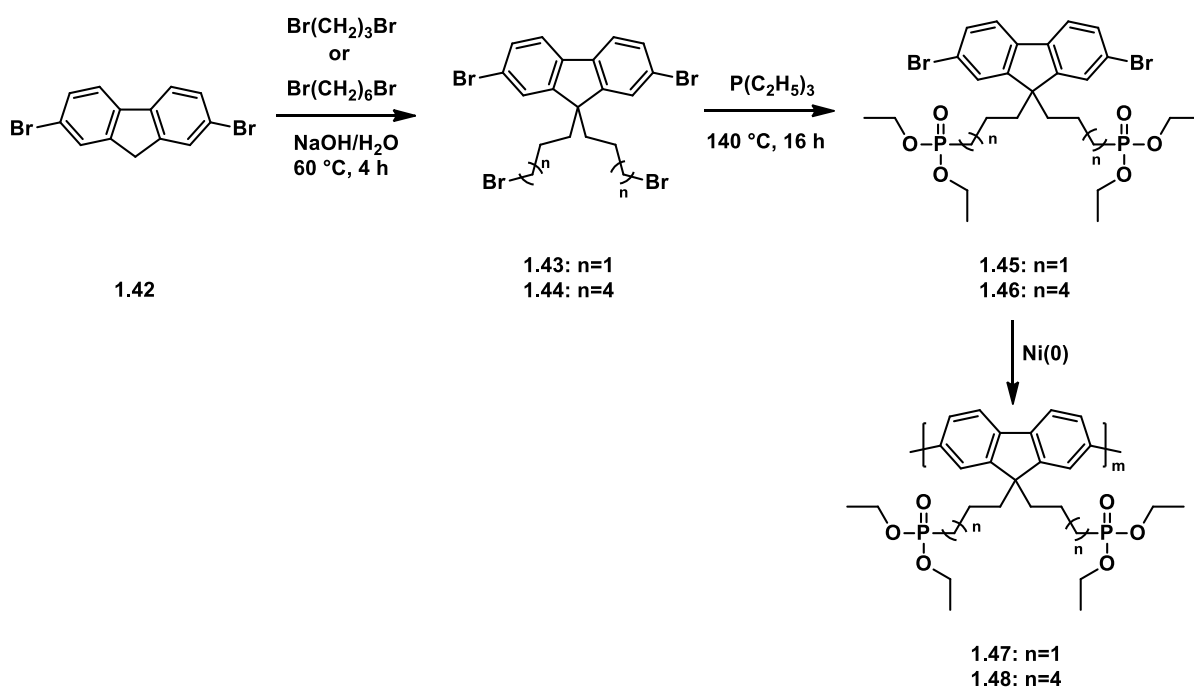


Scheme 1.9. Synthesis of polymer **1.41**.

1.3 Polymers Containing Fluorene Derivatives

Polyfluorenes are a class of conjugated fluorescent polymers that benefit from high Φ_F , and impressive thermal and chemical stability.²⁹⁻³¹ Polyfluorenes containing phosphonate groups in the side-chain (e.g., **1.47** and **1.48**) have been synthesized and their use as chemosensors has been explored.³² Synthesis of these polymers began by reacting 2,7-dibromofluorene (**1.42**) with 1,3-dibromopropane ($\text{Br}(\text{CH}_2)_3\text{Br}$) or 1,6-dibromohexane ($\text{Br}(\text{CH}_2)_6\text{Br}$) in an aqueous solution containing NaOH to afford **1.43** and **1.44**. These molecules were then refluxed in the presence of $\text{P}(\text{C}_2\text{H}_5)_3$ to obtain monomers **1.45** and **1.46**. Polymerization was then performed by Yamamoto polycondensation where monomers were reacted with nickel (0) catalyst (Scheme 1.10). The spectroscopic properties of these polymers were investigated, and it was found that their absorption depends on the solvent being used. For example, **1.47** has λ_{max} at 382 nm in CHCl_3 , but 338 nm in EtOH, and **1.48** has an λ_{max} at 392 nm in CHCl_3 and 401 nm

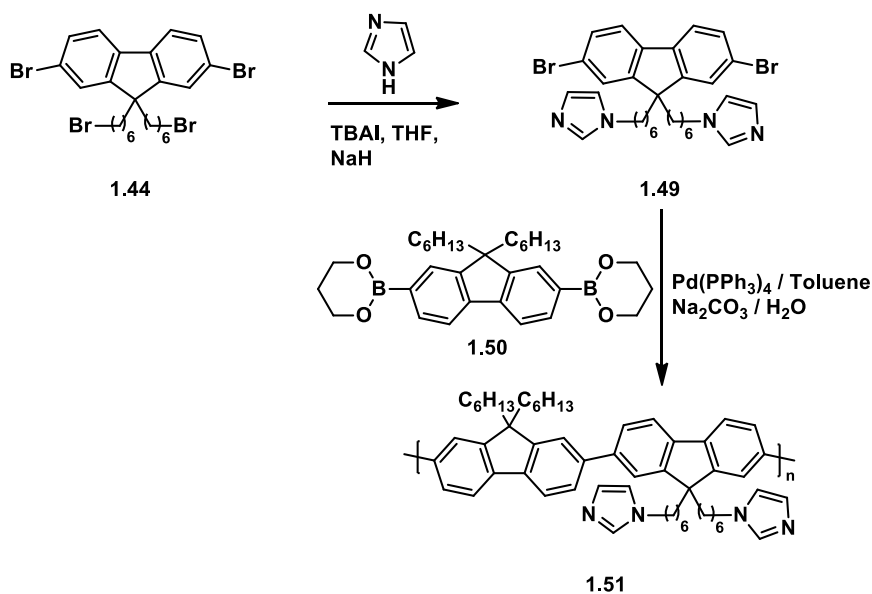
in EtOH. The emission spectra were also solvent dependent. Polymers **1.47** and **1.48** emit at 418 nm in CHCl_3 and 422 nm in EtOH. The Φ_F for both polymers in EtOH was found to be 74%, suggesting that there is no aggregation in solution since little to no quenching was observed. Furthermore, the sensing properties of these polymers to metal ions was investigated. This was done by adding various metal ions (Li^+ , Na^+ , K^2+ , Mg^{2+} , Ca^{2+} , Cd^{2+} , Zn^{2+} , Fe^{3+}) to a solution of polymers **1.47** or **1.48** in CHCl_3 . No significant changes to the emission of these solutions was observed for any of the ions, except for when Fe^{3+} was added. Addition of Fe^{3+} resulted in dramatic quenching of the emission intensity by 210 fold for **1.47** and 130 fold for **1.48**. These results demonstrate the efficacy of these polymer as sensitive and selective chemosensors of Fe^{3+} .



Scheme 1.10. Synthesis of polymers **1.47** and **1.48**.

Imidazole-functionalized polyfluorenes **1.51** have also been synthesized and investigated for their use as chemosensors.³³ The design of these polymers was based on the fact that the imidazole has been demonstrated to have ion coordinating abilities to various ions,³⁴ and the fluorene portion would have strong luminescence properties. Synthesis of this copolymer began by reacting **1.44** with imidazole in THF and NaH using TBAI. This resulted in the synthesis of monomer **1.49**, which was then copolymerized with **1.50** using Suzuki coupling

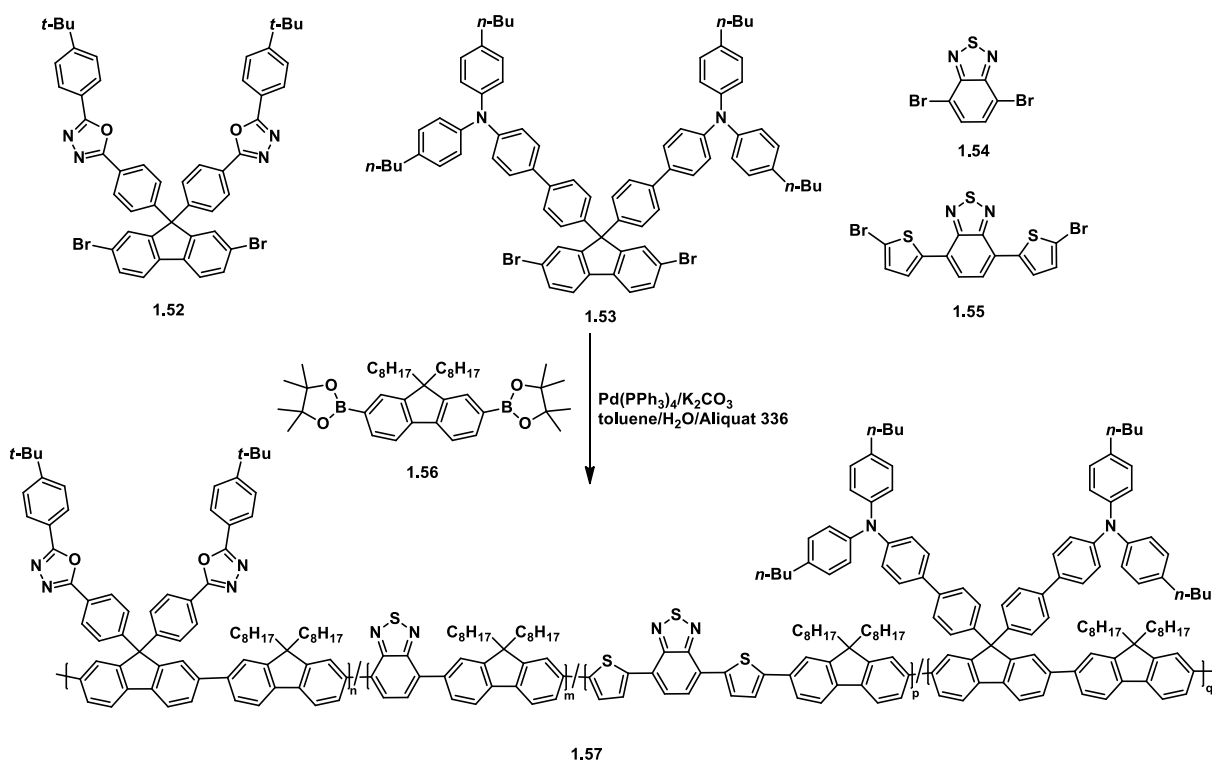
polymerization ($\text{Pd}(\text{PPh}_3)_4$ as the catalyst) to obtain polymer **1.51**. This polymer was shown to absorb in the UV-vis region, specifically having a λ_{max} at 390 nm. It was also emissive, with a λ_{em} at 404 nm, and a shoulder at 425 nm. Their use as chemosensors was explored by adding various metals (e.g., Fe^{2+} , Ni^{2+} , Cd^{2+} , Mn^{2+} , Al^{3+}) to polymer solutions in THF; however, no change in the absorbance of the polymers or their emission was detected. Nevertheless, when Cu^{2+} was added, a blue-shift in the λ_{max} of the polymer solution was detected ($\Delta\lambda = 7$ nm); this was due to the change in the electronic structure of the backbone upon metal binding. The emission properties of the polymers were affected more dramatically, whereby addition of 1–2 ppm Cu^{2+} solutions completely quenched the fluorescence. Films of these polymers were made, and placed into an aqueous solution of CuCl_2 where the same blue-shift in the λ_{max} , and quenching of the fluorescence was observed. Furthermore, when the films were placed into an ammonia solution, the fluorescence was rejuvenated. These properties showed the potential use of these polymers for applications as fluorescent chemosensors.



Scheme 1.11. Synthesis of polymer **1.51**.

Polymers containing derivatives of fluorene (**1.52**, **1.53**), benzothiadiazole (**1.54**) and bisthiophenylbenzothiadiazole (**1.55**) have also been synthesized, and their use as white-light-emitting polymers has been demonstrated.³⁵ These polymers (**1.57**) were made by using Suzuki polycondensation of monomers containing oxidiazole (**1.52**), triphenylamine (**1.53**), 4,7-dibromo-2,1,3-benzothiadiazole (**1.54**), 4,7-bis(5-bromothiophen-2-yl)-2,1,3benzothiadiazole

(**1.55**), and the diboronate (**1.56**), where Pd(PPh₃)₄ was used as the catalyst, and aliquat 336 was used as the phase-transfer reagent as this polymerization took place in a mixture of toluene and aqueous K₂CO₃ (2M) solution (Scheme 1.52). These polymers possessed *D* of 2.0, typical for condensation polymerizations, and λ_{max} at around 300 and 380 nm in CHCl₃. Emission spectra collected for these polymers in CHCl₃ showed two λ_{em} at approximately 430 and 460 nm. Thin film fabricated devices of these polymers were also made, and emission from these films ranged from 400–700 nm, having λ_{em} peaks at 430, 460, 518, and 602 nm (each pertaining to one of the chromophores in the polymer). The combination of these specific emission wavelengths led to the devices emitting white light when an electric field was applied. Furthermore, the different emissions from this polymer was concluded to be due to partial energy transfer from the blue-fluorescent polyfluorene backbone to the other chromophores. Controlling the contribution of light from each chromophores (by controlling the number of chromophores within the polymer) led to the emission of white light.

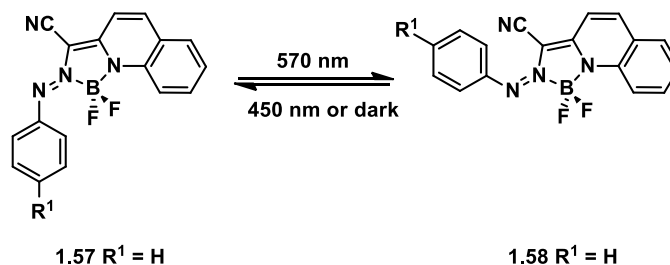


Scheme 1.12. Synthesis of polymer **1.57**.

1.4 Boron Containing Fluorophores and Polymers

BF₂ complexes of chelating *N,N*- and *N,O*- ligands have received a lot of interest and have been extensively researched due to their unique properties, which include: large absorption coefficients, high Φ_F , redox activity, and excellent stability. These compounds have found use as photosensitizers, fluorescent imaging agents, OLEDs, and as the functional component of sensors.³⁶⁻⁴²

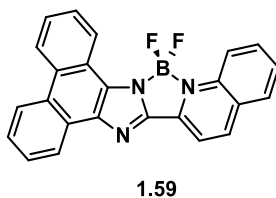
The ability to synthesize asymmetric BF₂ complexes has allowed for versatility in their applications as well as in their properties. For example, the Aprahamian group was able to synthesize *N,N*-chelated asymmetric BF₂ molecules containing an azo group (e.g., **1.58**) by reacting BF₃•OEt₂ boron trifluoride etherate with the corresponding hydrazone at room temperature.⁴³ Isomerization of this molecule from its *trans* (**1.57**) to *cis* (**1.59**) confirmation was induced by visible light (570 nm) (Scheme 1.13), and their photoisomerization properties could be studied using UV/vis spectroscopy thanks to their very distinct λ_{max} at 530 nm and 480 nm, respectively. Furthermore, they were able to obtain a red-shift in the activation wavelength of these complexes by the addition of an electron donating group in the R¹ position such as a methoxy or dimethyl amine group.⁴⁴ The activation wavelength of these complexes was shifted to the near-IR region of the spectrum (630 nm and 710 nm, respectively).



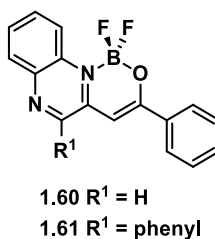
Scheme 1.13. Isomerization of *trans*-**1.57** to *cis*-**1.58** using visible light.

Besides being able to introduce interesting functional groups to BF₂ complexes, asymmetric synthesis can also be used as a means to create rigid BF₂ complexes so that fluorescence in the solid state can be obtained. For example, phenanthro[9,10-*d*]imidazole-quinoline BF₂ **1.59** was synthesized in hopes of obtaining solid-state fluorescence.⁴⁵ This approach was taken due to the fact that phenanthro[9,10-*d*]imidazole-quinoline dyes display large Stokes' shifts, which

aid in minimizing reabsorption and self-quenching in the solid state.⁴⁶ They found that compound **1.59** had strong absorbance in solution at 476 nm, and bright luminescence at 585 nm in solution with a Φ_F of 90% and also possessed emission in the solid state at 622 nm with a Φ_F of 18%.

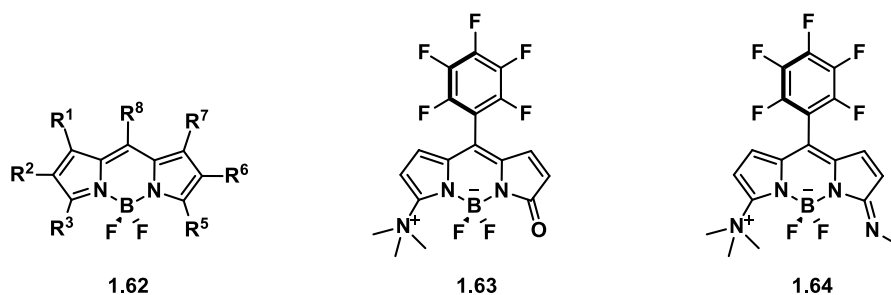


Emission in the solid state can also be realized by synthesizing molecules that undergo aggregation-induced emission (AIE), which is a phenomenon whereby the structure of the molecule becomes restricted in the solid state, thereby enhancing the emission of the chromophores.⁴⁷ For example, BF_2 complexes of quinoxaline- β -ketoiminates (e.g., **1.60** and **1.61**) have strong absorption and emission properties in solution.⁴⁸ However, in the solid state, **1.60** was essentially non-emissive ($\Phi_F = 2\%$) whereas **1.61** had a solid-state Φ_F of 22%. The difference in their behaviour was attributed to the phenyl group introduced at the R^1 position in **1.61**. This phenyl group was observed to be twisted in the solid-state structure, which in turn increased the π - π distance between adjacent molecules, decreased π - π stacking, and resulted in the impediment of intermolecular quenching, allowing the molecule to fluoresce in the solid state.



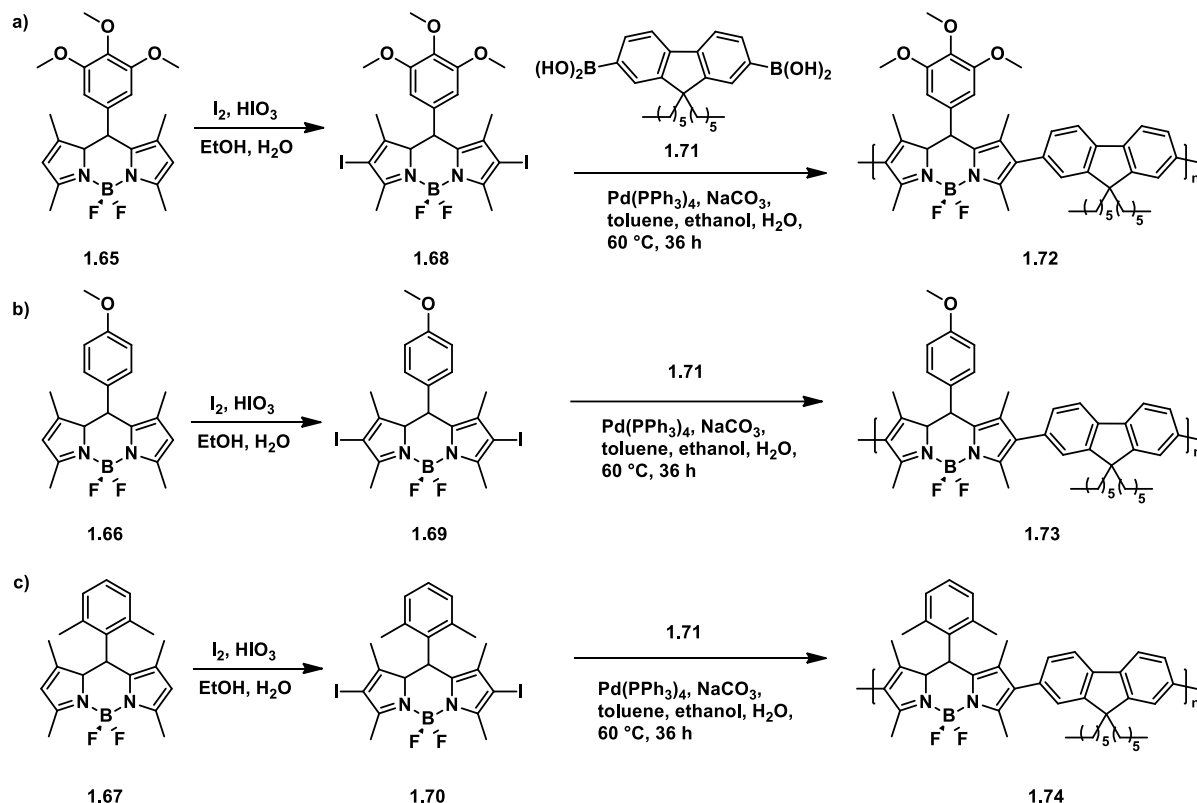
Another class of BF_2 dyes that have been extensively studied are those of chelating dipyrromethene ligands (e.g., **1.62**).⁴⁹ These molecules, known as boron dipyrromethenes (BODIPYs), benefit from tunable optical and chemical properties as well as high Φ_F . Recently, the first example of zwitterionic BODIPYs was described (**1.63** and **1.64**).⁵⁰ These asymmetric BODIPYs possessed large Stokes' shifts, intense emission, and were water soluble. Their absorption bands (in MeOH) were quite broad and ranged from 390–405 nm for compound

1.63 and 414–434 nm for compound **1.64**. Moreover, they displayed λ_{em} in EtOH at 461 nm with a Φ_F of 95% for **1.63**, and 506 nm with a Φ_F of 68% for **1.64**. Thanks to their solubility in water, their use as live cell imaging agents was demonstrated by subjecting both dyes to yeast cells and observing the specific staining of the cells in the granules of the yeast.



The Liu group synthesized copolymers of BODIPYs and fluorenes in order to take advantage of their interesting properties.⁵¹ The idea was to make three separate copolymers bearing fluorene units and BODIPY units; these copolymers would differ based on the BODIPY derivative used. Different functional groups on the BODIPYs would tune their spectroscopic properties, and thus the polymers would benefit from these differences. Synthesis began by the iodization of BODIPYs **1.65**, **1.66**, **1.67** by dissolving each BODIPY in an EtOH/water solution containing I₂ and HIO₃, stirred at 60 °C for 30 min. This yielded monomers **1.68**, **1.69**, **1.70** which were then copolymerized with fluorene **1.71** using palladium-catalyzed Suzuki polymerization to yield polymers **1.72**, **1.73**, **1.74** where both fluorenes and BODIPYs are found in the main chain. The spectroscopic properties of molecules **1.65**, **1.66**, **1.67** were studied, and it was found that they all had λ_{max} in CHCl₃ at approximately 500 nm, and emission at approximately 510 nm, with Φ_F ranging from 72% for compound **1.65** to 87% for compound **1.67**. Once iodine was installed, all compounds experienced a red-shift in the absorbance and emission spectra by 33–38 nm. The Φ_F decreased, now ranging from 6% for compound **1.69** to 9% for compound **1.70**; this was attributed to quenching by the heavy atom effect. Once the monomers were copolymerized with fluorene, their absorbance and emission spectra were further red-shifted by 14–22 nm for the absorbance spectra, and 37–39 nm for the emission spectra. The Φ_F also increased, ranging from 56% for **1.73** to 85% for **1.74**. This red-shift in the λ_{max} and λ_{em} for polymers **1.72**, **1.73**, **1.74** was attributed to the extended π -conjugation in the polymers. It was also observed that emission from the fluorene moiety in the backbone was no longer observed once it had been incorporated into the polymers; this was

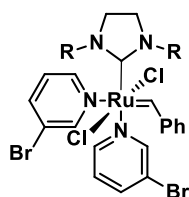
due to efficient photoinduced energy transfer from the fluorene moiety to the BODIPY moiety. Fluorescence quenching was observed for all polymers when titrated with fluoride or cyanide ions; this demonstrated their potential use in chemical and biological sensing applications.



Scheme 1.14. Synthesis of monomers **1.68–1.70** and polymers **1.72–1.74**.

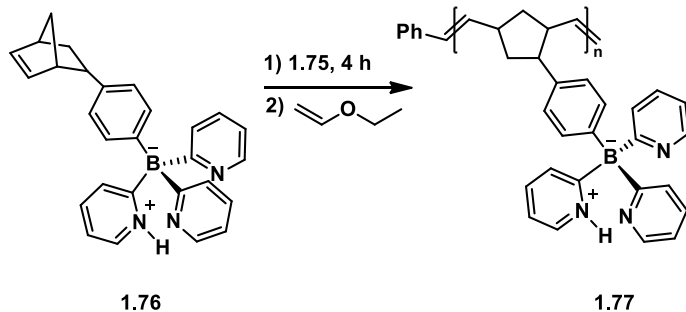
The Jäkle group incorporated boron-containing molecules **1.76** into polymers **1.77** and block copolymers **1.79** in order to study their potential metal complexation properties. Molecule **1.76** was chosen since this polydentate ligand has been previously studied for its potential metal complexation properties with various metals (e.g., Mg^{2+} , Fe^{2+} , Mn^{2+}).^{52–54} Synthesis of these polymers was achieved using ring-opening metathesis polymerization (ROMP) of the pendant norbornene group found in monomer **1.76** and the pendant oxabicycloheptene group on **1.78**. Monomer **1.77** was dissolved in CHCl_3 and the 3-bromo pyridine derivative of Grubbs' third generation catalyst (GIII, **1.75**) was added and the reaction was stirred for 1 h, yielding homo polymer **1.77**. Block copolymer **1.79** was synthesized by dissolving monomer **1.78** in CHCl_3 , adding GIII (**1.75**) and stirring for 1 h; then **1.77** was added and the reaction mixture was stirred

for an additional 4 h. The polymerization for both polymers was terminated using ethyl vinyl ether. Homopolymer **1.77** had \bar{D} of 1.29, while block copolymer **1.79** had \bar{D} of 1.16, which are within the range of living / step-growth polymerizations.⁵⁵ Monomer **1.76** was tested for its metal ion complexation properties. This was done by treating **1.76** with $\text{Cu}(\text{ClO}_4)_2 \cdot 6\text{H}_2\text{O}$ or FeCl_2 , in the presence of Et_3N . Once complexation was done, the UV-vis absorption spectra of the complexes were studied in CH_2Cl_2 and it was found that for the Fe^{2+} complexes, λ_{max} were found at 425 and 480 nm, whereas for complexes with Cu^{2+} , the λ_{max} was at 600 nm. Successful complexation of metals to the polydentate ligands led the group to test whether or not aggregates of block copolymers **1.79** would also form complexes with these metal ions which would lead to crosslinking of the polymers. First, aggregates of the blocks were made by taking advantage of their amphiphilic properties, where the borate containing block is soluble in EtOH, but the oxabicyclo dicarboxylate portion is not. Thus, a solution of these polymers in DMF was placed in a dialysis tube and allowed to stir in EtOH for 3 h; dynamic light scattering (DLS) of this solution concluded that the block copolymers had formed aggregates in solution. FeCl_2 was then added to the aggregate solution followed by addition of Et_3N . It was observed that a red precipitate began to form over time. Energy-dispersive X-ray (EDX) spectroscopy measurements proved that Fe(II) had successfully complexed with the aggregate molecules, and thus caused the polymers to crosslink and precipitate out of solution. Furthermore, metal exchange reactions could also be achieved by first complexing homo polymer **1.77** with $\text{Cu}(\text{ClO}_4)_2 \cdot 6\text{H}_2\text{O}$ in EtOH, yielding a green precipitate, and then adding FeCl_2 . Over a span of 2 days the colour of the precipitate began to change to beige; and EDX showed successful metal ion exchange. The complexation of these metal ions resulted in metal-rich cross-linked polymer networks.

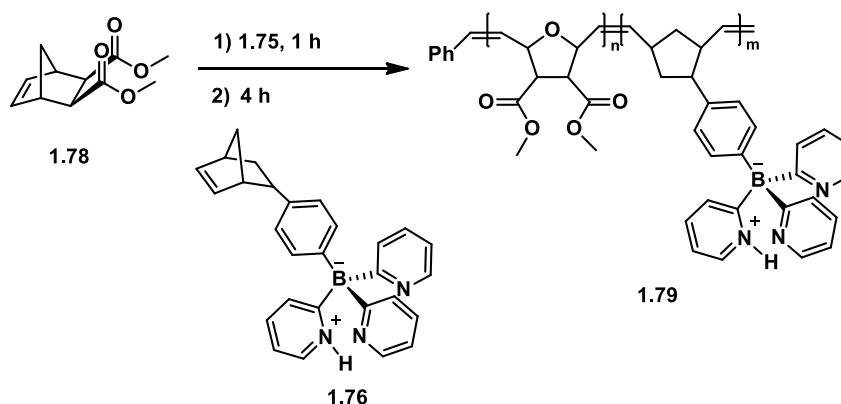


R = 2,4,6-trimethylphenyl

1.75



Scheme 1.15. ROMP of monomer **1.76** to yield homopolymer **1.77**.



Scheme 1.16. ROMP of monomer **1.78** and monomer **1.76** to yield block copolymer **1.79**.

1.5 Scope of Thesis

This thesis will focus on the synthesis of various novel asymmetric and symmetric 3-cyanoformazanate BF_2 complexes and the incorporation of these molecules into homo, block, and random copolymers by the use of ROMP. The interest in these studies lies in the observation that BF_2 formazanate complexes have low energy absorption/emission, which is advantageous in various applications such as cell imaging, as well as the fact that polymers are easier to solution process which is important in applications that would require formation of films, such as in OLEDs. These complexes also have similar properties to that of the widely researched BODIPYs, yet their synthesis is easier and yields of these complexes are much higher making them cost effective. Thus, my goal was to make fluorescent BF_2 cyanoformazanate containing polymers that can be used as cell imaging agents, as functional thin films, and to track block copolymer self-assembly.

Chapter 2 will focus on the synthesis of an asymmetric 3-cyanoformazan along with its corresponding BF₂ complex. Synthesis of other 3-cyanoformazanate BF₂ complexes will also be outlined, and a detailed comparison of their spectroscopic and electrochemical properties described. Furthermore, X-ray crystallographic studies of two specific BF₂ complexes will also be discussed.

Chapter 3 will outline the use of ROMP in order to synthesize various polymers that contain 3-cyanoformazanate BF₂ complexes. Block and random copolymer synthesis for these 3-cyanoformazanate BF₂ complexes with a second organic monomer will also be described. Spectroscopic, thermal and electrochemical properties of the polymers will be studied in detail.

Chapter 4 will summarize the work in this thesis as well as describe future work involving the synthesis of new BF₂ containing block copolymers that can self-assemble into fluorescent micelles.

1.6 References

1. Muller, C. D.; Falcou, A.; Reckefuss, N.; Rojahn, M.; Wiederhirn, V.; Rudati, P.; Frohne, H.; Nuyken, O.; Becker, H.; Meerholz, K., *Nature* **2003**, *421*, 829–833.
2. Swager, T. M., *Acc. Chem. Res.* **1998**, *31*, 201–207.
3. Zhu, Y.; Alam, M. M.; Jenekhe, S. A., *Macromolecules* **2003**, *36*, 8958–8968.
4. Zhan, X.; Liu, Y.; Wu, X.; Wang, S.; Zhu, D., *Macromolecules* **2002**, *35*, 2529–2537.
5. Tsai, Y.; Lai, C.; Chien, R.; Hong, J.; Yeh, A., *J. Polym. Sci., Part A: Polym. Chem.* **2012**, *50*, 237–249.
6. Li, C.; Li, Z.; Liu, J.; Zhao, X.; Yang, H.; Yang, S., *Polymer* **2010**, *51*, 3851–3858.
7. Agrawal, A. K.; Jenekhe, S. A., *Macromolecules* **1993**, *26*, 895–905.
8. Tong, H.; Wang, L.; Jing, X.; Wang, F., *Macromolecules* **2002**, *35*, 7169–7171.

9. Kalogianni, A.; Pefkianakis, E.; Stefopoulos, A.; Bokias, G.; Kallitsis, J. K., *J. Polym. Sci., Part B: Polym. Phys.* **2010**, *48*, 2078–2083.
10. Vohra, V.; Suresh, S.; Ponrathnam, S.; Rajan, C. R.; Kajzar, F., *J. Polym. Sci., Part A: Polym. Chem.* **2000**, *38*, 962–971.
11. Cai, H.; He, X.-H.; Zheng, D.-Y.; Qiu, J.; Li, Z.-C.; Li, F.-M., *J. Polym. Sci., Part A: Polym. Chem.* **1996**, *34*, 1245–1250.
12. He, G.; Yan, N.; Cui, H.; Liu, T.; Ding, L.; Fang, Y., *Macromolecules* **2011**, *44*, 7096–7099.
13. Feng, L.; Deng, Y.; Wang, X.; Liu, M., *Sens Actuators B Chem.* **2017**, *245*, 441–447.
14. Thivaios, I.; Kakogianni, S.; Bokias, G., *Macromolecules* **2016**, *49*, 3526–3534.
15. Zhang, H.; Zhou, N.; Zhu, X.; Chen, X.; Zhang, Z.; Zhang, W.; Zhu, J.; Hu, Z.; Zhu, X., *Macromol. Rapid Commun.* **2012**, *33*, 1845–1851.
16. Xue, X.; Zhu, J.; Zhang, Z.; Zhou, N.; Tu, Y.; Zhu, X., *Macromolecules* **2010**, *43*, 2704–2712.
17. Damaceanu, M.-D.; Rusu, R.-D.; Nicolescu, A.; Bruma, M., *J. Polym. Sci., Part A: Polym. Chem.* **2011**, *49*, 893–906.
18. Bouffard, J.; Swager, T. M., *Macromolecules* **2008**, *41*, 5559–5562.
19. Williams, D. F.; Schadt, M., *J. Chem. Phys.* **1970**, *53*, 3480–3487.
20. Raghunath, P.; Reddy, M. A.; Gouri, C.; Bhanuprakash, K.; Rao, V. J., *J. Phys. Chem. A* **2006**, *110*, 1152–1162.
21. Li, Y.; Kim, T.-H.; Zhao, Q.; Kim, E.-K.; Han, S.-H.; Kim, Y.-H.; Jang, J.; Kwon, S.-K., *J. Polym. Sci., Part A: Polym. Chem.* **2008**, *46*, 5115–5122.
22. Valentini, L.; Bagnis, D.; Marrocchi, A.; Seri, M.; Taticchi, A.; Kenny, J. M., *Chem. Mater.* **2008**, *20*, 32–34.

23. Dickert, F. L.; Tortschanoff, M.; Bulst, W. E.; Fischerauer, G., *Anal. Chem.* **1999**, *71*, 4559–4563.
24. Ji, H.-F.; Dabestani, R.; Brown, G. M., *J. Am. Chem. Soc.* **2000**, *122*, 9306–9307.
25. Zrida, H.; Hriz, K.; Jaballah, N.; Hrichi, H.; Kreher, D.; Majdoub, M., *J. Mater. Sci.* **2016**, *51*, 680–693.
26. Hrichi, H.; Hriz, K.; Jaballah, N.; Chaâbane, R. B.; Simonetti, O.; Majdoub, M., *J. Polym. Res.* **2013**, *20*, 241.
27. Gondek, E.; Kityk, I. V.; Danel, A., *Mater. Chem. Phys* **2008**, *112*, 301–304.
28. Huang, Y. F.; Shiu, Y. J.; Hsu, J. H.; Lin, S. H.; Su, A. C.; Peng, K. Y.; Chen, S. A.; Fann, W. S., *J. Phys. Chem. C* **2007**, *111*, 5533–5540.
29. Scherf, U.; List, E. J. W., *Adv. Mater.* **2002**, *14*, 477–487.
30. Leclerc, M., *J. Polym. Sci., Part A: Polym. Chem.* **2001**, *39*, 2867–2873.
31. Wong, W.-Y., *Coord. Chem. Rev.* **2005**, *249*, 971–997.
32. Zhou, G.; Qian, G.; Ma, L.; Cheng, Y.; Xie, Z.; Wang, L.; Jing, X.; Wang, F., *Macromolecules* **2005**, *38*, 5416–5424.
33. Zhou, X.-H.; Yan, J.-C.; Pei, J., *Macromolecules* **2004**, *37*, 7078–7080.
34. Ho, H. A.; Leclerc, M., *J. Am. Chem. Soc.* **2003**, *125*, 4412–4413.
35. Chuang, C.-Y.; Shih, P.-I.; Chien, C.-H.; Wu, F.-I.; Shu, C.-F., *Macromolecules* **2007**, *40*, 247–252.
36. Gorman, A.; Killoran, J.; O'Shea, C.; Kenna, T.; Gallagher, W. M.; O'Shea, D. F., *J. Am. Chem. Soc.* **2004**, *126*, 10619–10631.
37. Frath, D.; Massue, J.; Ulrich, G.; Ziessel, R., *Angew. Chem. Int. Ed.* **2014**, *53*, 2290–2310.

38. Cheng, F.; Jakle, F., *Chem. Commun.* **2010**, *46*, 3717–3719.
39. Fischer, G. M.; Daltrozzo, E.; Zumbusch, A., *Angew. Chem. Int. Ed.* **2011**, *50*, 1406–1409.
40. Firinci, E.; Bates, J. I.; Riddlestone, I. M.; Phillips, N.; Aldridge, S., *Chem. Commun.* **2013**, *49*, 1509–1511.
41. Lu, J.-S.; Ko, S.-B.; Walters, N. R.; Kang, Y.; Sauriol, F.; Wang, S., *Angew. Chem. Int. Ed.* **2013**, *52*, 4544–4548.
42. Frath, D.; Poirel, A.; Ulrich, G.; De Nicola, A.; Ziessel, R., *Chem. Commun.* **2013**, *49*, 4908–4910.
43. Yang, Y.; Hughes, R. P.; Aprahamian, I., *J. Am. Chem. Soc.* **2012**, *134*, 15221–15224.
44. Yang, Y.; Hughes, R. P.; Aprahamian, I., *J. Am. Chem. Soc.* **2014**, *136*, 13190–13193.
45. Li, W.; Lin, W.; Wang, J.; Guan, X., *Org. Lett.* **2013**, *15*, 1768–1771.
46. Lin, W.; Long, L.; Yuan, L.; Cao, Z.; Chen, B.; Tan, W., *Org. Lett.* **2008**, *10*, 5577–5580.
47. Mei, J.; Hong, Y.; Lam, J. W. Y.; Qin, A.; Tang, Y.; Tang, B. Z., *Adv. Mater.* **2014**, *26*, 5429–5479.
48. Liao, C.-W.; Rao M, R.; Sun, S.-S., *Chem. Commun.* **2015**, *51*, 2656–2659.
49. Loudet, A.; Burgess, K., *Chem. Rev.* **2007**, *107*, 4891–4932.
50. Sekhar, A. R.; Sariki, S. K.; Reddy, R. V. R.; Bisai, A.; Sahu, P. K.; Tomar, R. S.; Sankar, J., *Chem. Commun.* **2017**, *53*, 1096–1099.
51. Meng, G.; Velayudham, S.; Smith, A.; Luck, R.; Liu, H., *Macromolecules* **2009**, *42*, 1995–2001.
52. Pawar, G. M.; Lalancette, R. A.; Bonder, E. M.; Sheridan, J. B.; Jäkle, F., *Macromolecules* **2015**, *48*, 6508–6515.

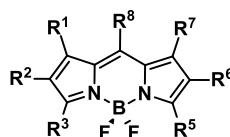
53. Cui, C.; Lalancette, R. A.; Jakle, F., *Chem. Commun.* **2012**, 48, 6930–6932.
54. Cui, C.; Shipman, P. R.; Lalancette, R. A.; Jäkle, F., *Inorg. Chem.* **2013**, 52, 9440–9448.
55. Slugovc, C., *Macromol. Rapid Commun.* **2004**, 25, 1283–1297.

Chapter 2

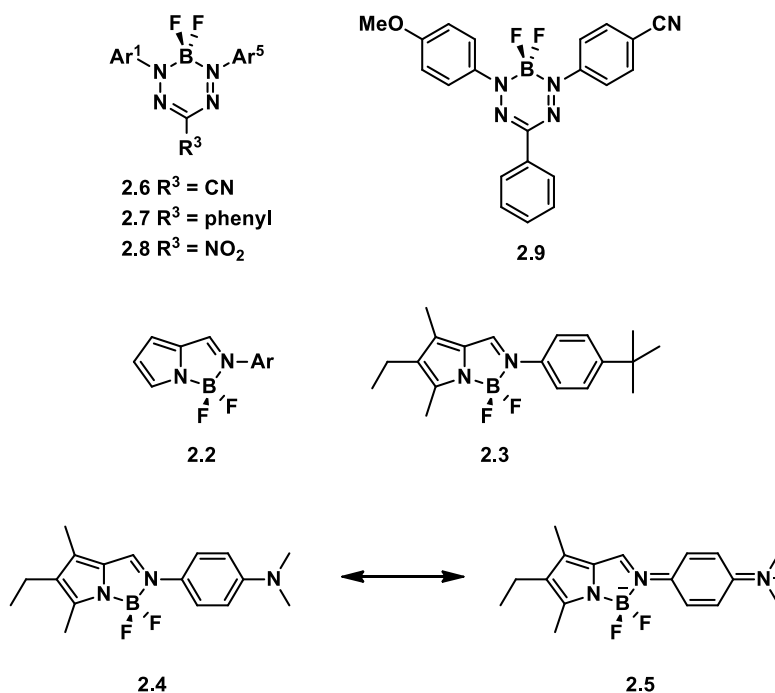
2 Asymmetric 3-Cyanoformazanate BF₂ Complexes

2.1 Introduction

Extensive research has been done on BF₂ containing complexes due to their interesting properties which include high molar extinction coefficients, high emission quantum yields, and redox activity.¹⁻³ One specific family of BF₂ molecules that has garnered a lot of attention are BODIPYs (**2.1**).⁴ Although BODIPYs possess a lot of the interesting properties described, they generally suffer from small Stokes' shifts which results in low Φ_F in concentrated solutions and in the solid state due to self-quenching. One way to increase the Stokes' shifts, is to break the *pseudo-C*₂-symmetry often found in symmetrical BODIPYs. Breaking the symmetry allows for a large distribution of charge upon excitation of the molecule thereby making the ground and excited states more energetically different and thus increasing Stokes' shifts.⁵ In an attempt to address this issue, boron complexes of iminopyrrolide ligands (BOIMPYs) were synthesized (e.g., **2.2**) as an asymmetric mimic to BODIPYs.⁶ BOIMPYs retained the interesting spectroscopic properties found in BODIPYs, such as high absorption coefficients and fluorescence, but possessed higher Stokes' shifts. It was also found that the de-excitation mechanism for these complexes relied on the substituents attached on the *para* position of Ar. For example, addition of a dimethylamino substituent in the *para* position (**2.4**) allowed the molecule to possess quinoid type resonance (**2.5**) that promoted charge separated character resulting in large Stokes' shifts (192 nm) and also solvatochromism (Scheme 2.1). Solvatochromism supported the idea that by obtaining such charge separated character, this complex had begun to develop charge transfer character. Conversely, having a *tert*-butyl group in the *para* position (**2.3**) also resulted in large Stokes' shifts (105 nm), but its emission was not solvent dependent, and thus relaxation most likely occurred from locally excited states and charge transfer.



2.1



Scheme 2.1. Benzoid (**2.4**) to quinoid (**2.5**) resonance structures.

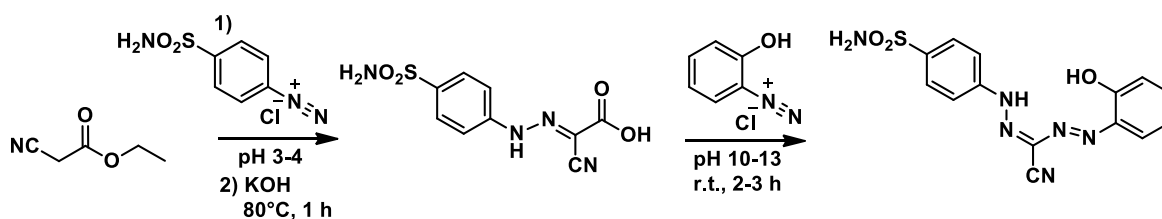
Another class of BF_2 dyes that has shown potential as alternatives to BODIPYs are those of chelating nitrogen ligands from a formazanate backbone (**2.6–2.8**). These BF_2 complexes exhibit tunable absorption, emission and electrochemical properties, as well as good Φ_{F} and high yielding syntheses.^{7,8} Triaryl BF_2 formazanate complexes (**2.7**) possess the largest Stokes' shifts (>100 nm) out of the three. Breaking the symmetry in these BF_2 complexes (e.g., **2.9**) has been shown to improve their Φ_{F} due to the push-pull electronics of the varying substituents in the Ar^1 and Ar^5 positions. Conversely, BF_2 complexes of 3-cyanoformazans (**2.6**) possess the highest Φ_{F} in comparison to those with phenyl or nitro groups at the R^3 position (**2.7**, **2.8**).⁸ These properties paved the way to pursue asymmetric 3-cyanoformazans, where the corresponding BF_2 complexes would benefit from an increase in emission intensity due to a combination of the presence of a cyano group in the R^3 position, and asymmetry. Moreover, synthesis of an asymmetric BF_2 complex would allow for functionalization of one of the *N*-aryl substituents with a polymerizable group. This would make it possible to synthesize polymers bearing BF_2 formazanate units appended to the polymer backbone.

This chapter describes the synthesis and characterization of various asymmetrically substituted BF_2 formazanate complexes. It also outlines the synthesis of the first reported asymmetric 3-cyanoformazan and its corresponding BF_2 complex. The use of CuAAC chemistry as a means of attaching a polymerizable group to one of the *N*-aryl substituents in the corresponding BF_2 complex is also described. The effect on the spectroscopic and electrochemical properties upon adding a triazole ring or coupling an alkyne group to one of the *N*-aryl substituents in the formazanate backbone was also investigated.

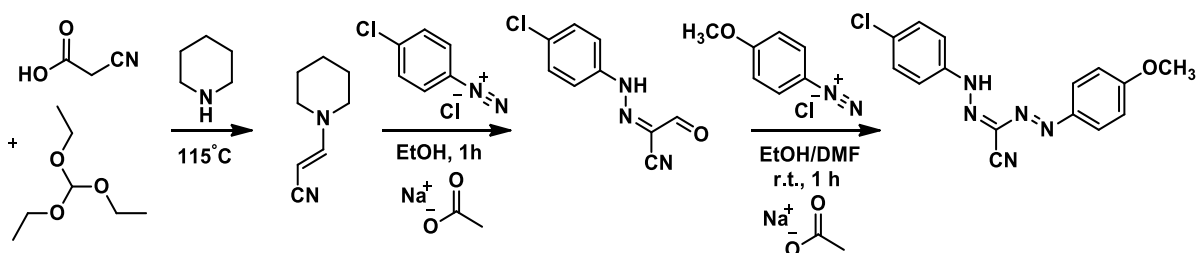
2.2 Results and Discussion

2.2.1 Synthesis of Asymmetric 3-Cyanoformazans

Two different methods were used in order to synthesize asymmetric 3-cyanoformazans (Scheme 2.2 and 2.3).^{9,10} Both of these methods were unsuccessful as yields and purification of the target formazans were low (Table 1). During optimization of both methods, it was observed that when the diazoniums of *p*-anisidine and *p*-toluidine were used in order to make either the hydrazone or the asymmetric formazan, a scrambling of aryl groups occurred where the symmetric formazans of the diazoniums used were observed along with the asymmetric formazan intended.



Scheme 2.2. Stolarski synthesis of asymmetric 3-cyanoformazans.⁹



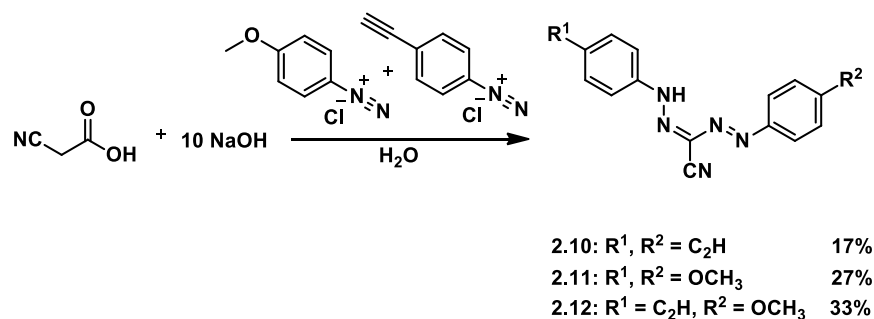
Scheme 2.3. Elnagdi synthesis for asymmetric 3-cyanoformazans.¹⁰

Table 2.1. Experimental yields for asymmetric syntheses.

Route	R ¹	R ²	Yield (%) ^b
Stolarski	H	Br	29
	H	OH	23*
Elnagdi ^a	Br	OCH ₃	65*
	Br	CH ₃	9*
	Cl	-	-
	OCH ₃	CH ₃	26*

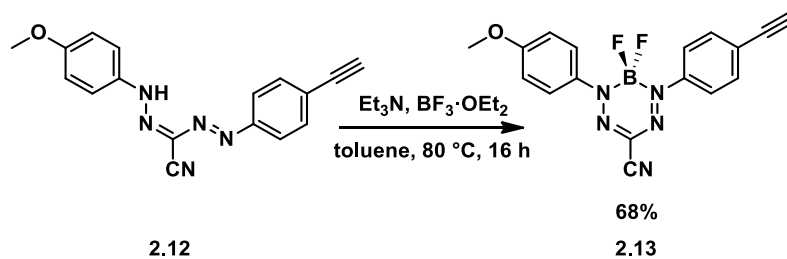
^aYield stated does not include the yield for the synthesis of enamionitrile (37%). ^bAsterisk denotes crude yield (due to failed purification).

After this discovery, the need to find a route that involved fewer steps and produced asymmetric formazans in a higher yield was necessary. Therefore, a different method for obtaining asymmetric 3-cyanoformazan **2.12** was employed (Scheme 2.4), whereby the asymmetric formazan desired was separated from the two corresponding symmetric formazans *via* column chromatography. This route has been previously reported for the synthesis of symmetric 3-cyanoformazans,¹¹ and although its use for asymmetric formazans is not elegant, it involves only one step and produces the same yields as the time-consuming methods mentioned above.

**Scheme 2.4.** Synthesis of asymmetric 3-cyanoformazan **2.12**.

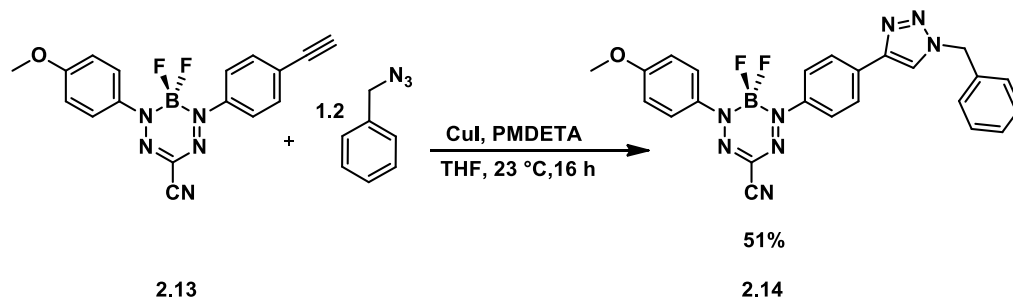
2.2.2 Synthesis of BF₂ 3-Cyanoformazanate Complexes

Formazan **2.12** was dissolved in toluene and excess Et₃N and BF₃•OEt₂ were added under an inert atmosphere. The solution was stirred overnight at 80 °C (Scheme 2.5). After aqueous work-up and column chromatography, ¹H NMR spectroscopy revealed the disappearance of the characteristic NH peak of the formazan seen at 12.5 ppm upon insertion of the BF₂ moiety. The introduction of the BF₂ moiety was also verified by a distinctive 1:1:1:1 quartet and a 1:2:1 triplet in the ¹⁹F NMR and ¹¹B NMR spectra, respectively.



Scheme 2.5. Synthesis of asymmetric BF_2 formazanate complex **2.13**.

In order to explore the possibility of using CuAAC chemistry to attach polymerizable groups to BF_2 complex **2.13**, benzyl azide was used to test the reaction. Copper (I) coordinated by PMDETA was the catalyst of choice. Benzyl azide and BF_2 complex **2.13** were added to the catalyst solution in dry and degassed THF and stirred at 23 °C for 16 h (Scheme 2.6). ^1H NMR spectroscopy (Figure 2.1) revealed the disappearance of the $\equiv\text{CH}$ peak at 3.28 ppm (triangle) and the appearance of the $=\text{CH}$ peak of the triazole ring at 7.76 ppm (circle). Further confirmation for the successful CuAAC reaction was evident when comparing the IR spectra of BF_2 complex **2.13** and benzyl-substituted BF_2 complex **2.14**. The IR spectrum for BF_2 complex **2.13** reveals the $\equiv\text{CH}$ stretch at 3282 cm^{-1} , while the IR spectrum of benzyl-substituted BF_2 complex **2.14** does not show the $\equiv\text{CH}$ stretch or the strong R-N_3 stretch of an azide which usually appears around $2170\text{--}2180\text{ cm}^{-1}$.¹² The unique 1:1:1:1 quartet in the ^{19}F NMR spectrum and 1:2:1 triplet in the ^{11}B NMR spectrum along with the persistent purple colour of the compound indicated the tolerance of the BF_2 moiety to the conditions for the CuAAC reaction. The synthesis of this compound also allowed for the study of the effects a triazole ring has on the spectroscopic and electrochemical properties of BF_2 complexes.



Scheme 2.6. CuAAC reaction for the synthesis of benzyl-substituted BF_2 complex **2.14**.

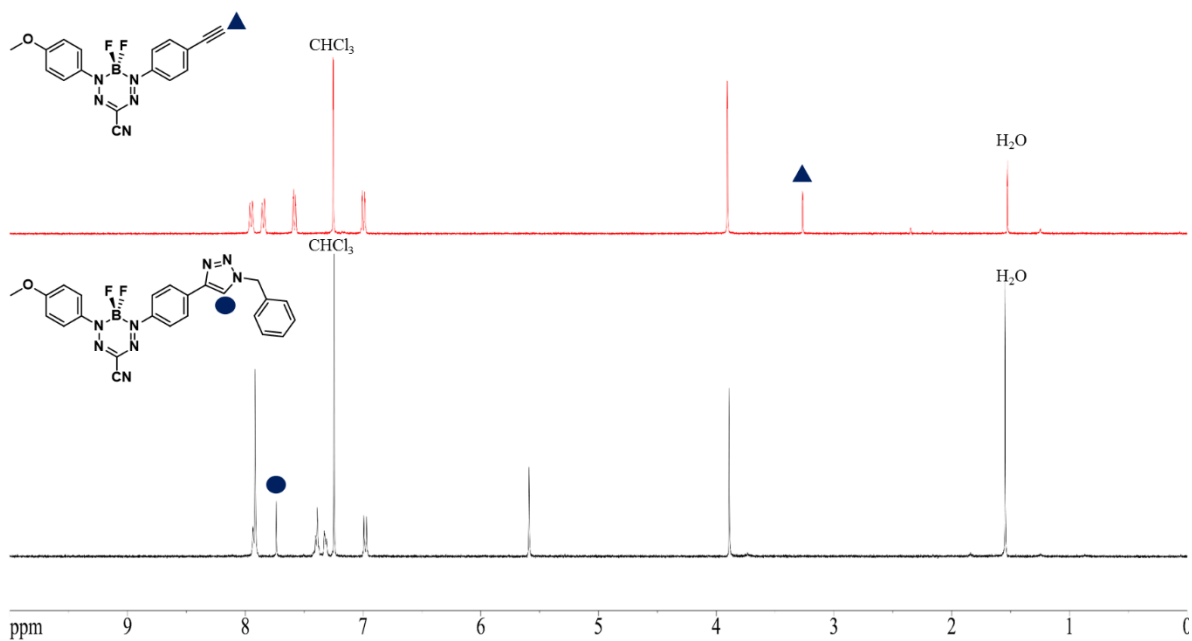
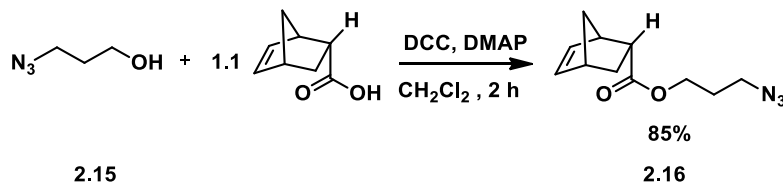


Figure 2.1. Overlay of ^1H NMR spectra of compounds **2.13** (red) and **2.14** (black) in CDCl_3 . The triangle represents the $\equiv\text{CH}$ proton and the circle represents $=\text{CH}$ peak of the triazole ring.

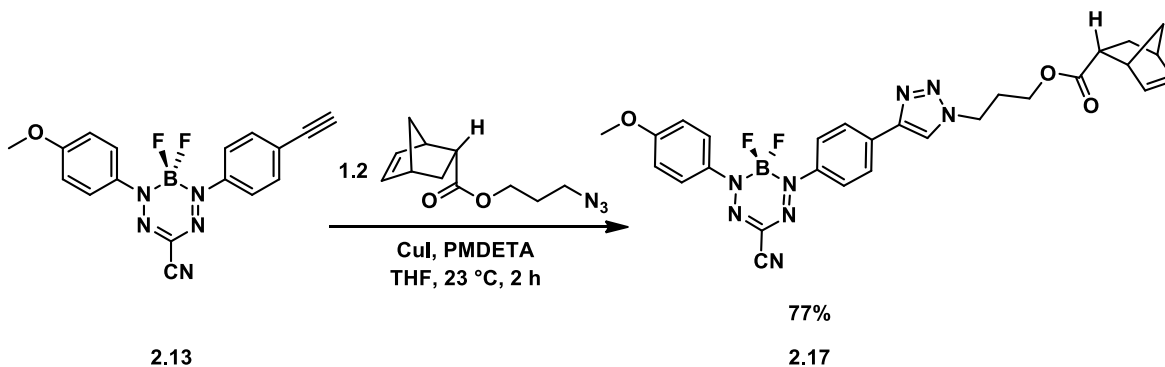
In pursuit of side-chain BF_2 formazanate polymers, azide-substituted norbornene **2.16** was synthesized (Scheme 2.7). This compound contains a polymerizable norbornene suitable for ROMP, along with an azide group that could be useful for clicking onto BF_2 complex **2.13**. Previously reported 3-azido-1-propanol **2.15**¹³ was added to a solution of 5-norbornene-*endo*-2-carboxylic acid, DCC, DMAP, and dry CH_2Cl_2 and stirred at 23 °C for 2 h. The reagent 5-norbornene-*endo*-2-carboxylic acid was separated from the *endo/exo* mixture purchased by reacting it with KI and I_2 in a basic solution, which resulted in the iodolactone formation of the *endo* isomer. The iodolactone was then isolated through an aqueous workup, and converted back to the *endo* isomer by stirring it in a solution of AcOH and zinc powder to afford pure 5-norbornene-*endo*-2-carboxylic acid.¹⁴

^1H NMR spectroscopy revealed the success of the coupling reaction, and the alkene protons corresponding to the *endo* isomer were found at 6.22 ppm and 5.93 ppm. The IR spectrum verified the presence of the azide functionality due to the strong R-N_3 stretch at 2095 cm^{-1} .



Scheme 2.7. DCC coupling for the synthesis of azide-substituted norbornene **2.16**.

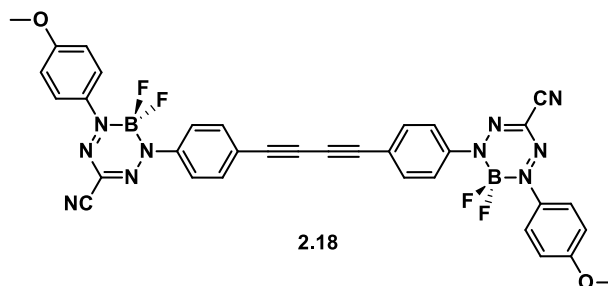
Azide-alkyne cycloaddition chemistry was then employed as a means of synthesizing a BF_2 containing monomer for future polymerization. Again, copper(I) coordinated by PMDETA was the catalyst of choice. BF_2 complex **2.13** was added to a solution of azide-substituted norbornene **2.16**, copper catalyst, and dry and degassed THF and stirred at 23 °C for 2 h (Scheme 2.8). ^1H NMR spectroscopy revealed the disappearance of the $\equiv\text{CH}$ peak at 3.28 ppm and the appearance of the $=\text{CH}$ peak of the triazole ring at 7.90 ppm. The IR spectrum of monomer **2.17** also verified the absence of $\equiv\text{CH}$ stretch at 3282 cm^{-1} from BF_2 complex **2.13**. ^{19}F and ^{11}B NMR spectroscopy revealed the unique 1:1:1:1 quartet and 1:2:1 triplet respectively, again verifying the stability of the BF_2 moiety under the conditions employed.



Scheme 2.8. Synthesis of monomer **2.17** by CuAAC.

During optimization experiments for the synthesis of monomer **2.17**, it was observed that when the reaction was left overnight, additional products formed. These products were isolated by column chromatography. One of the fractions was isolated in 7 % yield and was blue in colour. Its ^{19}F NMR and ^{11}B NMR spectra revealed the presence of a BF_2 moiety. Crystals of this compound (**2.18**) suitable for X-ray diffraction studies were grown (see below), and it was discovered that the compound was a dimer of BF_2 complex **2.13**. This structure was confirmed by ^1H NMR spectroscopy and mass spectrometry. Literature precedence confirmed that Cu(II) can catalyze the oxidative dimerization of alkynes,¹⁵⁻¹⁹ supporting the hypothesis that this side

product forms as a result of the gradual oxidation of Cu(I) in the reaction mixture to yield catalytic Cu(II).



2.2.3 X-ray Crystallography

Single crystals of BF₂ complex **2.13** were grown by slow diffusion of hexanes into a saturated solution of BF₂ complex **2.13** in slow evaporating CH₂Cl₂. The crystal displayed disorder at the alkyne and methoxy substituents as a result of a two-fold rotation axis. The solid-state structure revealed the boron centre to be found in a distorted tetrahedral geometry when looking at angles (°): F1'–B1–F1 112.01(15), F1'–B1–N1 108.75(5), F1'–B1–N1' 110.42(5), N1–B1–N1' 106.34(13). Furthermore, the structure is relatively planar with a torsion angle of 7.2° between the N1–N2–C1–N2–N1 plane of the formazanate backbone, and the C3–C8 plane of the *N*-aryl substituents.

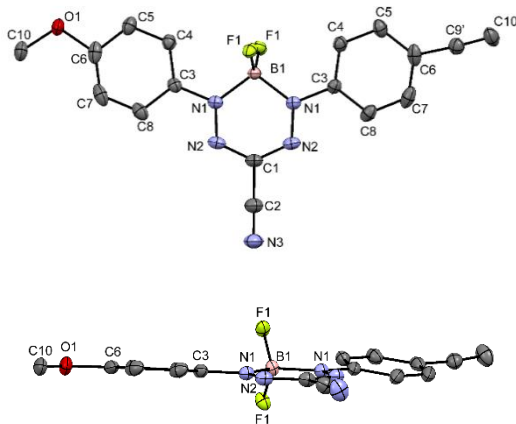


Figure 2.2. Solid-state structure of BF₂ complex **2.13** (top and side views). Hydrogen atoms have been omitted for clarity. Thermal displacement ellipsoids are shown at 50% probability.

Table 2.2. Selected bond lengths (Å) and angles (degrees) for **2.13** BF₂ complex.

2.13	
B1-F1	1.3732(14)
B1-N1	1.5759(15)
N1-N2	1.3023(15)
N2-C1	1.3351(13)
N3-C2	1.146(2)
C9'-C10'	1.191(7)
O1-C10	1.418(5)
N1-N2-C1	117.24(11)
N2 ¹ -C1-N2	130.03(16)
N2-C1-C2	114.99(8)
C10'-C9'-C6	174.8(6)
C10-O1-C6	112.7(3)
F1-B1-N1-N2	118.09(12)
N2-N1-C3-C8	6.26(16)
C7-C6-O1-C10	-1.3(5)
C5-C6-O1-C10	178.2(3)

Single crystals of dimer **2.18** were grown by slow evaporation of hexanes into a saturated solution of dimer **2.18** in benzene. The solid-state structure revealed the planar confirmation of this molecule with a torsion angle of 9.7° between the N1–N2–C1–N4–N3 plane of the formazanate backbone and the C10–C15 plane, and a torsion angle of 0.07° between the C10–C15 plane and the C10'–C15' plane. The boron centre is also found in a distorted tetrahedron geometry when looking at angles (°): F1–B1–F2 112.59(11), F1–B1–N3 111.12(11), F2–B1–N1 109.58(10), N3–B1–N1 106.52(9). The delocalized nature of the formazanate backbone is apparent when looking at the bond lengths (Å): N1–N2 1.3007(14), N3–N4 1.3066(14), N2–C1 1.3409(16), and N4–C1 1.3354(14), since these bond lengths are in between those expected for single and double bonds of the same atoms.²⁰ The torsion angle between the N1–N2–C1–N4–N3 plane of the formazanate backbone and the C3–C8 plane is 17.1°.

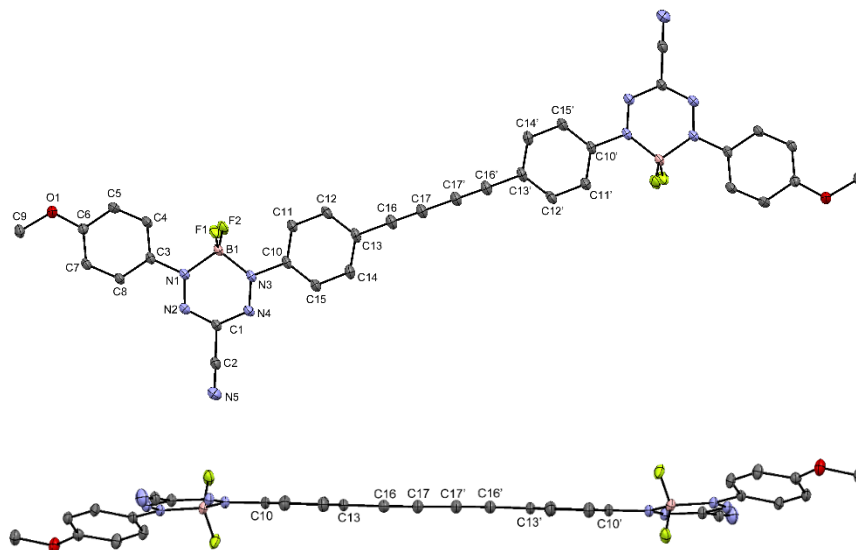


Figure 2.3. Solid-state structure of dimer **2.18** (top and side views). Hydrogen atoms have been omitted for clarity. Thermal displacement ellipsoids are shown at 50% probability.

Table 2.3. Selected bond lengths (Å) and angles (degrees) for **2.18** BF₂ complex.

2.18	
B1-F1	1.3671(17)
B1-F2	1.3736(15)
B1-N3	1.5648(18)
B1-N1	1.5793(16)
N5-C2	1.1453(16)
O1-C9	1.4344(15)
C16-C17	1.2063(16)
C17-C17 ¹	1.369(2)
N1-N2-C1	117.24(9)
N3-N4-C1	117.01(10)
N4-C1-N2	129.89(11)
N2-C1-C2	114.68(10)
C17-C16-C13	178.73(14)
C16-C17-C17 ¹	179.48(19)
N4-N3-C10-C15	5.74(16)
N2-N1-C3-C8	16.06(16)
C9-O1-C6-C5	-175.67(11)

2.2.4 Absorption/Emission Properties of BF₂ 3-Cyanoformazanate Complexes

The spectroscopic properties of the BF₂ formazanate complexes that were synthesized are summarized in Table 2.4. Figures 2.4a and 2.4b display the UV-vis absorption and emission spectra for selected compounds.

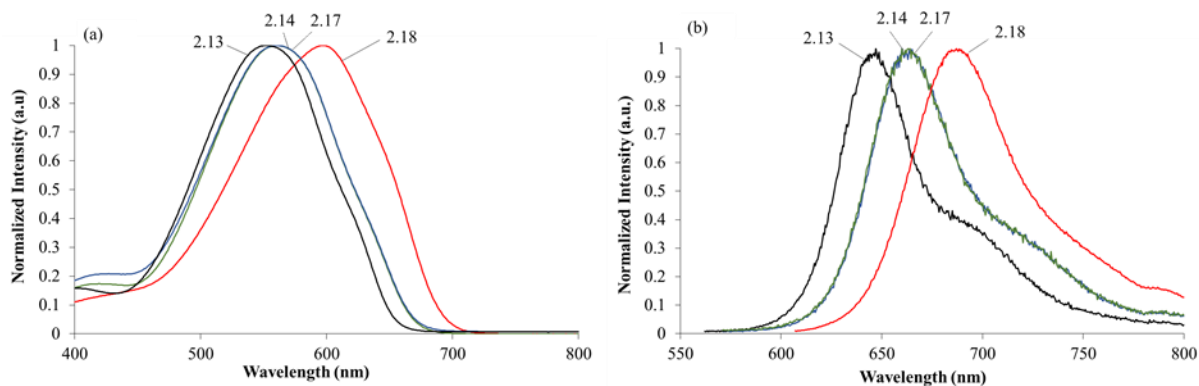


Figure 2.4. Normalized absorption (a) and emission (b) spectra for BF₂ complex **2.13** (black), benzyl-substituted BF₂ complex **2.14** (blue), monomer **2.17** (green), and dimer **2.18** (red) recorded in CH₂Cl₂.

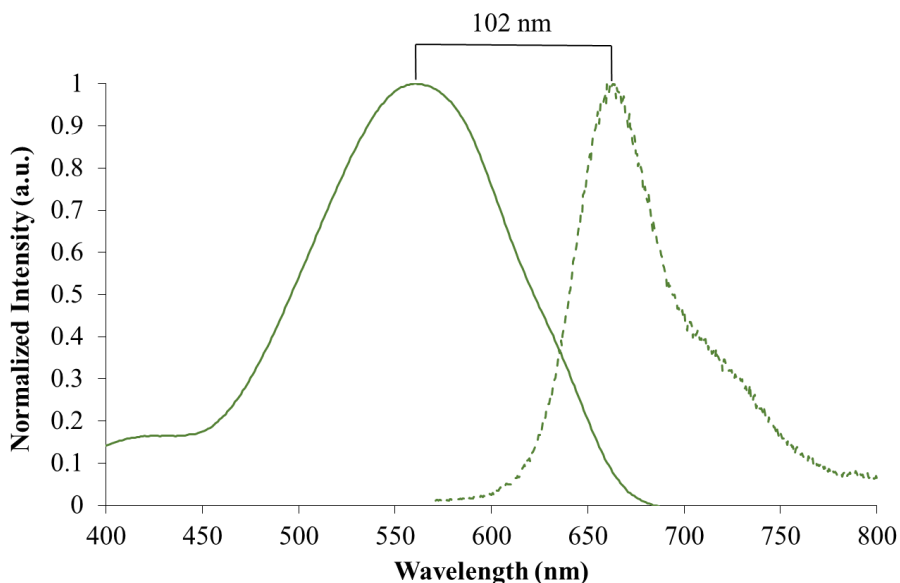


Figure 2.5. Normalized absorption (solid line) and emission (dashed line) spectra for monomer **2.17** recorded in CH₂Cl₂.

Table 2.4. Spectroscopic properties of BF₂ complex **2.13**, benzyl-substituted BF₂ complex **2.14**, monomer **2.17**, and dimer **2.18**.

	Solvent	λ_{\max} (nm)	ϵ (M ⁻¹ cm ⁻¹)	λ_{em} (nm)	Φ_{F} (%) ^a	ν_{ST} (nm)	ν_{ST} (cm ⁻¹)
2.13	CH ₂ Cl ₂	552	30,400	647	30	95	2660
	THF	550	32,500	650	27	100	2797
	Toluene	569	26,800	647	36	78	2119
2.14	CH ₂ Cl ₂	560	31,000	660	30	100	2706
	THF	560	33,900	671	25	111	2954
	Toluene	579	37,400	661	37	82	2143
2.17	CH ₂ Cl ₂	561	35,300	663	29	102	2742
	THF	560	23,100	668	20	108	2887
	Toluene	578	30,100	661	33	83	2172
2.18	CH ₂ Cl ₂	597	78,500	687	<1	90	2194
	THF	592	77,400	685	<1	93	2293
	Toluene	605	62,500	688	<1	83	1994

^aQuantum yields were measured according to published protocol using ruthenium tris(bipyridine) hexafluorophosphate as a relative standard^{21,22} and corrected for wavelength-dependent detector sensitivity (Figure A2.21). Due to error associated with the integration of the fluorescence spectra, we estimate that the quantum yields determined for dimer **2.18** are less than 1%.

These results reveal that, upon introduction of a triazole ring, the maximum absorption (λ_{\max}) and emission (λ_{em}) associated with the BF₂ formazanates red-shift by approximately 10 nm when comparing BF₂ complex **2.13** with benzyl-substituted BF₂ complex **2.14** and monomer **2.17**. This is likely a result of extended electronic conjugation. Furthermore, the oxidative dimerization of alkynes to yield dimer **2.18** also resulted in a red-shift of λ_{\max} and λ_{em} by approximately 45 nm and 40 nm, respectively. A larger red-shift can be attributed to the planarity of the two chromophores with respect to one another which results in an extent of conjugation along both chromophores as opposed to just the triazole ring in the previous examples.

BF₂ complex **2.13**, benzyl-substituted BF₂ complex **2.14** and monomer **2.17** all have moderate Φ_{F} (29–30% in CH₂Cl₂). It is worth noting that, upon introduction of a triazole ring, the quantum yields were not increased, which is opposite to a phenomenon often reported.²³ This can be rationalized by the fact that formation of a triazole ring causes the compound to no longer possess the push-pull electronics which has been shown to increase Φ_{F} .⁸ Dimer **2.18** is essentially non-emissive, which can be attributed to possible intramolecular quenching due to the proximity of both chromophores. The Stokes' shifts observed provide a range of values for these compounds that are within the range of typical Stokes' shifts found in other BF₂ formazanate complexes.⁷

Table 2.5. Electrochemical properties of BF₂ complex **2.13**, benzyl-substituted BF₂ complex **2.14**, monomer **2.17**, and dimer **2.18**.

	E _{red1} (V)	E _{red2} (V)
2.13	-0.67	-1.69
2.14	-0.69	-1.73
2.17	-0.69	-1.75
2.18^a	-0.65	-1.65

^aPotentials reported as the mid-point of two consecutive one-electron reduction processes.

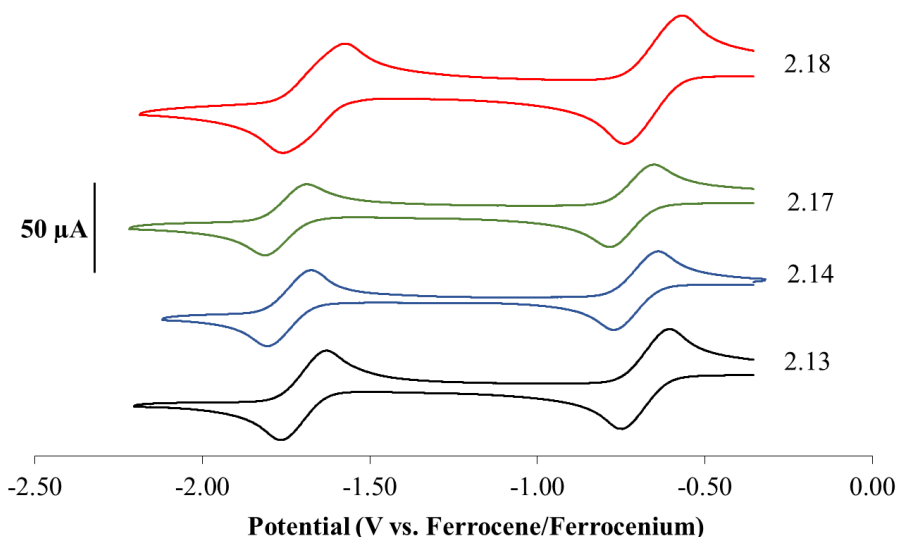


Figure 2.6. Cyclic voltammograms for BF₂ complex **2.13** (black), benzyl-substituted BF₂ complex **2.14** (blue), monomer **2.17** (green), and dimer **2.18** (red), were recorded at a scan rate of 250 mV s⁻¹ for 1 mM analyte solutions in CH₂Cl₂ containing 0.1 M [nBu₄N][PF₆] as the supporting electrolyte. All voltammograms were referenced internally against the ferrocene/ferrocenium redox couple.

2.3 Conclusion

Attempts to synthesize asymmetric 3-cyanoformazans using literature procedures was unsuccessful in giving high yields and pure formazans. Thus, a different method was employed that allowed for the synthesis of the first reported asymmetric 3-cyanoformazan **2.12**, which was then converted to the corresponding BF₂ complex **2.13**. CuAAC chemistry was used as a method for synthesizing various types of BF₂ complexes. All compounds showed strong λ_{max} ranging from 552–597 nm in CH₂Cl₂ and λ_{em} from 647–687 nm. The introduction of triazole rings was shown to red-shift the λ_{max} and λ_{em} by about 10 nm, and the oxidative coupling of alkynes caused a red-shift in the λ_{max} and λ_{em} by approximately 45 and 40 nm, respectively. All compounds were redox active, and had cyclic voltammograms comprised of two reversible

one-electron (**2.13**, **2.14** and **2.17**) or two sets of overlapping reversible one-electron reduction waves (**2.18**). Introduction of a triazole ring made it more difficult to reduce the BF₂ formazanate due to its electron donating character, while alkyne coupling caused reduction to be easier due to the increase in conjugation and the BF₂ complex-substituted alkyne's withdrawing effects. The next chapter will focus on the polymerization of monomer **2.17** by using ROMP of its pendant norbornene group.

2.4 Experimental

2.4.1 General Considerations

Reactions and manipulations were carried out under a nitrogen atmosphere using standard Schlenk techniques unless otherwise stated. Solvents were obtained from Caledon Laboratories, dried using an Innovative Technologies Inc. solvent purification system, collected under vacuum, and stored under a nitrogen atmosphere over 4 Å molecular sieves. *Endo*-5-norbornene-2-carboxylic acid was separated from the *endo/exo* mixture using a published procedure.¹⁴ All other reagents were purchased from Sigma Aldrich, Alfa Aesar or TCI America and used as received.

NMR spectra were recorded on a 400 MHz (¹H: 399.8 MHz, ¹¹B: 128.3 MHz, ¹⁹F: 376.1 MHz, ¹³C: 100.5 MHz), or a 600 MHz (¹³C: 150.7 MHz) Varian INOVA instruments. ¹H NMR spectra were referenced to residual CHCl₃ at 7.27 ppm and ¹³C{¹H} NMR spectra were referenced to CDCl₃ at 77.00 ppm. ¹¹B NMR spectra were referenced internally to BF₃•OEt₂ at 0 ppm. ¹⁹F NMR spectra were referenced internally to CFCl₃ at 0 ppm. Mass spectrometry data were recorded in positive-ion mode using a high-resolution Finnigan MAT 8200 spectrometer using electron impact ionization. UV-vis absorption spectra were recorded using a Cary 5000 Scan instrument using standard quartz cells (1 cm path length) with a scan range of 200 to 800 nm. Four separate concentrations were run for each sample, and molar extinction coefficients were determined from the slope of a plot of absorbance against concentration. Emission spectra were recorded using a Photon Technology International QM-4 SE spectrofluorometer. Emission quantum yields were estimated relative to [Ru(bpy)₃][PF₆]₂ and corrected for wavelength dependent detector sensitivity (Figure A2.21).²¹ FT-IR spectra were

recorded using a PerkinElmer Spectrum Two FT-IR spectrometer using an attenuated total reflectance (ATR) accessory.

2.4.2. X-ray Crystallography Methods

Single crystals for X-ray diffraction studies of BF₂ complex **2.13** and dimer **2.18** were grown by slow vapour diffusion of hexanes into a saturated solution of BF₂ complex **2.13** in CH₂Cl₂ and dimer **2.18** in benzene; these crystals were analyzed by Stephanie Barbon. The samples were mounted on a MiTeGen polyimide micromount with a small amount of Paratone *N* oil. All X-ray measurements were made on a Bruker Kappa Axis Apex2 diffractometer at a temperature of 110 K. The data collection strategy was a number of ω and φ scans which collected data over a range of angles, 2θ . The frame integration was performed using SAINT program.²⁴ The resulting data was scaled and absorption corrected using a multi-scan averaging of symmetry equivalent data using SADABS.²⁵ The structures were solved by dual space methodology using the SHELXT program.²⁶ All non-hydrogen atoms were obtained from the initial solution. The hydrogen atoms were introduced at idealized positions and were allowed to refine isotropically for BF₂ complex **2.13**, but for dimer **2.18** the hydrogen atoms were introduced at idealized positions and the positional parameters but not the displacement parameters were allowed to refine. The structural model was fit to the data using full matrix least-squares based on F^2 . The calculated structure factors included corrections for anomalous dispersion from the usual tabulation. The structure was refined using the SHELXL-2014 program from the SHELX suite of crystallographic software.²⁶ Graphic plots were produced using the Mercury software. See Table 2.6 for crystallographic data.

Table 2.6. Crystallographic data for compounds **2.13** and **2.18**.

	2.13	2.18
Formula	C ₁₇ H ₁₂ BF ₂ N ₅ O	C ₄₆ H ₃₄ B ₂ F ₄ N ₁₀ O ₂
Formula Weight (<i>g/mol</i>)	351.13	856.45
Crystal Dimensions (<i>mm</i>)	0.188 × 0.107 × 0.104	0.509 × 0.244 × 0.074
Crystal Color and Habit	purple prism	blue plate
Crystal System	monoclinic	triclinic
Space Group	C 2/c	P $\bar{1}$
Temperature (K)	110	110
<i>a</i> (Å)	10.248(6)	6.917(2)
<i>b</i> (Å)	14.634(7)	10.231(4)
<i>c</i> (Å)	11.146(5)	15.408(9)
α (°)	90	101.670(11)
β (°)	107.352(18)	92.500(12)
γ (°)	90	107.13(2)
<i>V</i> (Å ³)	1595.5(14)	1014.3(8)
<i>Z</i>	4	1
ρ (<i>g/cm</i>)	1.462	1.402
λ , Å, (Mo K α)	0.71073	0.71073
μ , (<i>cm</i> ⁻¹)	0.111	0.102
Diffractometer Type	Bruker Kappa Axis Apex2	Bruker Kappa Axis Apex2
R _{merge}	0.0406	0.0425
^a R ₁ [2 σ I > 2]	0.0428	0.054
^b wR ₂ [2 σ I > 2]	0.0963	0.1153
R ₁ (all data)	0.077	0.1232
wR ₂ (all data)	0.1107	0.1399
GOF	1.038	1.013

$$^a R_1 = \sum (|F_o| - |F_c|) / \sum F_o$$

$$^b wR_2 = [\sum w (F_o^2 - F_c^2)^2] / \sum (w F_o^4)]^{1/2}$$

$$GOF = [\sum w (F_o^2 - F_c^2)^2] / (\text{No. of reflns.} - \text{No. of params.})]^{1/2}$$

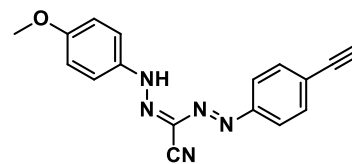
2.4.3 Electrochemical Methods

Cyclic voltammetry experiments were performed with a Bioanalytical Systems Inc. (BASi) Epsilon potentiostat and analyzed using BASi Epsilon software. Typical electrochemical cells consisted of a three-electrode setup including a glassy carbon working electrode, platinum counter electrode, and silver *pseudo* reference electrode. Experiments were run at 250 mV s⁻¹ in degassed CH₂Cl₂ solutions of the analyte (~1 mM) and electrolyte (0.1 M [*n*Bu₄N][PF₆]). Cyclic voltammograms were internally referenced against the ferrocene/ferrocenium redox couple (~1 mM internal standard) and corrected for internal cell resistance using the BASi Epsilon software.

2.4.4. Synthetic Procedures

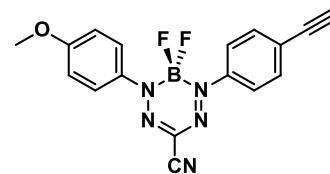
3-Cyanoformazan **2.12**

In air, cyanoacetic acid (1.00 g, 11.7 mmol) and NaOH (4.70 g, 11.7 mmol) were mixed with deionized H₂O (60 mL) and the solution was stirred in an ice bath for 20 min. Meanwhile, in a separate flask, 4-ethynylaniline (1.10 g, 9.39 mmol) was mixed with 12 M HCl (2.35 mL, 28.2 mmol) in deionized H₂O (2.3 mL). The solution was cooled in an ice bath for 15 min before a cooled solution of sodium nitrite (0.75 g, 11 mmol) in deionized H₂O (5 mL) was added dropwise. The resulting reaction mixture, which contained diazonium salt, was stirred in an ice bath for an additional 20 min. In the meantime, in a separate flask, *p*-anisidine (1.44 g, 11.7 mmol) was mixed with 12 M HCl (2.94 mL, 35.3 mmol) in deionized H₂O (2.9 mL). The solution was cooled in an ice bath for 15 min before a cooled solution of sodium nitrite (0.93 g, 13 mmol) in deionized H₂O (5 mL) was added dropwise. The resulting reaction mixture, which contained diazonium salt, was stirred in an ice bath for an additional 20 min. The diazonium salt solutions were then mixed together and stirred in an ice bath for 10 min. The diazonium-containing solution was then added dropwise to the cyanoacetic acid solution. The solution turned dark red after approximately 2 min. After complete addition, the mixture was stirred in an ice bath for an additional 60 min before being neutralized with 1 M HCl. The resulting red-brown solid was filtered off and purified by flash chromatography using a gradient strategy (starting at 1:1 *n*-hexanes: CH₂Cl₂ and ending with 2:8 *n*-hexanes: CH₂Cl₂) where the second coloured fraction contained the desired product. Removal of the solvent *in vacuo* afforded 3-cyanoformazan **2.12** as a dark red microcrystalline solid. Yield = 1.18 g, 33%. M.p 212–213 °C. ¹H NMR (400.1 MHz, DMSO-*d*₆): δ 12.49 (br s, 1H, NH), 8.08 (d, ³J_{HH} = 9 Hz, 2H, aryl CH), 7.54 (br d, 4H, aryl CH), 7.18 (d, ³J_{HH} = 9 Hz, 2H, aryl CH), 4.19 (s, 1H, ≡CH), 3.91 (s, 3H, OCH₃). ¹³C{¹H} NMR (100.6 MHz, DMSO-*d*₆): δ 163.4, 146.1, 142.7, 133.0, 127.0, 126.4, 116.8, 115.7, 115.0, 112.8, 83.5, 80.7, 55.9. FT-IR (ATR): 3308 (m), 3230 (m), 2942 (s), 2837 (s), 2224 (m), 2099 (m), 1605 (m), 1579 (m), 1514 (s), 1249 (s), 1183 (s), 1164 (s), 1140 (s), 1110 (m), 1028 (m) cm⁻¹. UV-vis (CH₂Cl₂): λ_{max} 444 nm (ε = 26,400 M⁻¹ cm⁻¹). Mass Spec. (EI, +ve mode): exact mass calculated for C₁₇H₁₃N₅O: 303.1120; exact mass found: 303.1111; difference: -3.0 ppm.



Asymmetric 3-cyanoformazanate BF₂ complex 2.13

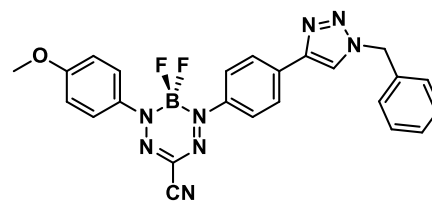
Asymmetric formazan **2.12** (0.40 g, 1.3 mmol) was dissolved in dry toluene (75 mL). Et₃N (0.40 g, 0.55 mL, 3.9 mmol) was then added slowly, and the solution was stirred for 10 min before BF₃•OEt₂ (0.94 g, 0.81 mL, 6.6 mmol) was added, and the solution



was heated to 80 °C with stirring for 16 h. The solution became dark purple during this time and after cooling to 23 °C, deionized H₂O (10 mL) was added to quench any excess boron-containing compounds. The toluene solution was then washed with deionized H₂O (3 × 20 mL), dried over MgSO₄, gravity filtered, and concentrated *in vacuo*. The resulting compound was purified by flash chromatography (THF, neutral alumina) to afford BF₂ complex **2.13** as a dark-purple solid. Yield = 0.31 g, 68%. M.p 199–200 °C. ¹H NMR (399.8 MHz, CDCl₃): δ 7.97 (d, ³J_{HH} = 9 Hz, 2H, aryl CH), 7.87 (d, ³J_{HH} = 9 Hz, 2H, aryl CH), 7.60 (d, ³J_{HH} = 9 Hz, 2H, aryl CH), 7.01 (d, ³J_{HH} = 9 Hz, 2H, aryl CH), 3.92 (br s, 3H, OCH₃), 3.28 (br s, 1H, ≡CH). ¹³C{¹H} NMR (150.7 MHz, CDCl₃): δ 163.6, 142.9, 136.8, 133.1, 125.4, 124.5, 122.5, 115.0, 114.1, 110.0, 82.6, 80.8, 55.9. ¹¹B NMR (128.3 MHz, CDCl₃): δ -0.7 (t, ¹J_{BF} = 31 Hz). ¹⁹F NMR (376.1 MHz, CDCl₃): δ -133.7 (q, ¹J_{FB} = 31 Hz). FT-IR (ATR): 3282 (m), 2928 (s), 2840 (s), 2240 (m), 1593 (s), 1505 (m), 1407 (s), 1343 (s), 1328 (s), 1307 (s), 1262 (s), 1166 (s), 1138 (s) cm⁻¹. UV-vis (CH₂Cl₂): λ_{max} 552 nm (ε = 30,400 M⁻¹ cm⁻¹). Mass Spec. (EI, +ve mode): exact mass calculated for C₁₇H₁₂BF₂N₅O: 351.1103; exact mass found: 351.1108; difference: +1.4 ppm.

Benzyl-substituted BF₂ complex 2.14

PMDETA (0.002 g, 0.003 mL, 0.01 mmol) was dissolved in dry THF (2 mL) and the solution was degassed *via* three freeze-pump-thaw cycles, before CuI (0.003 g, 0.01

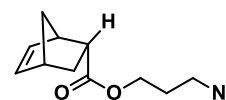


mmol) was added and the resulting mixture was stirred for 15 min at 23 °C. Benzyl azide (0.045 g, 0.043 mL, 0.34 mmol) and BF₂ complex **2.13** (0.100 g, 0.285 mmol) were then added and the reaction mixture was stirred at 23 °C for 16 h. Upon cooling, the THF solution was purified by flash chromatography (THF, neutral alumina) and recrystallized from MeOH to afford benzyl-substituted BF₂ complex **2.14** as a dark-purple microcrystalline solid. Yield = 0.14 g, 51%. M.p 188–189 °C. ¹H NMR (400.1 MHz, CDCl₃): δ 7.95–7.93 (m, 6H, aryl CH),

7.76 (br s, 1H, =CH), 7.42–7.40 (m, 3H, aryl CH), 7.34–7.32 (m, 2H, aryl CH), 7.00 (d, $^3J_{\text{HH}} = 9$ Hz, 2H, aryl CH), 5.61 (br s, 2H, CH₂), 3.91 (br s, 3H, OCH₃). ¹³C{¹H} NMR (150.7 MHz, CDCl₃): δ 162.7, 146.6, 142.6, 136.8, 134.3, 132.9, 129.2, 128.9, 128.1, 126.4, 125.2, 123.3, 120.4, 114.9, 114.2, 110.0, 55.8, 54.3. ¹¹B NMR (128.3 MHz, CDCl₃): δ -0.7 (t, $^1J_{\text{BF}} = 29$ Hz). ¹⁹F NMR (376.1 MHz, CDCl₃): δ -134.2 (q, $^1J_{\text{FB}} = 29$ Hz). FT-IR (ATR): 3123 (m), 2849 (m), 2250 (m), 1603 (s), 1509 (m), 1460 (m), 1375 (s), 1344 (s), 1326 (s), 1308 (s) cm⁻¹. UV-vis (CH₂Cl₂): λ_{max} 560 nm (ε = 31,000 M⁻¹ cm⁻¹). Mass Spec. (EI, +ve mode): exact mass calculated for C₂₄H₁₉BF₂N₈O: 484.1743; exact mass found: 484.1759; difference: +3.3 ppm.

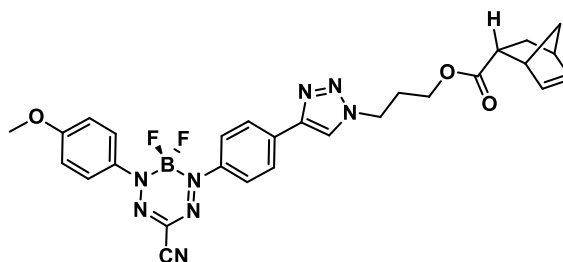
Azide-substituted norbornene **2.16**

As previously reported,²⁷ *endo*-5-norbornene-2-carboxylic acid (1.52 g, 11.0 mmol), DCC (2.47 g, 12.0 mmol) and DMAP (1.46 g, 12.0 mmol) were dissolved in dry CH₂Cl₂ (110 mL) and the solution was stirred for 15 min at 23 °C. 3-azido-1-propanol (1.01 g, 10.0 mmol) was then added to the reaction mixture and stirred at 23 °C for 2 h. The solvent was then removed *in vacuo* and the crude mixture was purified by flash chromatography (3:1 *n*-hexanes:EtOAc, silica) to afford azide-substituted norbornene **2.16** as a clear and colourless liquid. Yield = 1.88 g, 85%. ¹H NMR (399.8 MHz, CDCl₃): δ 6.21 (dd, 1H, $^3J_{\text{HH}} = 6$, $^3J_{\text{HH}} = 3$ Hz, =CH), 5.93 (dd, 1H, $^3J_{\text{HH}} = 6$, $^3J_{\text{HH}} = 3$ Hz, =CH), 4.12 (t, 2H, $^3J_{\text{HH}} = 6$ Hz, CH₂), 3.40 (t, 2H, $^3J_{\text{HH}} = 7$ Hz, CH₂), 3.22 (br s, 1H, CH), 2.99–2.95 (m, 1H, CH), 2.92 (br s, 1H, CH), 1.95–1.87 {m, 3H, CH₂ (2H) and diastereotopic CH₂ (1H)}, 1.47–1.41 (m, 2H, 2 x diastereotopic CH₂), 1.29 (d, 1H, $J_{\text{HH}} = 8$ Hz, diastereotopic CH₂). ¹³C{¹H} NMR (150.7 MHz, CDCl₃): δ 174.6, 137.9, 132.2, 61.0, 49.6, 48.3, 45.7, 43.3, 42.5, 29.2, 28.2. FT-IR (ATR): 3064 (w), 2968 (m), 2876 (m), 2095 (s), 1730 (s), 1455 (m), 1336 (m), 1270 (m), 1172 (s) cm⁻¹. Mass Spec. (EI, +ve mode): exact mass calculated for C₁₁H₁₅N₃O₂: 221.1164; exact mass found: 221.1158; difference: -2.7 ppm.



Monomer 2.17

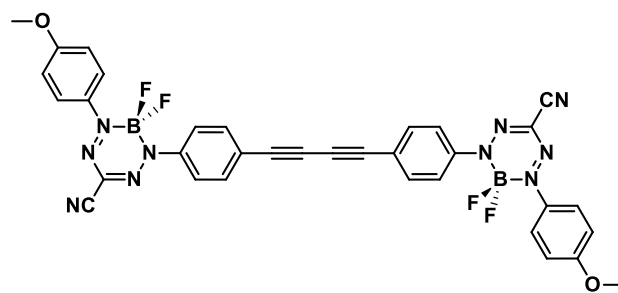
PMDETA (0.005 g, 0.006 mL, 0.03 mmol) and azide-substituted norbornene **2.16** (0.162 g, 0.732 mmol) were dissolved in dry THF (4 mL) and the solvent was degassed *via* three freeze-



pump-thaw cycles. CuI (0.006 g, 0.03 mmol) was then added and the mixture was stirred for 15 min at 23 °C. BF₂ complex **2.13** (0.214 g, 0.610 mmol) was then added and the reaction mixture was stirred at 23 °C for 2 h. The solvent was removed *in vacuo* and the mixture purified by flash chromatography; first a toluene/silica column was employed to remove purple and blue side products, then 1:1 toluene:EtOAc was added and the third coloured fraction contained the desired product. Removal of the solvent *in vacuo* afforded monomer **2.17** as a dark-purple microcrystalline solid. Yield = 0.27 g, 77%. M.p 75–76 °C. ¹H NMR (399.8 MHz, CDCl₃): δ 7.97–7.95 (m, 6H, aryl CH), 7.90 (br s, 1H, triazole =CH), 7.02–7.00 (m, 2H, aryl CH), 6.23 (dd, 1H, ³J_{HH} = 6, ³J_{HH} = 3 Hz, =CH), 5.95 (dd, 1H, ³J_{HH} = 6, ³J_{HH} = 3 Hz, =CH), 4.53 (t, ³J_{HH} = 7 Hz, 2H, CH₂), 4.15–4.11 (m, 2H, CH₂), 3.92 (s, 3H, OCH₃), 3.22 (br s, 1H, CH), 2.99–2.94 (m, 2H, 2CH), 2.35–2.29 (m, 2H, CH₂), 1.96–1.90 (m, 1H, diastereotopic CH₂), 1.48–1.41 (m, 2H, 2 × diastereotopic CH₂), 1.30–1.28 (m, 1H, diastereotopic CH₂). ¹³C{¹H} NMR (150.7 MHz, CDCl₃): δ 174.6, 162.7, 146.3, 142.7, 138.1, 138.0, 136.8, 132.9, 132.1, 126.4, 125.2, 123.4, 120.7, 114.9, 114.2, 60.6, 55.9, 49.7, 47.4, 45.8, 43.3, 42.5, 29.6, 29.2. ¹¹B NMR (128.3 MHz, CDCl₃): δ –0.7 (t, ¹J_{BF} = 30 Hz). ¹⁹F NMR (376.1 MHz, CDCl₃): δ –134.1 (q, ¹J_{FB} = 30 Hz). FT-IR (ATR): 3138 (w), 2933 (m), 2857 (m), 2241 (m), 1726 (s), 1597 (s), 1505 (m), 1334 (s), 1261 (s) cm⁻¹. UV-vis (CH₂Cl₂): λ_{max} 561 nm (ε = 35,300 M⁻¹ cm⁻¹). Mass Spec. (EI, +ve mode): exact mass calculated for C₂₈H₂₇BF₂N₈O₃: 572.2267; exact mass found: 572.2256; difference: –1.9 ppm.

Dimer 2.18

This product appeared when the synthesis for monomer **2.17** was left overnight. The dimer was purified by flash chromatography (silica gel, toluene), where the second blue coloured fraction contained the dimer. Yield = 0.02 g, 7%. M.p 249–250



°C. ^1H NMR (399.8 MHz, CD_2Cl_2): δ 7.96 (d, $^3J_{\text{HH}} = 9$ Hz 4H, aryl CH), 7.88 (d, $^3J_{\text{HH}} = 9$ Hz 4H, aryl CH), 7.66 (d, $^3J_{\text{HH}} = 9$ Hz 4H, aryl CH), 7.04 (d, $^3J_{\text{HH}} = 9$ Hz 4H, aryl CH), 3.91 (s, 6H, OCH_3). $^{13}\text{C}\{^1\text{H}\}$ NMR (150.7 MHz, CD_2Cl_2): δ 164.0, 144.1, 137.5, 134.2, 128.7, 126.1, 124.2, 123.3, 115.7, 114.7, 83.0, 77.5, 56.6. ^{11}B NMR (128.3 MHz, CD_2Cl_2): δ -0.7 (t, $^1J_{\text{BF}} = 31$ Hz). ^{19}F NMR (376.1 MHz, CD_2Cl_2): δ -134.3 (q, $^1J_{\text{FB}} = 31$ Hz). FT-IR (ATR): 3011 (w), 2936 (w), 2843 (w), 2247 (m), 1731 (w), 1599 (s), 1507 (m), 1406 (m) cm^{-1} . UV-vis (CH_2Cl_2): λ_{max} 597 nm ($\epsilon = 78,500 \text{ M}^{-1} \text{ cm}^{-1}$). Mass Spec. (EI, +ve mode): exact mass calculated for $\text{C}_{34}\text{H}_{22}\text{B}_2\text{F}_4\text{N}_{10}\text{O}_2$: 700.2049; exact mass found: 700.2061; difference: +1.7 ppm.

2.5 References

- Gorman, A.; Killoran, J.; O'Shea, C.; Kenna, T.; Gallagher, W. M.; O'Shea, D. F., *J. Am. Chem. Soc.* **2004**, *126*, 10619–10631.
- Frath, D.; Massue, J.; Ulrich, G.; Ziessel, R., *Angew. Chem. Int. Ed.* **2014**, *53*, 2290–2310.
- Frath, D.; Poirel, A.; Ulrich, G.; De Nicola, A.; Ziessel, R., *Chem. Commun.* **2013**, *49*, 4908–4910.
- Loudet, A.; Burgess, K., *Chem. Rev.* **2007**, *107*, 4891–4932.
- Araneda, J. F.; Piers, W. E.; Heyne, B.; Parvez, M.; McDonald, R., *Angew. Chem. Int. Ed.* **2011**, *50*, 12214–12217.
- Lee, B.; Park, B. G.; Cho, W.; Lee, H. Y.; Olsaz, A.; Chen, C.-H.; Park, S. B.; Lee, D., *Chem. Eur. J.* **2016**, *22*, 17321–17328.

7. Barbon, S. M.; Reinkeluers, P. A.; Price, J. T.; Staroverov, V. N.; Gilroy, J. B., *Chem. Eur. J.* **2014**, *20*, 11340–11344.
8. Barbon, S. M.; Price, J. T.; Reinkeluers, P. A.; Gilroy, J. B., *Inorg. Chem.* **2014**, *53*, 10585–10593.
9. Szymczyk, M.; Czajkowski, W.; Stolarski, R., *Dyes and Pigm.* **1999**, *42*, 227–235.
10. Abdallah, S. O.; Metwally, N. H.; Anwar, H. F.; Elnagdi, M. H., *J. Heterocycl Chem.* **2005**, *42*, 781–786.
11. Gilroy, J. B.; Otieno, P. O.; Ferguson, M. J.; McDonald, R.; Hicks, R. G., *Inorg. Chem.* **2008**, *47*, 1279–1286.
12. Lieber, E.; Rao, C. N. R.; Chao, T. S.; Hoffman, C. W. W., *Anal. Chem.* **1957**, *29*, 916–918.
13. Ma, Z.; Lin, Y.; Cheng, Y.; Wu, W.; Cai, R.; Chen, S.; Shi, B.; Han, B.; Shi, X.; Zhou, Y.; Du, L.; Li, M., *J. Med. Chem.* **2016**, *59*, 2151–2162.
14. Berson, J. A.; Ben-Efraim, D. A., *J. Am. Chem. Soc.* **1959**, *81*, 4083–4087.
15. Brandsma, L.; Verkruijse, H. D.; Walda, B., *Synth. Commun.* **1991**, *21*, 137–139.
16. Jones, E. R. H., *J. Chem. Soc.* **1950**, 754–761.
17. Hay, A. S., *J. Org. Chem.* **1962**, *27*, 3320–3321.
18. Vilhelmsen, M. H.; Jensen, J.; Tortzen, C. G.; Nielsen, M. B., *Eur. J. Org. Chem.* **2013**, *2013*, 701–711.
19. Wang, Z., *Comprehensive Organic Name Reactions and Reagents*, 3rd vol.; John Wiley & Sons, Inc.: 2010.
20. Haynes, W. M., *CRC Handbook of Chemistry and Physics* 96th Edition. Taylor & Francis Group: New York, 2015.
21. Fery-Forgues, S.; Lavabre, D., *J. Chem. Educ.* **1999**, *76*, 1260.

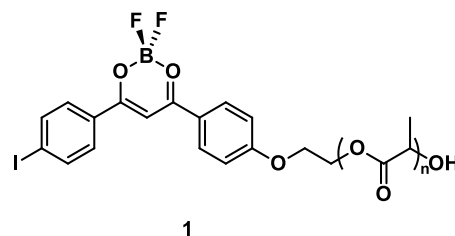
22. Suzuki, K.; Kobayashi, A.; Kaneko, S.; Takehira, K.; Yoshihara, T.; Ishida, H.; Shiina, Y.; Oishi, S.; Tobita, S., *Phys. Chem. Chem. Phys.* **2009**, *11*, 9850–9860.
23. Weissleder, R.; Ross, B. D.; Rehemtulla, A.; Gambhir, S. S., In *Molecular Imaging: Principles and Practice*. PMPH-USA: Shelton, 2010; p 1357.
24. Bruker-AXS, *SAINTE*, 2013.8; Bruker-AXS, Madison, WI 53711, USA., 2013.
25. Bruker-AXS, *SADABS*, 2012.1; Bruker-AXS, Madison, WI 53711, USA., 2012.
26. Sheldrick, G., *Acta Cryst.* **2015**, *71*, 3–8.
27. Paquette, J. A.; Rabiee Kenaree, A.; Gilroy, J. B., *Polym. Chem.* **2017**, *8*, 2164–2172.

Chapter 3

3 Fluorescent BF₂ 3-Cyanoformazanate Polymers

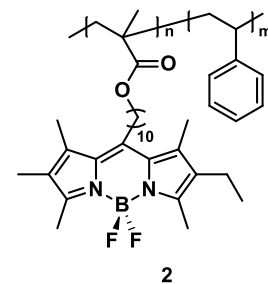
3.1 Introduction

Fluorescent, boron-containing molecules have been incorporated into polymers that have shown potential use in various areas such as: spectroscopic sensing, fluorescence imaging, gene and drug delivery, and light-harvesting materials.^{1,2,3-17} For example, the Fraser



group was able to modulate solid-state fluorescence and phosphorescence of polymer **1** by varying the length of appended polylactic acid (PLA) chains and using heavy atoms.¹⁸ Furthermore, they showed that low molecular-weight polymers had weak fluorescence but strong phosphorescence spectra in anaerobic/low-oxygen conditions. These properties allowed the group to carry out *in vivo* imaging of breast cancer mammary carcinoma tumour regions in mice, thereby demonstrating their use as tumour hypoxia imaging agents.

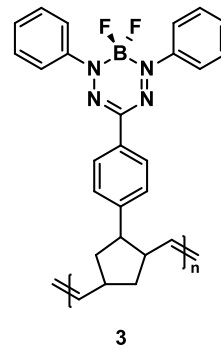
Chujo and coworkers synthesized a methacrylate derivative with a pendant BODIPY unit which was copolymerized with polystyrene using reversible addition-fragmentation chain transfer (RAFT) polymerization to yield polymer **2**.¹⁹ This polymer self-assembled into nanosized particles that exhibited absorption and emission properties similar to that of the free BODIPY monomer unit. The Φ_F of the



particles was much higher than that of the monomer which was due to the fact that polystyrene units inhibited the π - π stacking of the BODIPY units, which would otherwise cause collision quenching of the fluorescence.

The controlled ROMP of side-chain BF₂ formazanate containing polymers **3** has been reported previously.²⁰ These polymers retained the properties of the BF₂ monomer such as high molar extinction coefficients, fluorescence, and redox activity. However, the Φ_F for both the monomer and polymer were rather low ($\Phi_F = 1.5\%$ and 2.5% , respectively). These results

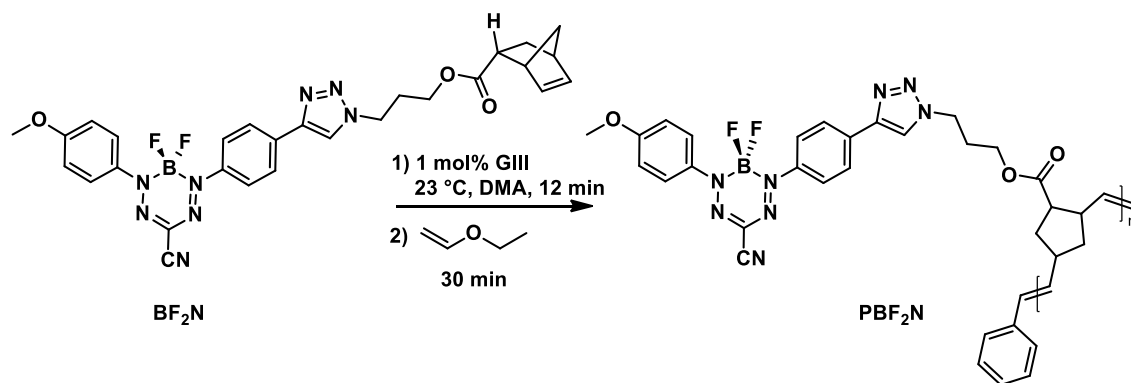
revealed the need to make a monomer with higher Φ_F , so that the corresponding polymer may also benefit from this property. This chapter describes the polymerization of monomer **2.21** (**BF₂N**) using ROMP. The synthesis of various block and random copolymers of **BF₂N** is also described, along with their thermal and spectroscopic properties.



3.2 Results and Discussion

3.2.1 Synthesis of Side-Chain Polymers

Attempts to polymerize monomer **BF₂N** using ROMP began by dissolving the monomer in dry and degassed CH_2Cl_2 at 50 mg mL^{-1} concentrations, at $23 \text{ }^\circ\text{C}$, using the 3-bromo pyridine derivative of Grubbs' third generation catalyst (GIII). However, after various attempts to optimize the conditions of the polymerization (such as temperature and time), there was no evidence of polymer formation using ^1H NMR spectroscopy. It was concluded that the polymer was likely not very soluble in CH_2Cl_2 and that short oligomers were crashing out of solution upon formation. Thus, dimethylacetamide (DMA) was used as a solvent since it solubilized the **BF₂N** monomer better than CH_2Cl_2 . The reactions were carried out in dry and degassed DMA at 50 mg mL^{-1} concentrations, at $23 \text{ }^\circ\text{C}$, using GIII. Ethyl vinyl ether was used as the terminating agent, and the polymer was purified by precipitation from pentane and isolated by centrifugation (Scheme 3.1). ^1H NMR spectroscopy of the **BF₂** polymer (**PBF₂N**) revealed the disappearance of the alkene protons of the norbornene group on **BF₂N** monomer, which appeared at 6.22 ppm and 5.93 ppm (triangles), and the appearance of broad signals between 5.25 and 5.35 ppm (circles) which are from the alkene protons found in the backbone of **PBF₂N** (Figure 3.1). Furthermore, all signals in the ^1H NMR spectrum were broad, which is often an indication of polymer formation. The **BF₂** moiety remained intact, which was evident by looking at the broad signal at -133.4 ppm in the ^{19}F NMR spectrum, and a 1:2:1 triplet at -0.8 ppm in the ^{11}B NMR spectrum (Figure A.3.9.). Cyclic voltammetry experiments were performed in CH_2Cl_2 and showed that the polymers exhibited two reversible one-electron reduction waves to yield first the poly radical anion, and then the poly dianion (Figure A.3.17.).



Scheme 3.1. ROMP of **BF₂N** monomer.

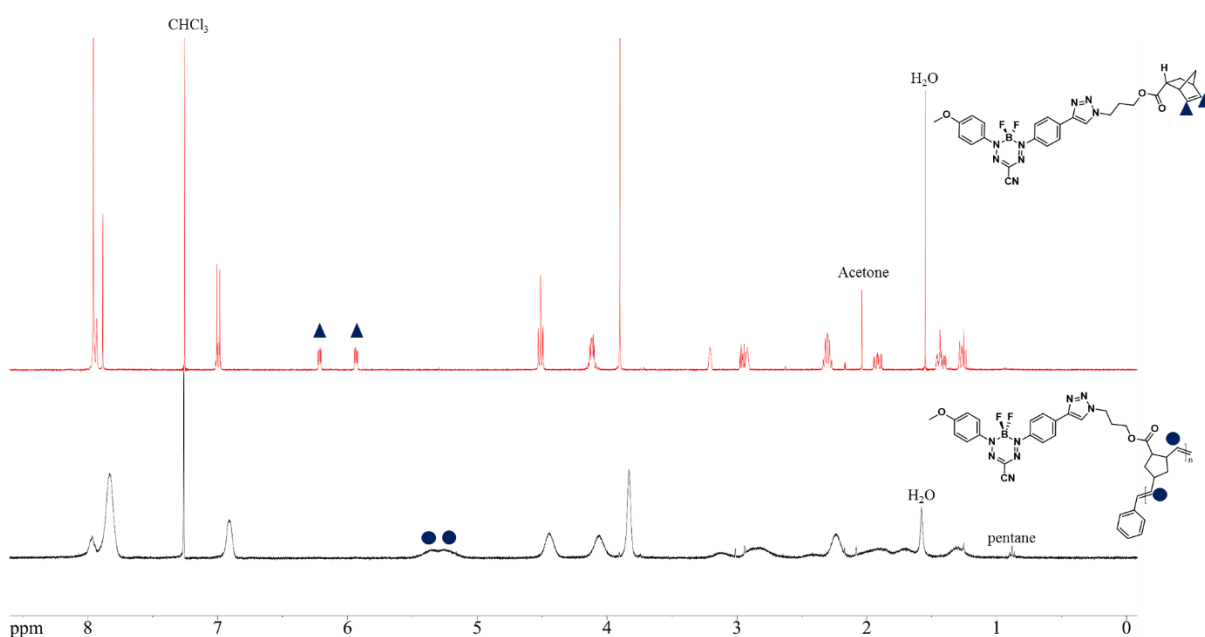


Figure 3.1. Overlay of the ¹H NMR spectra for **BF₂N** monomer (red) and **PBF₂N** (black) in CDCl₃. The triangles represent the norbornene alkene protons on **BF₂N** and the circles represents the new alkene protons found in the backbone of **PBF₂N**.

In order to determine the time at which the ROMP reaction was finished, it was monitored by taking aliquots of a reaction solution at different time intervals and terminating the polymerization with ethyl vinyl ether. Monitoring the reaction revealed that the polymerization was complete after approximately 10 min (Figure 3.2). The number average molecular weight (M_n), weight average molecular weight (M_w) and dispersity (D) for each of the aliquots of **PBF₂N** was then determined by gel permeation chromatography (GPC) relative to polystyrene standards and summarized in Table 3.1. ¹H NMR spectroscopy could not be used to determine the molecular weight of the **PBF₂N** since resonances associated with the phenyl end group

overlapped with those of the polymer repeating unit. Furthermore, the polymer absorbs at 630 nm, impeding the use of triple-detection GPC as a means for determining absolute molecular weight. Dispersity values ranged from 1.10–1.31 demonstrating the controlled polymerization of monomer **BF₂N** using ROMP, which is an important trait for future block and random copolymer synthesis. Molecular weight data for the **BF₂N** monomer was also collected. It is worth noting that the molecular weight of the monomer (572.37 g mol⁻¹) has been overestimated by GPC ($M_n = 4,140$ g mol⁻¹), and thus we postulate that all the molecular weights found for the polymers are also overestimated.

Table 3.1. Summary of molecular weight data determined by GPC for **PBF₂N** polymers.

Time (min)	M_n	M_w	\mathcal{D}
BF₂N	4,140	4,869	1.18
1	109,200	126,500	1.16
3	151,400	189,200	1.25
5	164,500	210,400	1.28
10	182,100	226,400	1.24
20	185,600	241,400	1.30
30	193,100	241,400	1.25
60	201,500	264,300	1.31

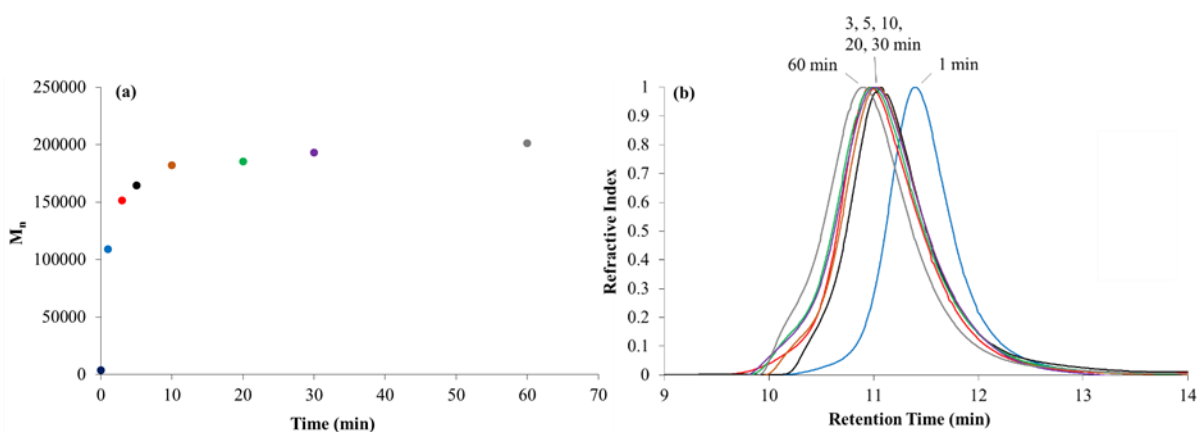
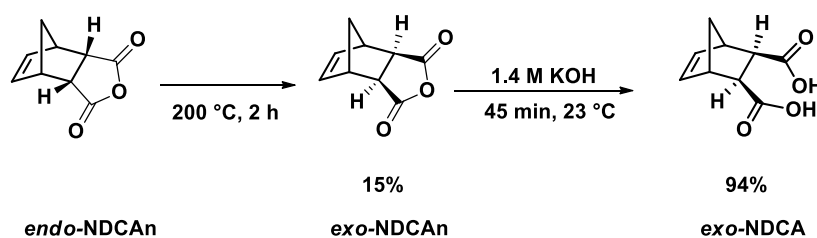


Figure 3.2. Relationship between M_n of **PBF₂N** as a function of time (a), and corresponding GPC traces (b). Dark blue dot at zero 0 min in (a) represents the M_n value determined for the **BF₂N** monomer. GPC traces in (b) are colour coded: 1 min (light blue), 3 min (red), 5 min (black), 10 min (dark yellow), 20 min (green), 30 min (purple), 60 min (grey).

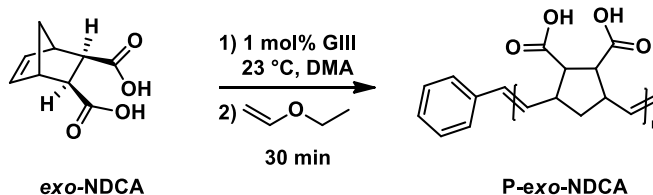
In order to synthesize copolymers containing **BF₂N** subunits, a second monomer containing a polymerizable norbornene group was synthesized according to a modified procedure developed by Alfred *et al.* (Scheme 3.2).²¹ First, *cis*-5-norbornene-*exo*-2,3-dicarboxylic

anhydride (**exo-NDCAn**) was synthesized by heating *cis*-5-norbornene-*endo*-2,3-dicarboxylic anhydride (**endo-NDCAn**) at 200 °C for 2 h, and separating **exo-NDCAn** from the remaining starting material (**endo-NDCAn**) by the use of column chromatography (1:1 *n*-hexanes:EtOAc). *Cis*-5-norbornene-*exo*-2,3-dicarboxylic acid (**exo-NDCA**) was then synthesized by stirring **exo-NDCAn** in a 1.4 M solution of KOH for 45 min. ¹H NMR spectroscopy confirmed the synthesis of solely the *exo* isomer for both **exo-NDCAn** and **exo-NDCA** (Figure A.3.1 and Figure A.3.2)



Scheme 3.2. Synthesis of monomer **exo-NDCA**.

Polymerization of **exo-NDCA** was carried out according to a modified procedure,²¹ where monomer **exo-NDCA** was dissolved in dry and degassed DMA at 50 mg mL⁻¹ concentrations, at 23 °C, using GIII; ethyl vinyl ether was once again used as the terminating agent (Scheme 3.3).

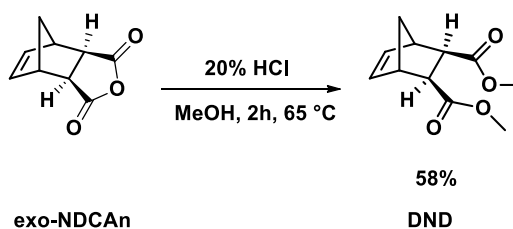


Scheme 3.3. Polymerization of monomer **exo-NDCA**.

¹H NMR spectroscopy revealed the disappearance of the alkene protons of the norbornene group on **exo-NDCA** which appeared as a multiplet at 6.24 ppm, and the appearance two broad signals at 5.25 and 5.43 ppm which are from the alkene protons found in the backbone of the *cis*-5-norbornene-*exo*-2,3-dicarboxylic acid polymer (**P-exo-NDCA**) (Figure A.3.3.). The polymerization of **exo-NDCA** was monitored as a function of time by taking aliquots of the reaction solution and terminating the polymerization with ethyl vinyl ether. The M_n , M_w and D for each of the aliquots of polymers was determined by GPC relative to polystyrene

standards and summarized in Table A.3.1. Prior to GPC analysis, the polymers were methylated by stirring in dry DMF with excess K_2CO_3 and CH_3I overnight. This was done to prevent any irreversible adsorption of the polymer to the GPC column due to the presence of the carboxylic acid groups in the **P-*exo*-NDCA**. Monitoring the reaction mechanism revealed that the polymerization was complete after approximately 6 min (Figure A.3.4). Dispersity values ranged from 1.07–1.38 showing controlled polymerization of monomer *exo*-NDCA.

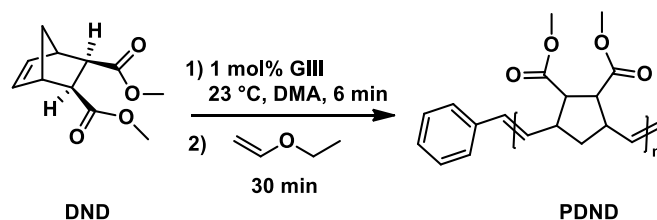
Initial attempts to synthesize block copolymers containing **BF₂N** and *exo*-NDCA subunits using ROMP were met with difficulties when trying to obtain a ¹H NMR spectrum. Although various solvents were used (e.g., $CDCl_3$, $DMSO-d_6$, or both) and variable temperature experiments were carried out (up to 125 °C in $DMSO-d_6$), all experiments were unsuccessful in revealing peaks pertaining to both polymers. This difficulty was most likely due to a difference in the solubility of both blocks rather than failed polymerization, since GPC traces suggest block copolymer synthesis was successful based on an increase in molecular weight of (**PBF₂N**)-*b*-(**P-*exo*-NDCA**) vs. solely the first block (**PBF₂N**) (Figure A.3.5). These difficulties, along with the inconvenience of having to methylate each polymer before GPC analysis, prompted the synthesis of a new monomer for block copolymer and random copolymer synthesis with **BF₂N**. *Cis*-dimethyl-5-norbornene-*exo*-2,3-dicarboxylate (**DND**) was synthesized by a modified procedure from Hennis *et al.*²² where sulfuric acid was substituted for hydrochloric acid (Scheme 3.4). ¹H NMR spectroscopy confirmed the synthesis of solely **DND** as the *exo* isomer (Figure 3.3).



Scheme 3.4. Synthesis of monomer **DND**.

Polymerization of **DND** was performed in the same manner as *exo*-NDCA, where **DND** was dissolved in dry and degassed DMA at 50 mg mL⁻¹ concentrations, at 23 °C, using GIII; ethyl vinyl ether was used as the terminating agent (Scheme 3.5). ¹H NMR spectroscopy revealed the disappearance of the alkene protons of the norbornene group of **DND** (triangle) which appeared as a broad singlet at 6.21 ppm, and the appearance of two

broad signals at 5.24 and 5.42 ppm (circles) due to the presence of the alkene protons found in the backbone of poly(*cis*-dimethyl-5-norbornene-*exo*-2,3-dicarboxylate) (**PDND**) (Figure 3.3).



Scheme 3.5. ROMP of **DND**.

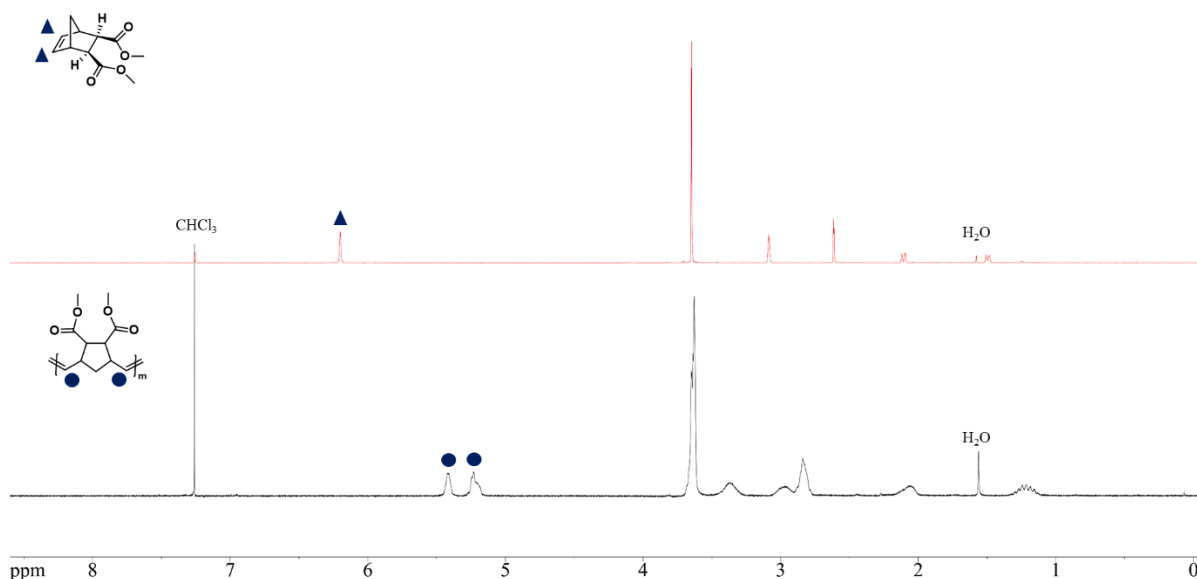


Figure 3.3. Overlay of the ^1H NMR spectra of compound **DND** (red) and **PDND** (black) in CDCl_3 . The triangle represents the norbornene alkene protons and the circles represent the new alkene protons found in the backbone of **PDND**.

The polymerization of **DND** was monitored over time by taking aliquots of the reaction solution at 0.5, 1, 3, 5, 7 and 9 min, prior to termination with ethyl vinyl ether. The M_n , M_w and D for each of the aliquots of polymers was determined by GPC (vs. polystyrene standards) (without the need of post-polymerization modification) and summarized in Table 3.2. Monitoring the reaction mechanism revealed that the polymerization was complete after approximately 3 min due to a plateauing of the M_n (Figure 3.4a), which is also seen by the overlap of GPC traces of 3, 5, 7, and 9 min seen in Figure 3.4b. The dispersity for all aliquots ranged from 1.12–1.14 which shows the controlled polymerization of **DND**, an important trait for future block and random copolymer synthesis.

Table 3.2. Summary of molecular weight data determined by GPC for **PDND**.

Time (min)	M_n	M_w	\bar{D}
0.5	36,900	41,250	1.12
1	39,510	44,360	1.12
3	43,680	49,280	1.13
5	42,520	48,510	1.14
7	43,060	48,730	1.13
9	43,190	48,910	1.13

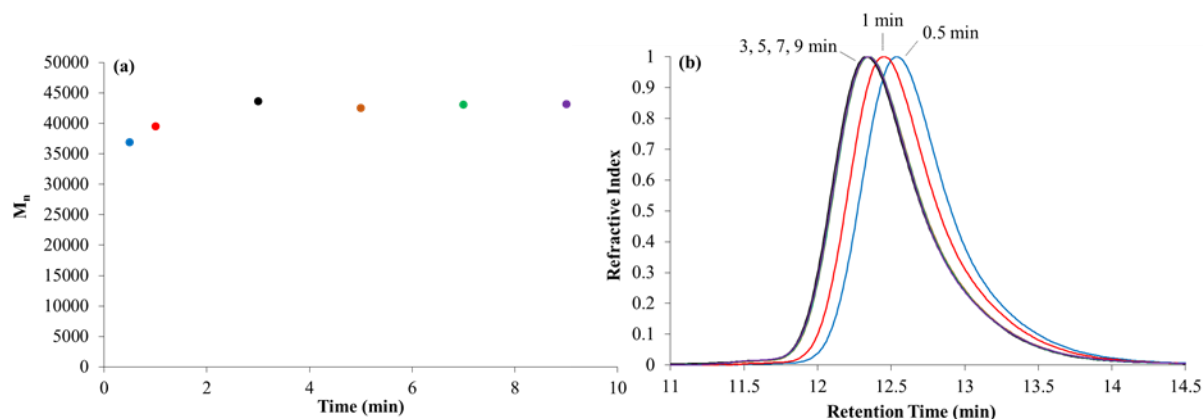
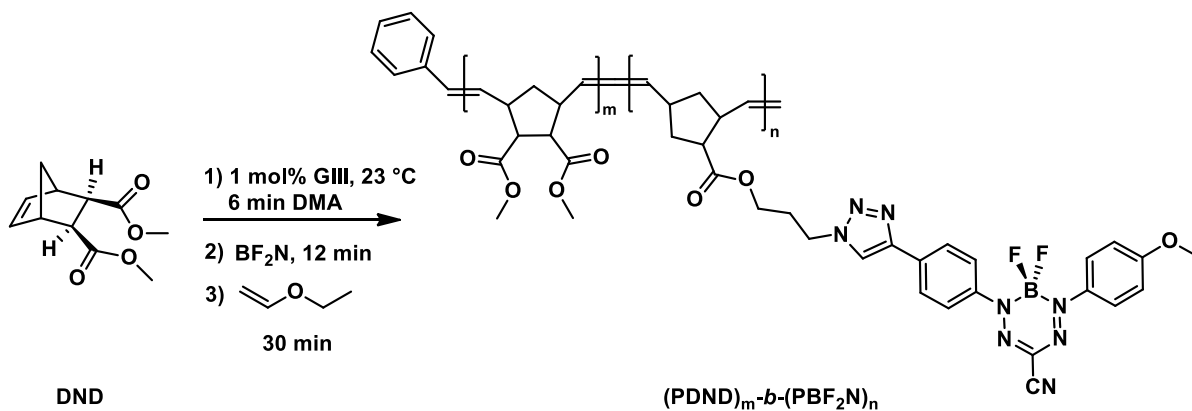


Figure 3.4. Relationship between the M_n of **PDND** as a function of time (a), and corresponding GPC traces (b). GPC traces in (b) are colour coded: 0.5 min (light blue), 1 min (red), 3 min (black), 5 min (dark yellow), 7 min (green), 9 min (purple).

3.2.2 Synthesis of Block Copolymers Containing BF_2 Complexes

A representative block copolymer $(\text{PDND})_m\text{-}b\text{-(PBF}_2\text{N)}_n$ containing subunits of **DND** and **BF₂N** was synthesized by first dissolving **DND** in dry degassed DMA at a concentration of 50 mg mL⁻¹, at 23 °C, and 1 mol % of GIII catalyst was added. The reaction mixture was stirred for 6 min. At this time, an aliquot of the first block (**PDND**) was removed and added to a solution containing ethyl vinyl ether; this was done so that the M_n of the first block could be found using GPC. A solution of monomer **BF₂N** was then added to the **PDND** reaction solution and the second monomer was allowed to polymerize from the active end of **PDND** for an additional 12 min and then quenched with ethyl vinyl ether (Scheme 3.6).



Scheme 3.6. Representative synthesis of (PDND)_m-b-(PBF₂N)_n polymers using ROMP.

As described, the synthesis of all block copolymers began by targeting 100 units of **DND** in **PDND** (1 mol% of GIII to **DND**). This method was used to synthesize three block copolymers that differed by the amount of BF₂ subunit allowed to grow off of the active **PDND** chain. The more BF₂N subunits allowed to grow off of the **PDND** live chain end, the greater the mole fraction of BF₂N subunit (f_{BF_2}) in each block copolymer, and thus a greater M_n for the block polymer (Table 3.3). This was also made evident by comparing the GPC traces for polymers (PDND)₂₇₆-b-(PBF₂N)₂₅₅, (PDND)₃₅₅-b-(PBF₂N)₅₃, (PDND)₂₆₆-b-(PBF₂N)₂₀, and **PDND** (Figure 3.5). As the f_{BF_2} increased, the M_n of the block copolymers also increased. \bar{D} values for the first blocks of all block copolymers ranged from 1.11–1.16, and \bar{D} from the block copolymers ranged from 1.16–1.45, consistent with controlled ROMP.²³

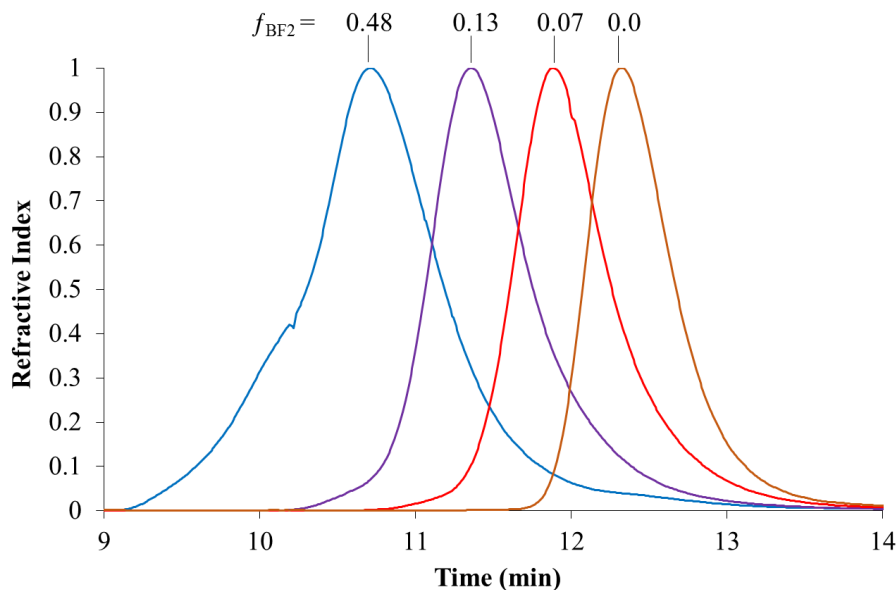


Figure 3.5. GPC traces (in DMF) of polymer **PDND** ($f_{\text{BF}_2} = 0.0$, dark yellow) and block copolymers **(PDND)_{276-b}-(PBF₂N)₂₅₅** ($f_{\text{BF}_2} = 0.48$, blue), **(PDND)_{355-b}-(PBF₂N)₅₃** ($f_{\text{BF}_2} = 0.13$, purple) and **(PDND)_{266-b}-(PBF₂N)₂₀** ($f_{\text{BF}_2} = 0.07$, red).

¹H NMR spectroscopy confirmed the synthesis of the block copolymers described above, along with the f_{BF_2} in each polymer (Figure A.3.10. – A.3.12.). Figure 3.6 shows the ¹H NMR spectrum of block copolymer **(PDND)_{276-b}-(PBF₂N)₂₅₅**, **PBF₂N** and **PDND**. The alkene protons of the norbornene group on **BF₂N** which appear between 5.94–5.96 and 6.22–6.24 ppm and the alkene protons of **DND** which appear as a broad singlet at 6.21 ppm have disappeared and new alkene protons that pertain to the backbone of **(PDND)_{276-b}-(PBF₂N)₂₅₅** have appeared as two broad signals at 5.25 and 5.43 ppm (circles). Integration of these signals with respect to the broad singlet at 6.92 ppm (star), which pertains to two aryl protons on the **BF₂N** containing block, was used in order to determine the block ratio of these polymers. In the case of block copolymer **(PDND)_{276-b}-(PBF₂N)₂₅₅**, the integrations of these signals is 2.00 to 4.20. As the signal that integrates to 4.20 contains two protons from **PBF₂N**, the remaining integration is attributed to **PDND** (2.20), thus the mole ratio of **BF₂N** subunit to **DND** subunits is 1:1.1, and thus **(PDND)_{276-b}-(PBF₂N)₂₅₅** contains $f_{\text{BF}_2} = 0.48$. Signals pertaining to the methoxy substituent on **PBF₂N** (triangle) and methyl ester groups on **PDND** (squares) are found at 3.83 ppm and 3.64 ppm, respectively. These signals are found in the ¹H NMR spectrum of **(PDND)_{276-b}-(PBF₂N)₂₅₅** as well; the ¹H NMR spectrum of **(PDND)_{276-b}-(PBF₂N)₂₅₅** is essentially an overlay of ¹H NMR spectrum of **PBF₂N** and **PDND**. All signals in the ¹H NMR spectrum were broad, which is an indication of polymer formation, and the **BF₂**

moiety remained intact, as evidenced by looking at the broad signal at -133.4 ppm in the ^{19}F NMR spectrum, and the broad 1:2:1 triplet at -0.75 ppm in the ^{11}B NMR spectrum (Figure A.3.16.). Cyclic voltammetry experiments were performed in CH_2Cl_2 and showed that the copolymers exhibited two reversible one-electron reduction waves to yield the poly radical anion and the poly dianion (Figure A.3.17).

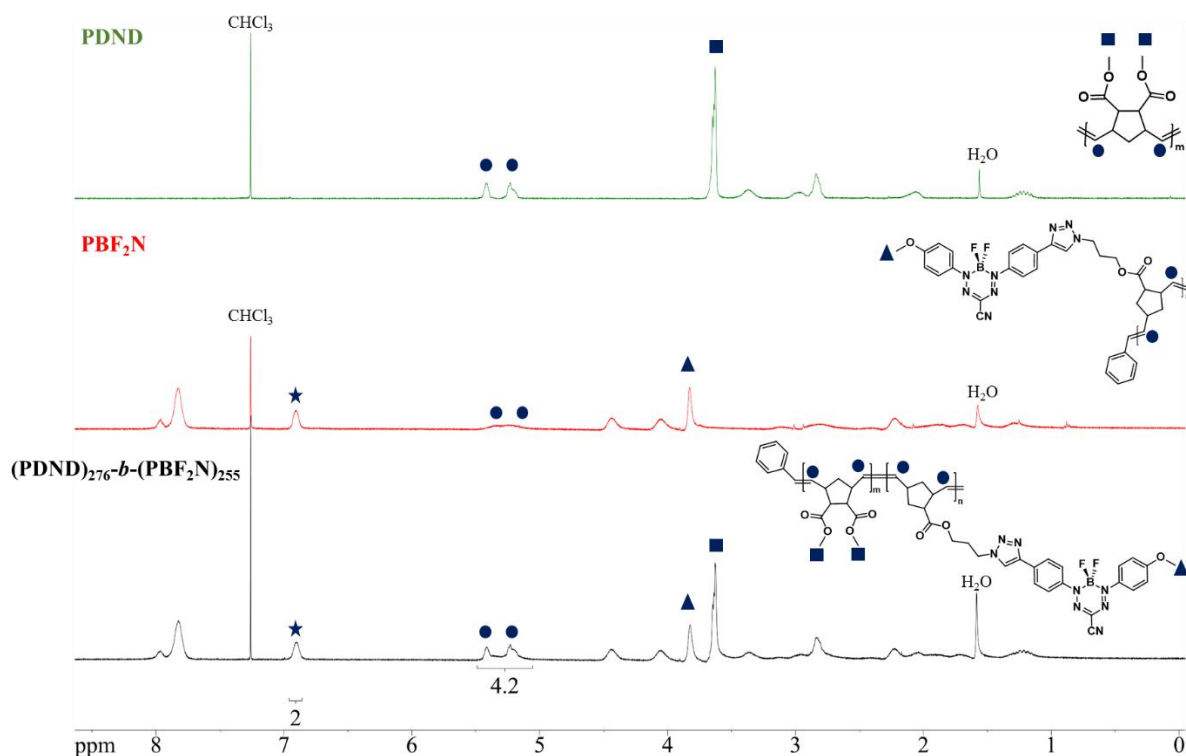


Figure 3.6. Overlay of ^1H NMR spectra of compound **PDND** (green), **PBF₂N** (red) and polymer **(PDND)₂₇₆-b-(PBF₂N)₂₅₅** (black) in CDCl_3 . The circles represent the new alkene protons found in the backbone of **(PDND)₂₇₆-b-(PBF₂N)₂₅₅**, the triangle represents the protons on the methoxy substituent of **PBF₂N**, the square represents the methyl groups on **PDND**, and the star represents two aryl protons on the **PBF₂N** subunit.

The number of repeating units for each block of **(PDND)_m-b-(PBF₂N)_n** were determined in two ways using GPC analysis in DMF (vs. polystyrene) and ^1H NMR spectroscopy. Method 1 involved the use f_{BF_2} found using ^1H NMR spectroscopy, and the M_n value found using GPC analysis. The following formula was used:

Block copolymer **(PDND)₂₇₆-b-(PBF₂N)₂₅₅**

$M_n = 204,300 \text{ g mol}^{-1}$ (determined by GPC)

n is mole fraction of **BF₂N** subunit =

$$\frac{n}{n+m} = 0.48 \text{ (based on } ^1\text{H NMR spectroscopy)} \quad 3.1$$

m is mole fraction of **DND** subunit =

$$\frac{m}{n+m} = 0.52 \text{ (based on } ^1\text{H NMR spectroscopy)} \quad 3.2$$

$$mMM_{\text{DND}} + nMM_{\text{BF}_2} = 204,300 \text{ g mol}^{-1} \quad 3.3$$

where: $MM_{\text{DND}} = 210.2265 \text{ g mol}^{-1}$ and $MM_{\text{BF}_2} = 572.3736 \text{ g mol}^{-1}$

Thus, using Equation 3.1 and 3.2 we know:

$$m = \frac{0.52}{0.48} n \quad 3.4$$

Substituting Equation 3.4 into Equation 3.3:

$$\frac{0.52}{0.48} n * MM_{\text{DND}} + nMM_{\text{BF}_2} = 204,300 \text{ g mol}^{-1} \quad 3.5$$

$$n = \frac{204,300 \text{ g mol}^{-1}}{\left(\frac{0.52}{0.48}\right) * MM_{\text{DND}} + MM_{\text{BF}_2}} \quad 3.6$$

Therefore:

$$n = 255$$

Substituting n into Equation 3.4 results in:

$$m = 276$$

Therefore, the degree of polymerization (DP_n) for each subunit within block copolymer **(PDND)_{276-b-(PBF₂N)₂₅₅}** is 276 units for the **DND** portion, and 255 for the **BF₂** portion.

Method 2 is more common, and involves finding the DP_n of the **DND** portion of the block copolymer by determining the M_n for an aliquot of the first block (**PDND**), and dividing it by the molar mass of **DND** ($38,820 \text{ g mol}^{-1}/210.23 \text{ g mol}^{-1}$). This resulted in a number average DP_n of 185 units of **DND** in **PDND**. As previously discussed, $^1\text{H NMR}$ spectroscopy revealed

that the ratio of **DND** subunit to **BF₂N** subunit in the block copolymer was 1.1 to 1. Using this information, the number of subunits of **BF₂N** in the second block (**PBF₂N**) was found to be 168. The M_n of the second block (**PBF₂N**) can then be found by multiplying the DP_n by the molar mass of **BF₂N** ($168 * 572.3736 \text{ g mol}^{-1}$), which resulted in a molar mass of $96,159 \text{ g mol}^{-1}$. Using this information, the M_n of **(PDND)_{276-b-(PBF₂N)₂₅₅}** was found to be $134,979 \text{ g mol}^{-1}$ ($38,820 \text{ g mol}^{-1} + 96,159 \text{ g mol}^{-1}$). The results for both methods are summarized in Table 3.3. Although Method 2 is the most widely used, Method 1 was the only way the degree of polymerization for the random copolymers could be calculated. Therefore, for consistency, the DP_n for both block and random copolymers will be reported using Method 1.

Table 3.3. Summary of molecular weight data determined for the first block and diblock copolymers **(PDND)_{276-b-(PBF₂N)₂₅₅}** ($f_{BF_2} = 0.48$), **(PDND)_{355-b-(PBF₂N)₅₃}** ($f_{BF_2} = 0.13$) and **(PDND)_{266-b-(PBF₂N)₂₀}** ($f_{BF_2} = 0.07$).

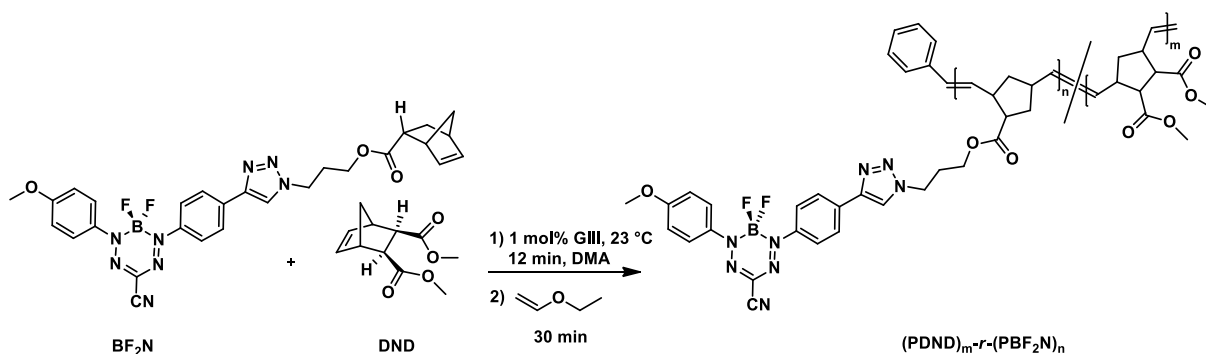
$f_{BF_2}^a$	Method 1					Method 2					
	(PDND)_{m-b-(PBF₂N)_n}					PDND_m				(PDND)_{m-b-(PBF₂N)_n}	
	M_n^b	$m^{a,b}$	$n^{a,b}$	M_w^b	\bar{D}^b	M_n^b	m^b	M_w^b	\bar{D}^b	$n^{a,b}$	$M_n^{a,b}$
0.48	204,300	276	255	295,400	1.45	38,820	185	43,070	1.11	168	134,980
0.13	104,000	355	53	126,300	1.21	54,910	261	62,670	1.14	38	76,580
0.07	66,040	266	20	76,370	1.16	42,810	204	48,610	1.14	16	52,140

^aDetermined from the relative integrations of unique ¹H NMR spectroscopic signals. ^bDetermined by GPC analysis (vs. polystyrene standards).

3.2.3 Synthesis of Random Copolymers Containing BF₂ Complexes

Random copolymers of monomers **DND** and **BF₂N** were synthesized by dissolving **DND** and **BF₂N** in dry, degassed DMA at a total monomer concentration of 50 mg mL^{-1} , at $23 \text{ }^\circ\text{C}$, and adding 1 mol % of GIII catalyst. The reaction mixture was stirred for 12 min and then quenched with ethyl vinyl ether (Scheme 3.7). The targeted DP_n of the three random copolymers that were synthesized was 100 (1 mol% GIII). Each random copolymer differed by the f_{BF_2} within the polymer, and this was calculated using the ¹H NMR methods described above for the block copolymers. ¹H NMR spectroscopy confirmed the synthesis of the copolymers (e.g., Figure 3.7). Two broad signals pertaining to the alkene protons found in the backbone of the random copolymers were found in the range of 5.40–5.23 ppm (circles). The methoxy group of the

BF₂N unit of the polymer was found as a broad singlet at 3.88 ppm (triangle), and the methyl groups pertaining to the **DND** portion of the polymer were found as one broad singlet at 3.62 ppm (square). For random copolymer **(PDND)_{316-r}-(PBF₂)₃₁₆** the ratio of **BF₂N** subunit to **DND** subunit was 1.0:1.0, and thus $f_{\text{BF}_2} = 0.50$. The BF₂ moiety remained intact, which was made evident by looking at the broad signal at -133.8 ppm in the ¹⁹F NMR spectrum, and the broad 1:2:1 triplet at -0.7 ppm in the ¹¹B NMR spectrum (Figure A.3.16). GPC (vs. polystyrene standards) was used to find the M_n, M_w, and *D* of the remaining random copolymers, and Method 1 was used to find the DP_n. Cyclic voltammetry experiments were performed in CH₂Cl₂ and showed that the polymers exhibited two reversible one-electron reduction waves to yield first the poly radical anion, and then the poly dianion (Figure A.3.17).



Scheme 3.7. Synthesis for random block copolymers **(PDND)_{m-r}-(PBF₂N)_n**. *m* represents the DP_n for the **DND** subunit, and *n* represents the DP_n for the **BF₂N** subunit.

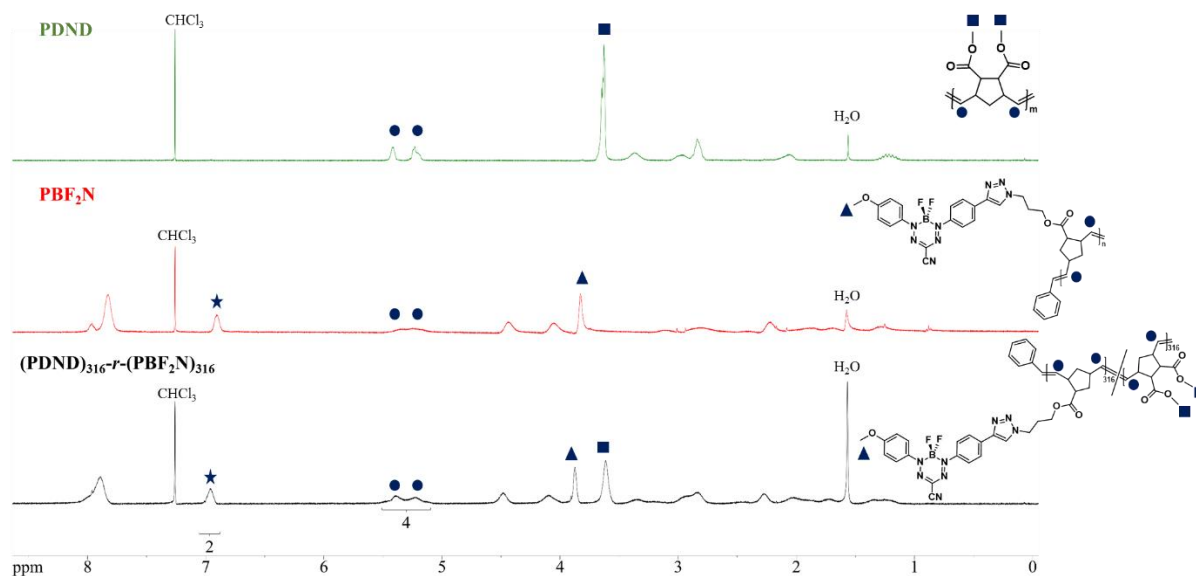


Figure 3.7. ^1H NMR spectra of $(\text{PDND})_{316}\text{-}r\text{-}(\text{PBF}_2\text{N})_{316}$ in CDCl_3 . The circles represent the alkene protons found in the backbone of the polymer, the triangle represents the protons on the methoxy group on the PBF_2N subunit, and the square represents the methyl groups on the DND subunit. The star represents two aryl protons on the PBF_2N subunit.

Table 3.4. Summary of molecular weight data for random copolymers $(\text{PDND})_{316}\text{-}r\text{-}(\text{PBF}_2\text{N})_{316}$ ($f_{\text{BF}_2} = 0.50$), $(\text{PDND})_{292}\text{-}r\text{-}(\text{PBF}_2\text{N})_{52}$ ($f_{\text{BF}_2} = 0.15$) and $(\text{PDND})_{298}\text{-}r\text{-}(\text{PBF}_2\text{N})_{26}$ ($f_{\text{BF}_2} = 0.08$).

$f_{\text{BF}_2}^{\text{a}}$	$(\text{PDND})_{\text{m}}\text{-}r\text{-}(\text{PBF}_2\text{N})_{\text{n}}$			$(\text{PDND})_{\text{m}}\text{-}r\text{-}(\text{PBF}_2\text{N})_{\text{n}}$	
	M_{n}^{b}	M_{w}^{b}	\mathcal{D}^{b}	m^{c}	n^{c}
0.50	247,300	335,200	1.36	316	316
0.15	90,890	107,000	1.18	292	52
0.08	77,490	88,820	1.15	298	26

^aDetermined by relative integrations of ^1H NMR spectroscopic signals. ^bDetermined by GPC analysis (vs. polystyrene standards). ^cDetermined by relative integrations of ^1H NMR spectroscopic signals and M_{n} from GPC.

The GPC data shows that as the f_{BF_2} increases the M_{n} of the polymer will also increase which makes sense since the BF_2N subunit has a molar mass that is 2.7 times greater than that of the DND subunit. Comparison of the GPC traces of all three random copolymers and PDND ($f_{\text{BF}_2} = 0.0$) also displays this trend (Figure 3.8). The dispersity values for the all three random copolymers range from 1.15–1.36, owing to the controlled polymerization of these polymers.

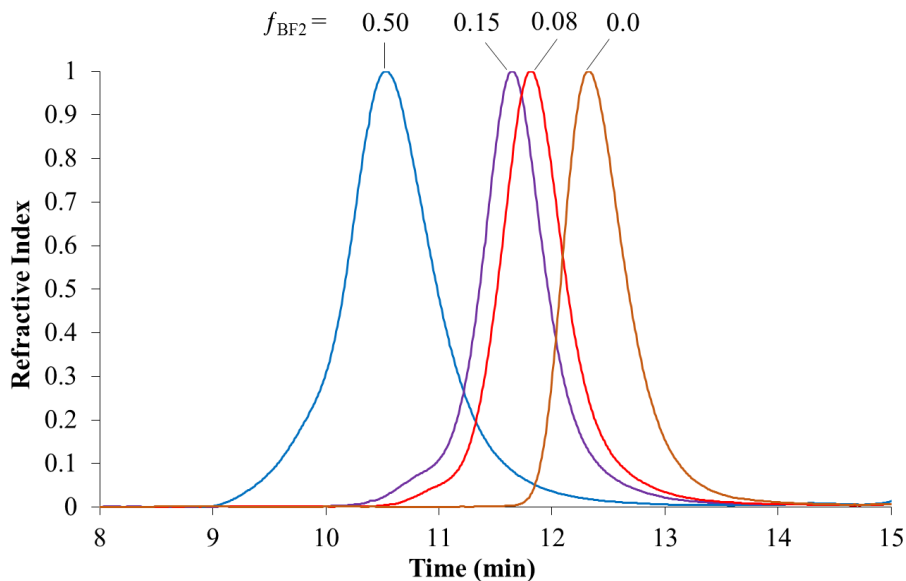


Figure 3.8. GPC traces (in DMF) of polymer **PDND** ($f_{\text{BF}_2} = 0.0$, dark yellow) and random copolymers **(PDND)₃₁₆-*r*-(PBF₂)₃₁₆** ($f_{\text{BF}_2} = 0.50$), **(PDND)₂₉₂-*r*-(PBF₂N)₅₂** ($f_{\text{BF}_2} = 0.15$) and **(PDND)₂₉₈-*r*-(PBF₂N)₂₆** ($f_{\text{BF}_2} = 0.08$).

3.2.4 Thermal Properties

Thermal gravimetric analysis (TGA) of the block and random copolymers, along with **PBF₂N** and **PDND** was used to determine the temperature corresponding to the onset of decomposition (2% mass loss, O.D.) for each polymer as well as to study their degradation over a range of temperatures (25 – 1000 °C). In general, **PDND** was found to be more thermally stable (O.D. = 155 °C) than **PBF₂N** (O.D. = 136 °C) as it survives a higher temperature range before losing a significant amount of its mass (Figure 3.9 and 3.10). The block (Figure 3.9) and random (Figure 3.10) copolymers followed a similar trend whereby thermal stability increased as f_{BF_2} decreased.

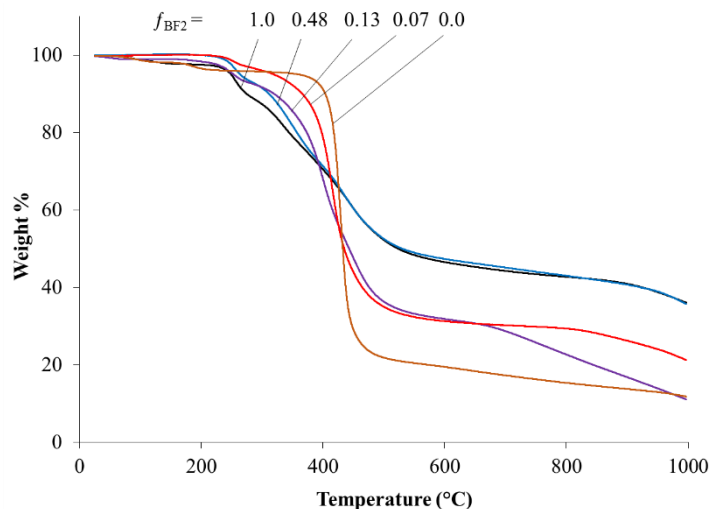


Figure 3.9. TGA graphs of **PBF₂N** ($f_{\text{BF}_2} = 1.0$, black), **(PDND)_{276-b}-(PBF₂N)₂₅₅** ($f_{\text{BF}_2} = 0.48$, blue), **(PDND)_{355-b}-(PBF₂N)₅₃** ($f_{\text{BF}_2} = 0.13$, purple), **(PDND)_{266-b}-(PBF₂N)₂₀** ($f_{\text{BF}_2} = 0.07$, red), and **PDND** ($f_{\text{BF}_2} = 0.0$, dark yellow).

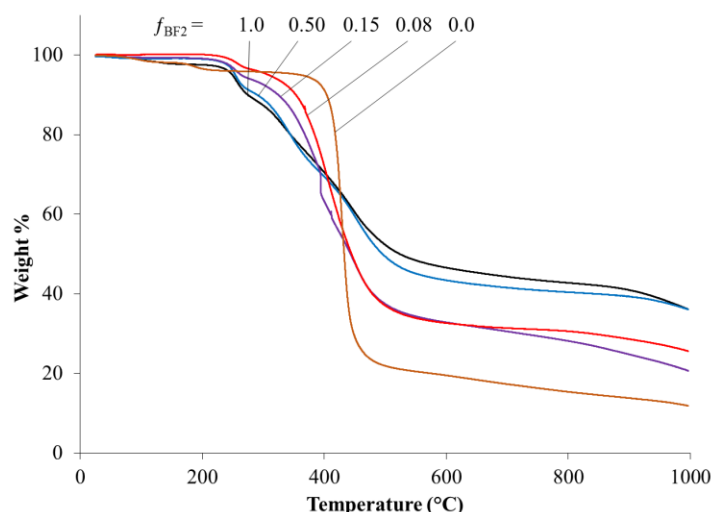


Figure 3.10. TGA graphs of **PBF₂N** ($f_{\text{BF}_2} = 1.0$, black), **(PDND)_{316-r}-(PBF₂N)₃₁₆** ($f_{\text{BF}_2} = 0.50$, blue), **(PDND)_{292-r}-(PBF₂N)₅₂** ($f_{\text{BF}_2} = 0.15$, purple), **(PDND)_{298-r}-(PBF₂N)₂₆** ($f_{\text{BF}_2} = 0.08$, red), and **PDND** ($f_{\text{BF}_2} = 0.0$, dark yellow).

Differential scanning calorimetry (DSC) studies of all of the polymers described in this work revealed their glass transition temperatures (T_g). **PDND** ($f_{\text{BF}_2} = 0.0$) was found to have a T_g of 83 °C while **PBF₂N** ($f_{\text{BF}_2} = 1.0$) had a T_g of 136 °C. When looking at the DSC traces for the block copolymers they revealed two T_g s, which proves we have made block copolymers (except for **(PDND)_{266-b}-(PBF₂N)₂₀** ($f_{\text{BF}_2} = 0.07$) (Figure 3.11)).²⁴ This behaviour is likely due to the small percentage of the **PBF₂N** block, making the transition difficult to observe. The first T_g corresponds to the transition from the glassy state to the rubbery state of the **PDND**

portion of the block copolymer. The temperatures at which this transition occurs ranged from 81–85 °C. The second T_g corresponds to the change in state from glassy to rubbery for the **PBF₂N** block portion. As the f_{BF_2} increases the temperature at which this transition occurred also increased. This second transition was not observed for **(PDND)_{266-b-(PBF₂N)₂₀}** ($f_{\text{BF}_2} = 0.07$) since the fraction of **BF₂N** units was small. DSC traces for the random copolymers reveal only one T_g , which suggests that we have synthesized random copolymers, and also supports the idea that polymerization of both monomers occurs at the same rate (Figure 3.12). It was observed that as the f_{BF_2} increases, the T_g also increased. The first derivative of all DSC traces was also plotted so that the transitions could be seen more clearly (Figure 3.11b and Figure 3.12b). No melt or crystallization events were observed.

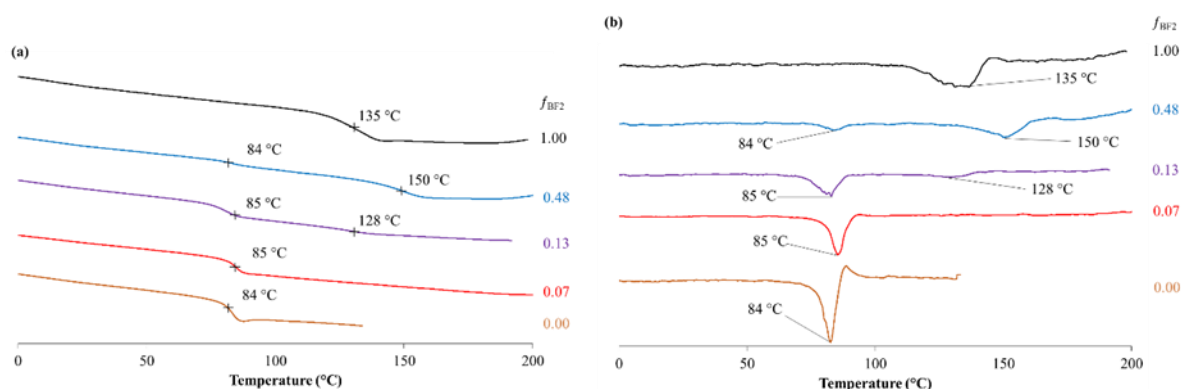


Figure 3.11. DSC traces (a) and first derivative traces (b) for polymer **PDND** ($f_{\text{BF}_2} = 0.0$, dark yellow), **PBF₂N** ($f_{\text{BF}_2} = 1.0$, black), and block copolymers **(PDND)_{276-b-(PBF₂N)₂₅₅}** ($f_{\text{BF}_2} = 0.48$, blue), **(PDND)_{355-b-(PBF₂N)₅₃}** ($f_{\text{BF}_2} = 0.13$, purple) and **(PDND)_{266-b-(PBF₂N)₂₀}** ($f_{\text{BF}_2} = 0.07$, red). Decomposition point of **PDND** was lower than the other polymers, and thus DSC could only be done up to 130 °C.

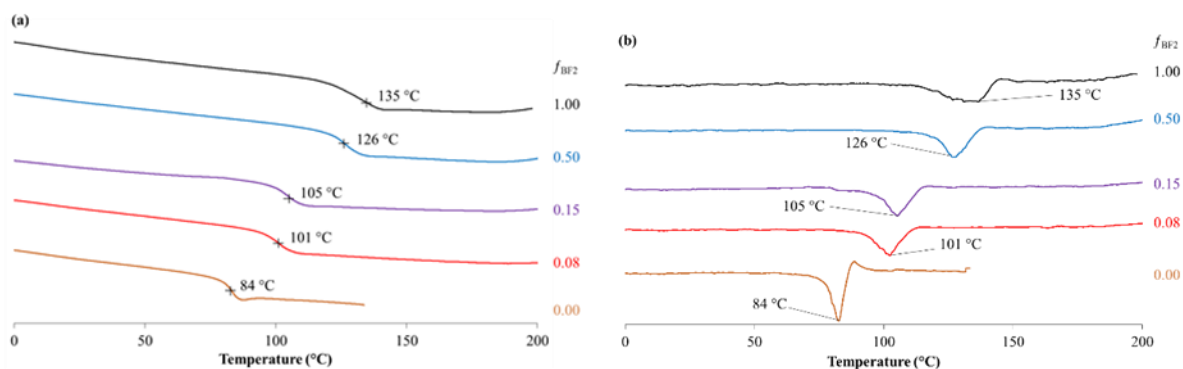


Figure 3.12. DSC traces (a) and first derivative traces (b) for polymer **PDND** ($f_{\text{BF}_2} = 0.0$, dark yellow), **PBF₂N** ($f_{\text{BF}_2} = 1.0$, black), and random copolymers **(PDND)_{316-r-(PBF₂N)₃₁₆}** ($f_{\text{BF}_2} = 0.50$, blue), **(PDND)_{292-r-(PBF₂N)₅₂}** ($f_{\text{BF}_2} = 0.15$, purple) and **(PDND)_{298-r-(PBF₂N)₂₆}** ($f_{\text{BF}_2} = 0.08$, red).

3.2.5 Spectroscopic Properties

The spectroscopic properties of **BF₂N** and all of the polymers synthesized in this study are summarized in Table 3.5. Figure 3.13 and 3.14 display the UV-vis absorption and emission spectra for selected compounds. Figure 3.15 displays the Φ_F for the random copolymers, **BF₂N** and **PBF₂N**. All of the spectroscopic data were collected in CH₂Cl₂.

Table 3.5. Spectroscopic properties of **BF₂N**, **PBF₂N**, and all block copolymers (**PDND**)_m-**b**-(**PBF₂N**)_n and random copolymers (**PDND**)_m-**r**-(**PBF₂N**)_n.

	f_{BF_2}	λ_{max} (nm)	ϵ (M ⁻¹ cm ⁻¹)	λ_{em} (nm)	Φ_F (%) ^a	ν_{ST} (nm)	ν_{ST} (cm ⁻¹)
BF₂N	1	561	35,300	663	35	102	2742
PBF₂N	1	559	27,500	663	12	104	2806
(PDND) _m - b - (PBF₂N) _n	0.48	559	-	667	2	108	2897
b - (PBF₂N) _n	0.13	559	-	665	3	106	2851
(PDND) _m - r - (PBF₂N) _n	0.50	558	-	664	8	106	2861
r - (PBF₂N) _n	0.15	560	-	664	19	104	2797
(PBF₂N) _n	0.08	561	-	664	26	103	2765

^aQuantum yields were measured according to published protocol²⁵ using ruthenium tris(bipyridine) hexafluorophosphate as a relative standard²⁶ and corrected for wavelength-dependent detector sensitivity (Figure A2.21).

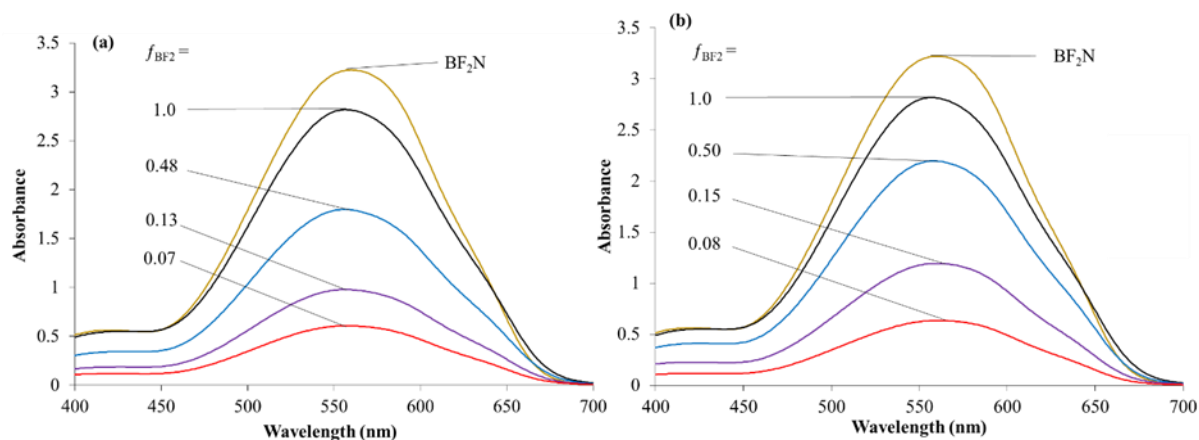


Figure 3.13. UV-vis absorption spectra of **BF₂N** (dark yellow) and **PBF₂N** ($f_{\text{BF}_2} = 1.0$, black) (a, b), and block copolymers (**PDND**)_m-**b**-(**PBF₂N**)_n (a), and random copolymers (**PDND**)_m-**r**-(**PBF₂N**)_n (b). All spectra were recorded in CH₂Cl₂ using 0.00005 g mL⁻¹ solutions.

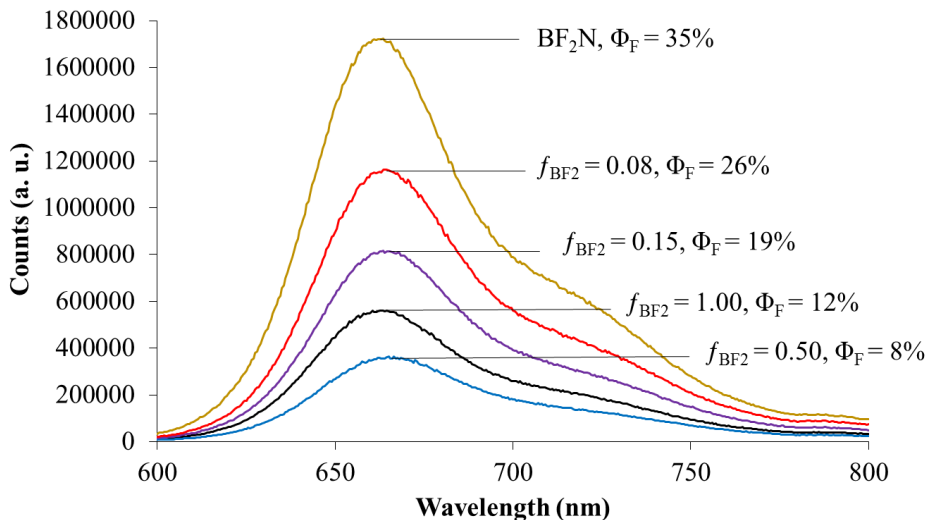


Figure 3.14. Emission spectra for BF_2N (dark yellow), PBF_2N ($f_{\text{BF}_2} = 1.0$, black) and random copolymers $(\text{PDND})_{316}\text{-}r\text{-}(\text{PBF}_2\text{N})_{316}$ ($f_{\text{BF}_2} = 0.50$, blue), $(\text{PDND})_{292}\text{-}r\text{-}(\text{PBF}_2\text{N})_{52}$ ($f_{\text{BF}_2} = 0.15$, purple) and $(\text{PDND})_{298}\text{-}r\text{-}(\text{PBF}_2\text{N})_{26}$ ($f_{\text{BF}_2} = 0.08$, red) (b). All spectra were recorded in CH_2Cl_2 and their absorbance in the UV-vis region was approximately 0.1.

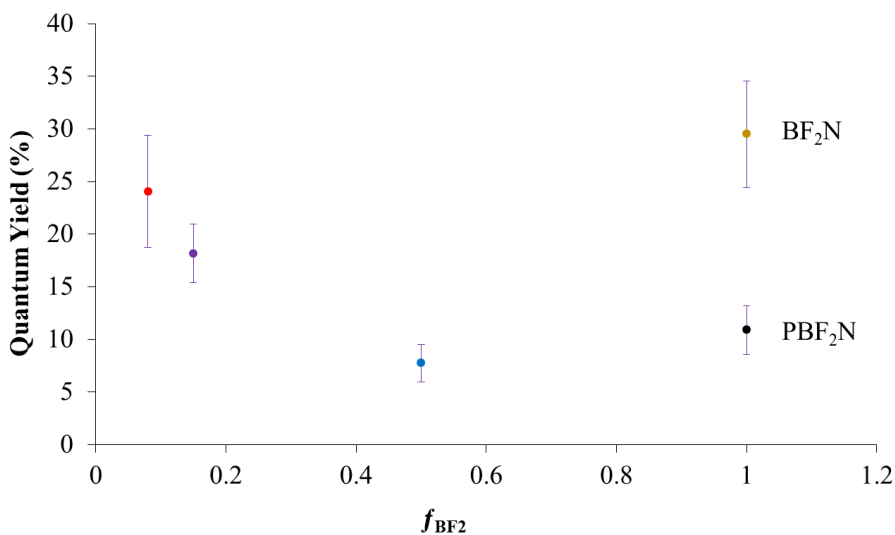


Figure 3.15. Summary of the quantum yields of fluorescence (red dots) for the random copolymers $(\text{PDND})_m\text{-}r\text{-}(\text{PBF}_2\text{N})_n$, as well as for BF_2N (defined as $f_{\text{BF}_2} = 1.0$), and PBF_2N ($f_{\text{BF}_2} = 1.0$). Errors bars associated with the quantum yields calculated were placed by using the standard deviation for three repeated experiments of each. Spectra were recorded in CH_2Cl_2 and their maximum absorbance in solution was approximately 0.1.

These results reveal that the polymers have a λ_{max} from 558–561 nm and a λ_{em} from 663–667 nm. The UV-vis absorption spectra were recorded in $0.00005 \text{ g mL}^{-1}$ solutions in CH_2Cl_2 and show that as the f_{BF_2} in the polymer increases, the λ_{max} at approximately 560 nm also increases (Figure 3.13). The Stokes' shifts for all polymers ranged from 103–106 nm. The Φ_F for the

block copolymers ranged from 1–3%, and were essentially non-emissive. In the case of the random copolymers, it was observed that as the f_{BF_2} decreased, the Φ_{F} increased. Figure 3.15 summarizes the average of the Φ_{F} found for three separate runs; error bars were included and calculated using the standard deviation from three unique measurements. Examining this graph reveals a clear correlation between the Φ_{F} and the average distance between **BF₂N** subunits in the polymer. For **PBF₂N**, for example, the quantum yield is low (12%) compared to **BF₂N** monomer (35%) and this is most likely due to the close proximity of the **BF₂N** units within the polymer resulting in reabsorption of emitted photons, due to the overlap between the absorption and emission spectra. However, as the f_{BF_2} decreases in the polymer, the average distance between each **BF₂N** subunit increases, and thus reabsorption from nearby **BF₂N** units is less likely. This results in an increase in Φ_{F} , with **(PDND)_{298-r}-(PBF₂N)₂₆** ($f_{\text{BF}_2} = 0.08$) having the highest Φ_{F} of 26%. Another argument for the decrease in Φ_{F} of polymers relative to monomer **BF₂N** could be π -stacking of **BF₂N** subunits in the polymer solution.²⁷ However, solutions were prepared to have absorbance values of approximately 0.1, and thus the amount of **BF₂N** in solution was approximately the same for all. Also, π -stacking in solution is usually accompanied by a red-shift in the absorbance and emission maxima, which was not observed for these systems.²⁸⁻²⁹ Thus, π -stacking is likely not occurring. Similar approaches have been employed in order to increase the quantum yield of fluorescence of polymers.^{19, 30-31}

3.3. Conclusions

ROMP was used to synthesize a variety of polymers containing 3-cyanoformazanate **BF₂** complexes (**PBF₂N**) and *cis*-dimethyl-5-norbornene-*exo*-2,3-dicarboxylate polymer (**PDND**). Homopolymers, block copolymers and random copolymers were characterized using ¹H NMR, ¹⁹F NMR, and ¹¹B NMR spectroscopy, UV-vis absorption/emission spectroscopy, IR spectroscopy, GPC, TGA, and DSC. In order to find the ratio of **BF₂N** and **DND** subunit in the copolymers, ¹H NMR spectroscopy was used where integrations of the backbone alkene protons and 2 aryl protons on the **BF₂N** subunit were used. GPC was used in order to determine the time at which the polymerizations of **PBF₂N** and **PDND** were finished, as well as to find M_n , M_w , and D values for all polymers. For the block copolymers, it was found that the M_n increased as the f_{BF_2} increased since more **BF₂N** was allowed to grow off of the initial **PDND** chain. For the random copolymers, it was found that as the f_{BF_2} increased the M_n also increased;

this is because the BF_2 portion of the polymer is much heavier than the **DND**. TGA was used to determine the decomposition point of all polymers. DSC was used to find the T_g of all polymers, and it was found that the block copolymers possessed two distinct T_g s, one for the **PDND** block, and the other for the **PBF₂N** block. The random copolymers possessed only one T_g ; this T_g increased as f_{BF_2} increased. All polymers showed strong λ_{max} ranging from 558–561 nm in CH_2Cl_2 and λ_{em} from 663–667 nm. The absorbance of all the polymers increased as the f_{BF_2} increased. The Φ_F for the random copolymers increased as f_{BF_2} decreased; this was attributed to the fact that in the chain with less **BF₂N** subunits, each **BF₂N** subunit would be further apart from the other, minimizing self-absorption. In developing this random copolymerization process, we have also created a dilution strategy allowing for emission intensity of BF_2 formazanate polymers to be maximized. It was also concluded that no π -stacking was occurring due to the absence of a red-shift in the absorbance and/or emission spectra. The block copolymers had a low Φ_F and were essentially non-emissive. **PBF₂N**, **(PDND)_{276-b}-(PBF₂N)₂₅₅**, and **(PDND)_{316-r}-(PBF₂N)₃₁₆** were found to be redox active, and exhibited two reversible one-electron reduction waves.

3.4. Experimental

3.4.1 General Considerations

Reactions and manipulations were carried out under a nitrogen atmosphere using standard Schlenk techniques unless otherwise stated. Solvents were obtained from Caledon Laboratories, dried using an Innovative Technologies Inc. solvent purification system, collected under vacuum, and stored under a nitrogen atmosphere over 4 Å molecular sieves. All other reagents were purchased from Sigma Aldrich, Alfa Aesar or TCI America and used as received.

NMR spectra were recorded on a 400 MHz (^1H : 399.8 MHz, ^{11}B : 128.3 MHz, ^{19}F : 376.1 MHz, ^{13}C : 100.5 MHz) or 600 MHz (^{13}C : 150.7 MHz) Varian INOVA instruments. ^1H NMR spectra were referenced to residual CHCl_3 at 7.27 ppm and ^{13}C NMR spectra were referenced to CDCl_3 at 77.00 ppm. ^{11}B NMR spectra were referenced internally to $\text{BF}_3\cdot\text{OEt}_2$ at 0 ppm. ^{19}F NMR spectra were referenced internally to CFCl_3 at 0 ppm. UV-vis absorption spectra were recorded using a Cary 5000 Scan instrument using standard quartz cells (1 cm path length) with a scan

range of 200 to 800 nm. Emission spectra were recorded using a Photon Technology International QM-4 SE spectrofluorometer. Emission quantum yields were estimated relative to $[\text{Ru}(\text{bpy})_3][\text{PF}_6]_2$ and corrected for wavelength dependent detector sensitivity (Figure C1).²⁵ FT-IR spectra were recorded using a Perkin Elmer Spectrum Two FT-IR spectrometer.

3.4.2 Electrochemical Methods

Cyclic voltammetry experiments were performed with a Bioanalytical Systems Inc. (BASi) Epsilon potentiostat and analyzed using BASi Epsilon software. Typical electrochemical cells consisted of a three-electrode setup including a glassy carbon working electrode, platinum counter electrode, and silver *pseudo* reference electrode. Experiments were run at 250 mV s^{-1} in degassed CH_2Cl_2 solutions of the analyte ($\sim 1 \text{ mM}$) and electrolyte ($0.1 \text{ M } [n\text{Bu}_4\text{N}][\text{PF}_6]$). Cyclic voltammograms were internally referenced against the ferrocene/ferrocenium redox couple ($\sim 1 \text{ mM}$ internal standard) and corrected for internal cell resistance using the BASi Epsilon software.

3.4.3 Gel Permeation Chromatography

GPC was carried out at a flow rate of 1 mL min^{-1} in DMF with 10 mM LiBr and $1\% \text{ (v/v) Et}_3\text{N}$ added at a regulated temperature of $85 \text{ }^\circ\text{C}$ using a Waters 515 pump, equipped with a Wyatt Optilab REx detector and two PLgel $5 \text{ }\mu\text{m}$ mixed-D ($300 \text{ mm} \times 7.5 \text{ mm}$) columns from Polymer Laboratories connected in series. Calibration was performed using monodisperse polystyrene standards supplied by Polymer Lab.

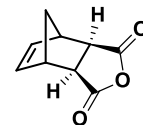
3.4.4 Thermal Analysis

Thermal degradation studies were performed using a TA Instruments Q50 TGA. The samples were placed in a platinum pan and heated at a rate of $10 \text{ }^\circ\text{C min}^{-1}$ from $25 \text{ }^\circ\text{C}$ to $1000 \text{ }^\circ\text{C}$ under a flow of nitrogen (100 mL min^{-1}). Glass transition temperatures (T_{gs}) were determined using Differential Scanning Calorimetry (DSC) on a TA Instruments DSC Q2000. The polymer samples were placed in an aluminum Tzero pan and heated to varying temperature ranges at $10 \text{ }^\circ\text{C min}^{-1}$ under a flow of nitrogen (50 mL min^{-1}) and cooled down to $-75 \text{ }^\circ\text{C}$ at $10 \text{ }^\circ\text{C min}^{-1}$, before the sample underwent two more heating/cooling cycles. T_{gs} were determined from the third heating/cooling cycle.

3.4.5 Synthetic Procedures

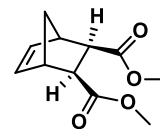
***Cis*-5-norbornene-*exo*-2,3-dicarboxylic anhydride (*exo*-NDCAn)**

***exo*-NDCAn** was synthesized according to a modified version of a procedure previously reported by Alfred *et al.*²¹ *Cis*-5-norbornene-*endo*-2,3-dicarboxylic anhydride ***endo*-NDCAn** (20.0 g, 122 mmol) was stirred at 210 °C for 2 h. The solution was cooled to 80 °C and 20 mL of toluene were added, which allowed white crystals to crash out. The resulting white crystals were isolated by vacuum filtration and purified by flash chromatography (1:1 *n*-hexanes:EtOAc, silica gel) where the first fraction contained the desired product. Removal of the solvent *in vacuo* yielded ***exo*-NDCAn** as a white solid. Yield = 3.11 g, 15%. ¹H NMR (399.8 MHz, CDCl₃): δ 6.34 (br s, 2H, =CH), 3.46 (br s, 2H, CH), 3.00 (br s, 2H, CH), 1.67 (d, ³J_{HH} = 10 Hz, 1H, CH₂), 1.45 (d, ³J_{HH} = 10 Hz, 1H, CH₂). These data are consistent with previous reports.²¹



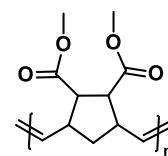
***Cis*-dimethyl-5-norbornene-*exo*-2,3-dicarboxylate (DND)**

***Cis*-dimethyl-5-norbornene-*exo*-2,3-dicarboxylate (DND)** was synthesized by a modified version of a procedure reported by Hennis *et al.*²² In air, ***exo*-NDCAn** (2.47 g, 15.0 mmol) was dissolved in 5.5 mL of MeOH and 0.25 mL of 12 M HCl. This solution was refluxed for 2 h. After cooling to room temperature, the solution was concentrated *in vacuo* and then washed with 2 x 25 mL of a saturated solution of NaHCO₃ and 1 x 25 mL of H₂O and dried over MgSO₄, gravity filtered and concentrated *in vacuo* to afford monomer **DND** as a white solid. Yield = 1.83 g, 58%. ¹H NMR (399.8 MHz, CDCl₃): δ 6.21 (br s, 2H, =CH), 3.66 (br s, 6H, CH₃), 3.10 (m, 2H, CH), 2.63 (m, 2H, CH), 2.12 (d, ³J_{HH} = 9 Hz, 1H, diastereotopic CH₂), 1.51 (d, ³J_{HH} = 9 Hz, 1H, diastereotopic CH₂). These data are consistent with previous reports.²²



Representative ROMP of DND

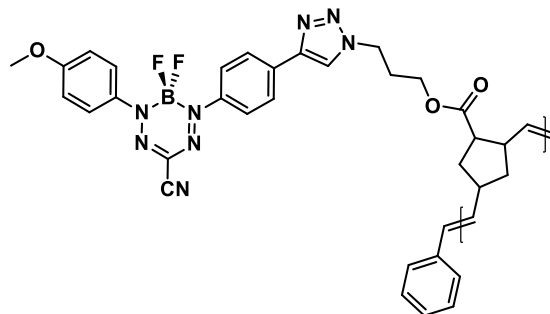
Monomer **DND** (0.100 g, 0.476 mmol) was dissolved in 1.9 mL of dry and degassed (*via* three freeze-pump-thaw cycles) DMA, and the solution was stirred at 23 °C for 15 min. Meanwhile, GIII (0.0126 g, 0.0142 mmol) was dissolved in 0.3 mL of dry and degassed (*via* three freeze-pump-thaw cycles) DMA. A 0.1 mL



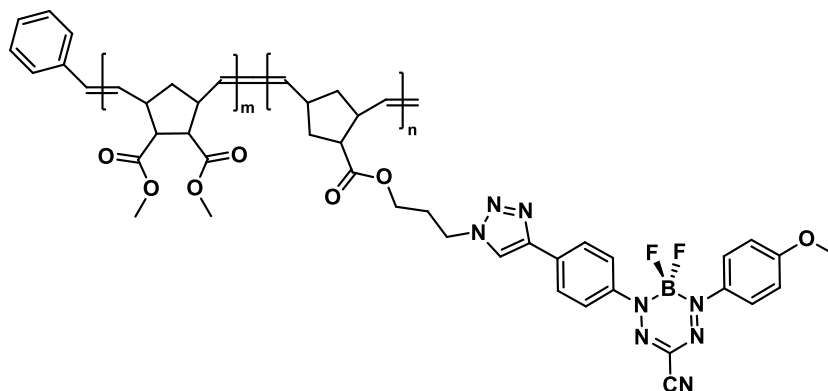
portion of the solution of GIII (0.0042 g, 1 mol %) was then added to the solution of monomer **DND** and stirred at 23 °C for 6 min. After 6 min, ethyl vinyl ether (0.857 g, 0.62 mL, 11.9 mmol) was added and the solution was stirred at 23 °C for 30 min. The product was precipitated from pentane, isolated by centrifugation, and dried at 23 °C *in vacuo* for 16 h to afford **PDND** as a white solid. Yield = 0.075 g, 75%. ¹H NMR (399.8 MHz, CDCl₃): δ 5.42 and 5.24 (br m, 2H, =CH), 3.64 (br s, 6H, 2 x OCH₃), 3.38 (br s, 1H, CH), 2.98 (br m, 1H, CH), 2.85 (br m, 2H, 2 x CH), 2.07 (br m, 1H, diastereotopic CH₂), 1.23 (br m, 1H, diastereotopic CH₂). GPC: M_n = 38820 g mol⁻¹, M_w = 43070 g mol⁻¹, *D* = 1.11. These data are consistent with previous reports.²⁷

Representative polymerization of BF₂N

Monomer **BF₂N** (0.050 g, 0.087 mmol) was dissolved in 1.9 mL of dry and degassed (*via* three freeze-pump-thaw cycles) DMA, and the solution was stirred at 23 °C for 15 min. Meanwhile, GIII (0.003 g, 1 mol %) was dissolved in 0.3 mL of dry and degassed (*via* three freeze-pump-thaw cycles) DMA. A 0.1 mL portion of the solution of GIII (0.001 g, 1 mol %) was then added to the solution of monomer **BF₂N** and stirred at 23 °C for exactly 1 h. After 1 h, ethyl vinyl ether (0.157 g, 2.18 mmol) was added and the solution was stirred at 23 °C for 30 min. The resulting dark-purple solution was purified by flash chromatography (THF, neutral alumina), and the product was precipitated from pentane, isolated by centrifugation, and dried at 23 °C *in vacuo* for 16 h to afford polymer **PBF₂N** as a purple solid. Yield = 0.030 g, 66%. ¹H NMR (399.8 MHz, CDCl₃): δ 7.97 (br s, 1 H, triazole CH), 7.84 (br s, 6 H, aryl CH), 6.92 (br s, 2 H, aryl CH), 5.35–5.25 (2 x br m, 2H, =CH), 4.45 (br s, 2H, CH₂), 4.07 (br s, 2H, CH₂), 3.84 (br s, 3H, OCH₃), 3.13 (br s, 1H, CH), 2.84 (br m, 2H, 2CH), 2.24 (br s, 2H, CH₂), 1.90 (br m, 2H, diastereotopic CH₂), 1.71 (br m, 1H, diastereotopic CH₂), 1.30 (br m, 1H, diastereotopic CH₂). ¹¹B NMR (128.3 MHz, CDCl₃): δ -0.8 (t, ¹J_{BF} = 30 Hz). ¹⁹F NMR (376.1 MHz, CDCl₃): δ -133.4 (br s). FT-IR (ATR): 3153 (w), 2952 (m), 2843 (m), 2243 (m), 1729 (s), 1598 (s), 1506 (m), 1343 (s), 1263 (s) cm⁻¹. UV-vis (CH₂Cl₂): λ_{max} = 555 nm (ε = 27,500 M⁻¹ cm⁻¹). GPC: M_n = 201,500 g mol⁻¹, M_w = 264,300 g mol⁻¹, *D* = 1.31.



Block Copolymers:



Representative procedure for the preparation of block copolymers (PDND)_m-b-(PBF₂N)_n

(PDND)₂₇₆-b-(PBF₂N)₂₅₅ ($f_{\text{BF}_2} = 0.48$)

Monomer **DND** (0.150 g, 0.713 mmol) was dissolved in 2.9 mL of dry and degassed (*via* three freeze-pump-thaw cycles) DMA, and the solution was stirred at 23 °C for 15 min. Meanwhile, **GIII** (0.019 g, 0.021 mmol) was dissolved in 0.3 mL of dry and degassed (*via* three freeze-pump-thaw cycles) DMA, and **BF₂N** (0.272 g, 0.475 mmol) was dissolved in 0.64 mL of dry and degassed (*via* three freeze-pump-thaw cycles) DMA. A 0.1 mL portion of the solution of **GIII** (0.0063 g, 1 mol %) was then added to the solution of monomer **DND** and stirred at 23 °C for 6 min. After 6 min, 1 mL of the reaction solution was removed and added to ethyl vinyl ether (0.429 g, 0.31 mL, 5.95 mmol) and stirred at 23 °C for 30 min. After removal of the 1 mL aliquot of the reactant solution, the **BF₂N** solution was added and stirred at 23 °C for 12 min. After 12 min, ethyl vinyl ether (0.857 g, 0.62 mL, 11.9 mmol) was added and the solution was stirred at 23 °C for 30 min. The aliquot removed after 6 min was clear and the product colourless and was precipitated from pentane, isolated by centrifugation, and dried *in vacuo* for 16 h to afford polymer **PDND** as a white solid. GPC: $M_n = 38,820 \text{ g mol}^{-1}$, $M_w = 43,070 \text{ g mol}^{-1}$, $D = 1.11$. The second solution was dark-purple, and the product was purified by precipitation into pentane, isolated by centrifugation and dried at 23 °C *in vacuo* for 16 h to afford polymer **(PDND)₂₇₆-b-(PBF₂N)₂₅₅** as a purple solid in quantitative yield. ¹H NMR (399.8 MHz, CDCl₃): δ 7.97 (br s, 1H, triazole CH), 7.83 (br m, 6H, aryl CH), 6.91 (br s, 2H, aryl CH), 5.42–5.24 (2 x br m, 4.2H, =CH), 4.44 (br s, 2H, CH₂), 4.07 (br s, 2H, CH₂), 3.83 (br s, 3H, OCH₃), 3.64 (br s, 6.6H, 2 x OCH₃), 3.38 (br s, 1H, CH), 3.13 (br s, 1H, CH),

2.98–2.85 (br m, 5H, *CH*), 2.25 (br s, 2H, *CH*₂), 2.05 (br m, 1H, diastereotopic *CH*₂), 1.92 (br m, 2H, diastereotopic *CH*₂), 1.72 (br m, 1H, diastereotopic *CH*₂), 1.34–1.16 (br m, 2H, diastereotopic *CH*₂). ¹¹B NMR (128.3 MHz, CDCl₃): δ –0.8 (t, ¹J_{BF} = 30 Hz). ¹⁹F NMR (376.1 MHz, CDCl₃): δ –133.4 (br s). FT-IR (ATR): 3138 (w), 2955 (m), 2849 (m), 2241 (m), 1733 (s), 1597 (s), 1505 (m), 1343 (s), 1261 (s) cm⁻¹. UV-vis (CH₂Cl₂): λ_{max} = 556 nm. GPC: M_n = 204,300 g mol⁻¹, M_w = 295,400 g mol⁻¹, Đ = 1.45.

(PDND)_{355-b}-(PBF₂N)₅₃ (*f*_{BF₂} = 0.13)

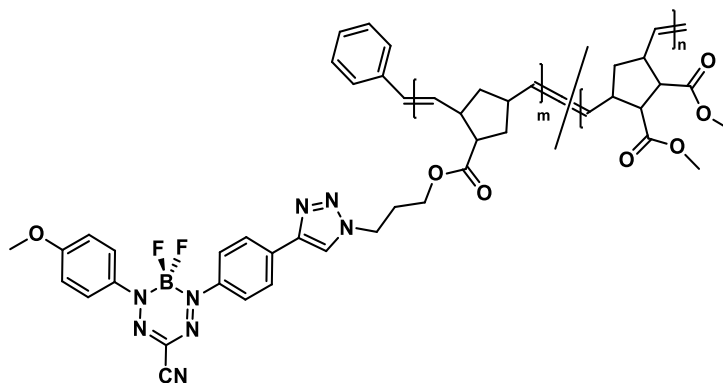
From monomer **DND** (0.250 g, 1.19 mmol) and **BF₂N** (0.109 g, 0.190 mmol). The aliquot removed at 6 min yielded polymer **PDND**. GPC: M_n = 54,910 g mol⁻¹, M_w = 62,670 g mol⁻¹, Đ = 1.14. The second solution afforded polymer **(PDND)_{355-b}-(PBF₂N)₅₃** in quantitative yield. ¹H NMR (399.8 MHz, CDCl₃): δ 7.97 (br s, 1 H, triazole *CH*), 7.85 (br s, 6 H, aryl *CH*), 6.93 (br s, 2 H, aryl *CH*), 5.43–5.24 (2 x br m, 15.8 H, =*CH*), 4.46 (br s, 2H, *CH*₂), 4.08 (br s, 2H, *CH*₂), 3.85 (br s, 3H, O*CH*₃), 3.64 (br s, 41H, O*CH*₃), 3.38 (br s, 7H, *CH*), 3.13 (br s, 1H, *CH*), 3.02–2.85 (br m, 21H *CH*), 2.25 (br s, 2H, *CH*₂), 2.07 (br m, 7H, diastereotopic *CH*₂), 1.91 (br m, 2H, diastereotopic *CH*₂), 1.70 (br m, 1H, diastereotopic *CH*₂), 1.33–1.14 (br m, 8H, diastereotopic *CH*₂). ¹¹B NMR (128.3 MHz, CDCl₃): δ –0.8 (t, ¹J_{BF} = 30 Hz). ¹⁹F NMR (376.1 MHz, CDCl₃): δ –133.5 (br s). FT-IR (ATR): 2989 (w), 2950 (m), 2849 (w), 2240 (s), 1733 (s), 1599 (s), 1436 (m), 1345 (s), 1263 (s) cm⁻¹. UV-vis (CH₂Cl₂): λ_{max} = 556 nm. GPC: M_n = 104,000 g mol⁻¹, M_w = 126,300 g mol⁻¹, Đ = 1.21.

(PDND)_{266-b}-(PBF₂N)₂₀ (*f*_{BF₂} = 0.07)

From monomer **DND** (0.300 g, 1.43 mmol) and **BF₂N** (0.068 g, 0.119 mmol). The aliquot removed at 6 min yielded polymer **PDND**. GPC: M_n = 42,810 g mol⁻¹, M_w = 48,610 g mol⁻¹, Đ = 1.13. The second solution afforded polymer **(PDND)_{266-b}-(PBF₂N)₂₀** in quantitative yield. ¹H NMR (399.8 MHz, CDCl₃): δ 7.98 (br s, 1 H, triazole *CH*), 7.89 (br s, 6 H, aryl *CH*), 6.96 (br s, 2 H, aryl *CH*), 5.43–5.24 (2 x br m, 27H, =*CH*), 4.47 (br s, 2H, *CH*₂), 4.09 (br s, 2H, *CH*₂), 3.88 (br s, 3H, O*CH*₃), 3.64 (br s, 73H, O*CH*₃), 3.38 (br s, 13H, *CH*), 3.13 (br s, 1H, *CH*), 3.02–2.85 (br m, 40 H, *CH*), 2.27 (br s, 2H, *CH*₂), 2.07 (br m, 13H, diastereotopic *CH*₂), 1.91 (br m, 2H, diastereotopic *CH*₂), 1.70 (br m, 1H, diastereotopic *CH*₂), 1.30–1.17 (br m, 14H, diastereotopic *CH*₂). ¹¹B NMR (128.3 MHz, CDCl₃): δ –0.7 (t, ¹J_{BF} = 30 Hz). ¹⁹F NMR

(376.1 MHz, CDCl₃): δ -134.0 (br s). FT-IR (ATR): 3000 (w), 2951 (m), 2848 (m), 1733 (s), 1599 (m), 1436 (s), 1362 (m), 1264 (s) cm⁻¹. UV-vis (CH₂Cl₂): λ_{\max} = 558 nm. GPC: M_n = 66,040 g mol⁻¹, M_w = 76,370 g mol⁻¹, D = 1.16.

Random Copolymers:



Representative procedure for the preparation of random copolymers (PDND)_m-b-(PBF₂N)_n

(PDND)_{316-r}-(PBF₂N)₃₁₆ ($f_{\text{BF}_2} = 0.50$)

Monomer **BF₂N** (0.150 g, 0.262 mmol) and **DND** (0.055g, 0.262 mmol) was dissolved in 3.9 mL of dry and degassed (*via* three freeze-pump-thaw cycles) DMA, and the solution was stirred at 23 °C for 15 min. Meanwhile, **GIII** (0.0092 g, 0.0104 mmol) was dissolved in 0.4 mL of dry and degassed (*via* three freeze-pump-thaw cycles) DMA. A 0.2 mL portion of the solution of **GIII** (0.0046 g, 1 mol %) was then added to the solution of monomer **BF₂N** and **DND** and stirred at 23 °C for exactly 12 min. After 12 min, ethyl vinyl ether (0.945 g, 0.69 mL, 13.1 mmol) was added and the solution was stirred at 23 °C for 30 min. The resulting dark-purple solution was purified by precipitation from pentane, isolated by centrifugation, and dried at 23 °C *in vacuo* for 16 h to afford **(PDND)_{316-r}-(PBF₂N)₃₁₆** as a purple solid. Yield = 0.248 g, 60%. ¹H NMR (399.8 MHz, CDCl₃): δ 7.90 (br m, 7 H, triazole CH + aryl CH), 6.97 (br s, 2 H, aryl CH), 5.41–5.23 (2 x br m, 4H, =CH), 4.49 (br s, 2H, CH₂), 4.11 (br s, 2H, CH₂), 3.88 (br s, 3H, OCH₃), 3.63 (br s, 6H, 2 x OCH₃), 3.35 (br s, 1H, CH), 3.13 (br s, 1H, CH), 2.98–2.85 (br m, 5H, CH), 2.29 (br s, 2H, CH₂), 2.07–1.91 (br m, 3H, diastereotopic CH₂), 1.72 (br m, 1H, diastereotopic CH₂), 1.36–1.20 (br m, 2H, diastereotopic CH₂). ¹¹B NMR

(128.4 MHz, CDCl₃): δ -0.7 (t, $^1J_{\text{BF}} = 30$ Hz). ^{19}F NMR (376.4 MHz, CDCl₃): δ -133.8 (br s). FT-IR (ATR): 2980 (w), 2951 (m), 2845 (m), 2240 (m), 1736 (s), 1604 (s), 1505 (m), 1348 (s), 1263 (s) cm⁻¹. UV-vis (CH₂Cl₂): $\lambda_{\text{max}} = 558$ nm. GPC: $M_n = 247,300$ g mol⁻¹, $M_w = 335,200$ g mol⁻¹, $D = 1.36$.

(PDND)_{292-r}-(PBF₂N)₅₂ ($f_{\text{BF}_2} = 0.15$)

From monomer **BF₂N** (0.030 g, 0.053 mmol) and **DND** (0.056 g, 0.265 mmol). Yield = 0.81 g, 94%. ^1H NMR (399.8 MHz, CDCl₃): δ 8.04 (br s, 1 H, triazole CH), 7.95 (br s, 6 H, aryl CH), 7.00 (br s, 2 H, aryl CH), 5.42–5.24 (2 x br m, 13H, =CH), 4.51 (br s, 2H, CH₂), 4.14 (br s, 2H, CH₂), 3.91 (br s, 3H, OCH₃), 3.63 (br s, 33H, OCH₃), 3.38 (br s, 6H, CH), 3.13 (br s, 1H, CH), 2.98–2.85 (br m, 19 H, CH), 2.29 (br s, 2H, CH₂), 2.06 (br m, 6H, diastereotopic CH₂), 1.90 (br m, 2H, diastereotopic CH₂), 1.72 (br m, 1H, diastereotopic CH₂), 1.38 (br m, 1H, diastereotopic CH₂), 1.30–1.16 (br m, 5.5 H, diastereotopic CH₂). ^{11}B NMR (128.3 MHz, CDCl₃): δ -0.7 (t, $^1J_{\text{BF}} = 31$ Hz). ^{19}F NMR (376.1 MHz, CDCl₃): δ -134.0 (br s). FT-IR (ATR): 3002 (w), 2951 (m), 2852 (w), 1743 (s), 1597 (s), 1439 (m), 1344 (s), 1267 (s) cm⁻¹. UV-vis (CH₂Cl₂): $\lambda_{\text{max}} = 560$ nm. GPC: $M_n = 90,890$ g mol⁻¹, $M_w = 107,000$ g mol⁻¹, $D = 1.18$.

(PDND)_{298-r}-(PBF₂N)₂₆ ($f_{\text{BF}_2} = 0.08$)

From monomer **BF₂N** (0.021 g, 0.036 mmol) and **DND** (0.076 g, 0.362 mmol). Yield = 0.85 g, 88%. ^1H NMR (399.8 MHz, CDCl₃): δ 8.05 (br s, 1 H, triazole CH), 7.94 (br s, 6 H, aryl CH), 7.01 (br m, 2 H, aryl CH), 5.42–5.24 (2 x br m, 26.6 H, =CH), 4.51 (br s, 2H, CH₂), 4.14 (br s, 2H, CH₂), 3.91 (br s, 3H, OCH₃), 3.63 (br s, 74H, OCH₃), 3.37 (br s, 12H, CH), 3.14 (br s, 1H, CH), 3.02–2.84 (br m, 36 H, CH), 2.28 (br s, 2H, CH₂), 2.07 (br m, 12H, diastereotopic CH₂), 1.90 (br m, 2H, diastereotopic CH₂), 1.73 (br m, 1H, diastereotopic CH₂), 1.33–1.19 (br m, 13 H, diastereotopic CH₂). ^{11}B NMR (128.3 MHz, CDCl₃): δ -0.7 (t, $^1J_{\text{BF}} = 33$ Hz). ^{19}F NMR (376.1 MHz, CDCl₃): δ -134.0 (br s). FT-IR (ATR): 2998 (m), 2952 (m), 2850 (m), 1733 (s), 1599 (w), 1436 (m), 1363 (w), 1264 (m) cm⁻¹. UV-vis (CH₂Cl₂): $\lambda_{\text{max}} = 561$ nm. GPC: $M_n = 77,490$ g mol⁻¹, $M_w = 88,820$ g mol⁻¹, $D = 1.15$.

3.5 References

1. Kim, H. N.; Guo, Z.; Zhu, W.; Yoon, J.; Tian, H., *Chem. Soc. Rev.* **2011**, *40*, 79–93.
2. Zhu, C.; Liu, L.; Yang, Q.; Lv, F.; Wang, S., *Chem. Rev.* **2012**, *112*, 4687–4735.
3. Qiao, J.; Liu, Z.; Tian, Y.; Wu, M.; Niu, Z., *Chem. Commun.* **2015**, *51*, 3641–3644.
4. Sanchez, J. C.; Trogler, W. C., *J. Mater. Chem.* **2008**, *18*, 5134–5141.
5. Jäkle, F., *Chem. Rev.* **2010**, *110*, 3985–4022.
6. Lorenz, T.; Crumbach, M.; Eckert, T.; Lik, A.; Helten, H., *Angew. Chem. Int. Ed.* **2017**, *56*, 2780–2784.
7. Long, X.; Ding, Z.; Dou, C.; Zhang, J.; Liu, J.; Wang, L., *Adv. Mater.* **2016**, *28*, 6504–6508.
8. Lorenz, T.; Lik, A.; Plamper, F. A.; Helten, H., *Angew. Chem. Int. Ed.* **2016**, *55*, 7236–7241.
9. Zhao, R.; Dou, C.; Xie, Z.; Liu, J.; Wang, L., *Angew. Chem. Int. Ed.* **2016**, *55*, 5313–5317.
10. Yin, X.; Guo, F.; Lalancette, R. A.; Jäkle, F., *Macromolecules* **2016**, *49*, 537–546.
11. Dou, C.; Long, X.; Ding, Z.; Xie, Z.; Liu, J.; Wang, L., *Angew. Chem. Int. Ed.* **2016**, *55*, 1436–1440.
12. Cheng, F.; Bonder, E. M.; Jäkle, F., *J. Am. Chem. Soc.* **2013**, *135*, 17286–17289.
13. Kim, T.; Lim, S.; Park, S.-R.; Han, C. J.; Lee, M. H., *Polymer* **2015**, *66*, 67–75.
14. Lessard, B. H.; Sampson, K. L.; Plint, T.; Bender, T. P., *J. Polym. Sci., Part A: Polym. Chem.* **2015**, *53*, 1996–2006.
15. Cataldo, S.; Fabiano, S.; Ferrante, F.; Previti, F.; Patanè, S.; Pignataro, B., *Macromol. Rapid Commun.* **2010**, *31*, 1281–1286.

16. Barbon, S. M.; Gilroy, J. B., *Polym. Chem.* **2016**, *7*, 3589–3598.
17. Pawar, G. M.; Lalancette, R. A.; Bonder, E. M.; Sheridan, J. B.; Jäkle, F., *Macromolecules* **2015**, *48*, 6508–6515.
18. Zhang, G.; Palmer, G. M.; Dewhirst, M. W.; Fraser, C. L., *Nat. Mater.* **2009**, *8*, 747–751.
19. Nagai, A.; Kokado, K.; Miyake, J.; Chujo, Y., *Macromolecules* **2009**, *42*, 5446–5452.
20. Novoa, S.; Paquette, J. A.; Barbon, S. M.; Maar, R. R.; Gilroy, J. B., *J. Mater. Chem. C* **2016**, *4*, 3987–3994.
21. Alfred, S. F. Water-Soluble Polymers from Norbornene Monomers. Ph. D. Dissertation, University of Massachusetts Amherst, Amherst, MA, 2008.
22. Hennis, A. D.; Polley, J. D.; Long, G. S.; Sen, A.; Yandulov, D.; Lipian, J.; Benedikt, G. M.; Rhodes, L. F.; Huffman, J., *Organometallics* **2001**, *20*, 2802–2812.
23. Slugovc, C., *Macromol. Rapid Commun.* **2004**, *25*, 1283–1297.
24. You, J.; Yoon, J. A.; Kim, J.; Huang, C.-F.; Matyjaszewski, K.; Kim, E., *Chem. Mater.* **2010**, *22*, 4426–4434.
25. Fery-Forgues, S.; Lavabre, D., *J. Chem. Educ.* **1999**, *76*, 1260.
26. Suzuki, K.; Kobayashi, A.; Kaneko, S.; Takehira, K.; Yoshihara, T.; Ishida, H.; Shiina, Y.; Oishi, S.; Tobita, S., *Phys. Chem. Chem. Phys.* **2009**, *11*, 9850–9860.
27. Birks, J. B., *Photophysics of Aromatic Molecules*. Wiley: New York, 1970.
28. Wang, W.-J.; Hao, L.; Chen, C.-Y.; Qiu, Q.-M.; Wang, K.; Song, J.-B.; Li, H., *RSC Adv.* **2017**, *7*, 20488–20493.
29. Wang, H.; Wang, Y.; Ye, X.; Hayama, H.; Sugino, H.; Nakano, H.; Nakano, T., *Polym. Chem.* **2017**, *8*, 708–714.

30. Becker, M. R.; Stefani, V.; Forte, M. M. C., *React. Funct. Polym.* **2006**, *66*, 1664–1669.
31. Hudson, Z. M.; Lunn, D. J.; Winnik, M. A.; Manners, I., *Nat. Commun.* **2014**, *5*, 3372.
32. Riegler, S.; Demel, S.; Trimmel, G.; Slugovc, C.; Stelzer, F., *J. Mol. Catal. A: Chem.* **2006**, *257*, 53–58.

Chapter 4

4 Conclusions and Future Work

4.1 Conclusions

This thesis describes the development of synthetic procedures required to produce asymmetric and symmetric 3-cyanoformazanate BF₂ complexes and the incorporation of the first reported asymmetric 3-cyanoformazanate BF₂ complex (**2.13**) into polymers using ROMP. The work began by synthesizing asymmetric 3-cyanoformazans using a different whereby the asymmetric formazan was isolated from a mixture containing symmetric derivatives through column chromatography. The BF₂ complex of this formazan was then synthesized by stirring it in a solution of toluene and excess Et₃N and BF₃•OEt₂ under an inert atmosphere at 80 °C overnight. Using CuAAC chemistry two additional BF₂ complexes were synthesized, one containing a benzyl group (**2.14**) and the other a polymerizable norbornene group (**2.17**); the latter would become the monomer used for future polymerization studies. The reaction used to make the monomer yielded a side product which was identified to be a dimer (**2.18**) of BF₂ complex **2.13**; connectivity of both of these structures was determined through X-ray crystallographic studies. Spectroscopic properties of all the BF₂ complexes synthesized revealed strong λ_{max} ranging from 552–597 nm in CH₂Cl₂ and λ_{em} from 647–687 nm. It was observed that the introduction of a triazole ring in compound **2.14** and monomer **2.17** caused a red-shift in the λ_{max} and λ_{em} (relative to **2.13**). This was attributed to an increase in the extent in electronic conjugation. A greater red-shift was observed for dimer **2.18**; this was concluded to be due to the extent of conjugation along both chromophores. Quantum yields of fluorescence for compounds **2.13**, **2.14** and **2.17** ranged from 29–30% in CH₂Cl₂. Dimer **2.18** was found to be non-emissive, most likely due to intramolecular quenching of the adjacent chromophores. All compounds were redox active and possessed two reversible reduction processes in their cyclic voltammograms that yielded a radical anion, and dianion. Introduction of a triazole ring resulted in the need for a more negative potential to be attained before reduction occurred (relative to **2.13**); this was due to the electron donating character of this group. Conversely, dimer **2.18** could be reduced at a lower potential (relative to **2.13**); this was

attributed to the increase in conjugation and the BF_2 complex-substituted alkyne's withdrawing effects.

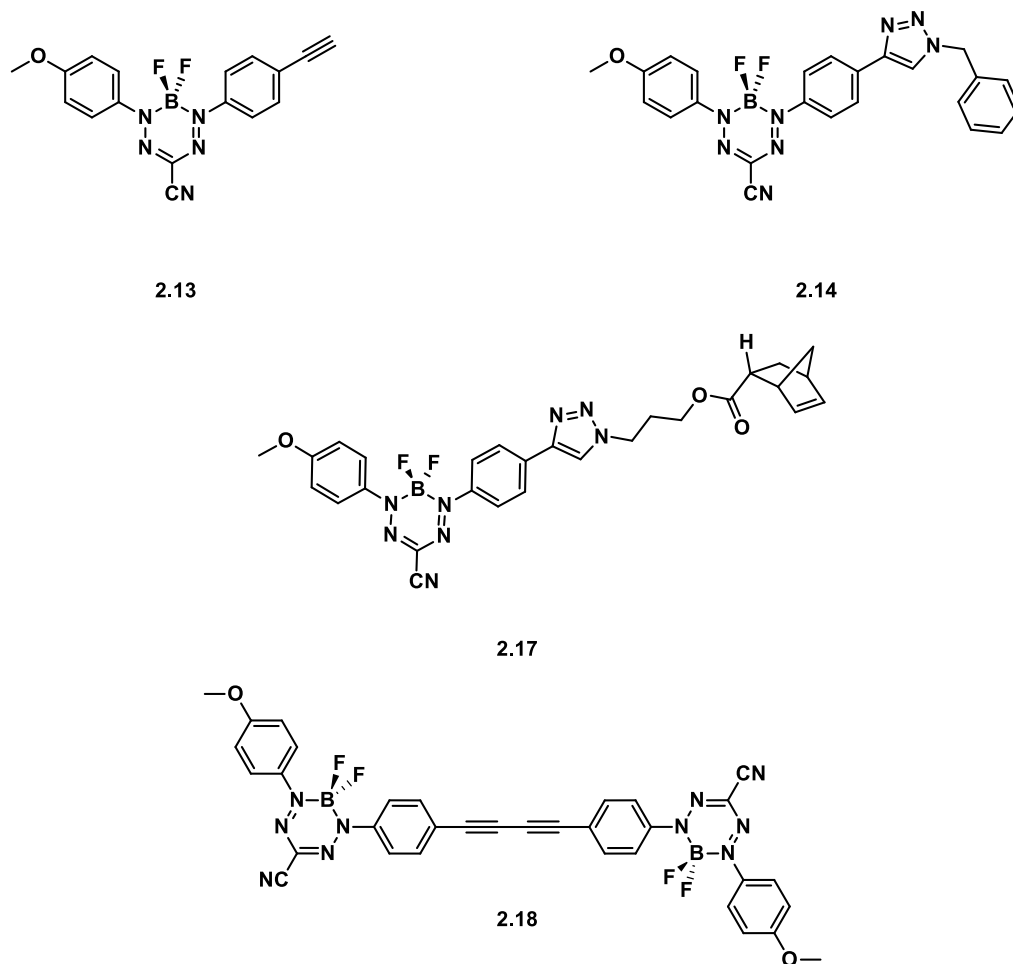


Figure 4.1. BF_2 complexes studied in Chapter 2.

Polymers containing 3-cyanoformazanate BF_2 complex (**2.13/BF₂N**) in the side chain were synthesised using ROMP. Homopolymers (**PBF₂N**) were synthesized by using GIII; the DP_n per polymer chain was targeted to be 100 (1 mol % catalyst). Block and random copolymers of **BF₂N** and *cis*-dimethyl-5-norbornene-*exo*-2,3-dicarboxylate (**DND**) were also synthesized. For block copolymers (**PDND**)_m-*b*-(**PBF₂N**)_n, the first block (**PDND**) was targeted to have a DP_n of 100, whereas the second block (**PBF₂N**) differed in length based on the mole ratio of **BF₂N** added to the living end of the first block. This difference gave rise to three separate block copolymers that differed in the f_{BF_2} . In the case of the random copolymers (**PDND**)_m-*r*-

(**PBF₂N**)_n, they all had targeted degrees of polymerization of 100 and differing f_{BF_2} . ¹H NMR, ¹⁹F NMR, and ¹¹B NMR spectroscopy, UV-vis absorption/emission spectroscopy, IR spectroscopy, GPC, TGA, and DSC were used in order to characterize all of the polymers synthesized. GPC data for the block copolymers and **PDND** revealed that as the f_{BF_2} increased, the M_n of the polymers also increased. This was also true for the random copolymers. In both cases, molecular weights for polymers containing **BF₂N** were over estimated. TGA revealed **PDND** to be more thermally stable than **PBF₂N**, and the block and random copolymers increased in thermal stability as the f_{BF_2} decreased. DSC revealed two T_g s for the block copolymers, the first one pertaining to the **PDND** block, and the second to the **PBF₂N** block. Random copolymers had one T_g , and it was observed that as the f_{BF_2} increased, the T_g also increased. All **BF₂** containing polymers had strong λ_{max} ranging from 558–561 nm in CH₂Cl₂ and λ_{em} from 663–667 nm. The block copolymers were found to be non-emissive, while the random copolymers showed an increase in the Φ_F as the f_{BF_2} decreased (Figure 4.1). This was attributed to the fact that in the random copolymers, **BF₂N** subunits would be further apart as the f_{BF_2} decreased, which would lead to less self-absorption and thus a higher Φ_F . All **BF₂** containing polymers were also found to be redox active, and exhibited two reversible one-electron reduction waves.

Synthesis of the first asymmetric **BF₂** complex has opened up a way to synthesize various functional fluorescent molecules by using CuAAC chemistry. ROMP was demonstrated to be an efficient way to incorporate these complexes into polymers; these polymers demonstrated interesting properties, which showed their potential use as functional fluorescent materials.

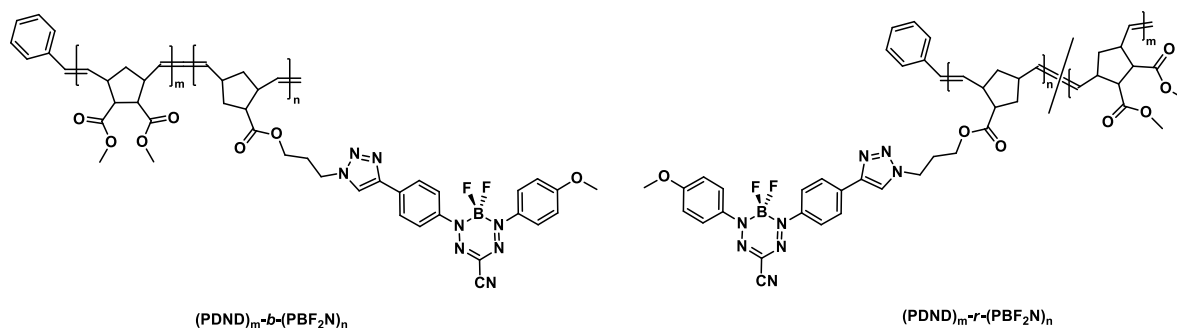


Figure 4.2. Block and random copolymers of **PBF₂N** and **PDND** studied in Chapter 3.

4.2 Future Work

Future work in this area will involve the synthesis of amphiphilic fluorescent block copolymers (e.g., **4.1** and **4.2**) that can self-assemble into micelles. The first block will ideally have very different solubility properties than the second.¹⁻² The second block will be a random copolymer of **PBF₂N** and **PDND**, where the f_{BF_2} should be less than 0.10 so that the Φ_{F} is high enough to eventually make fluorescent micelles whereby the fluorescence will allow for micelle formation to be followed using laser confocal microscopy. It is hypothesized that when the **PBF₂N** / **PDND** block is found on the outside of micelles (the corona) fluorescence from the subunit will be observed. However, if the **PBF₂N** / **PDND** containing block is found on the inside of the micelles, the close proximity of the **PBF₂N** subunits may quench the fluorescence.

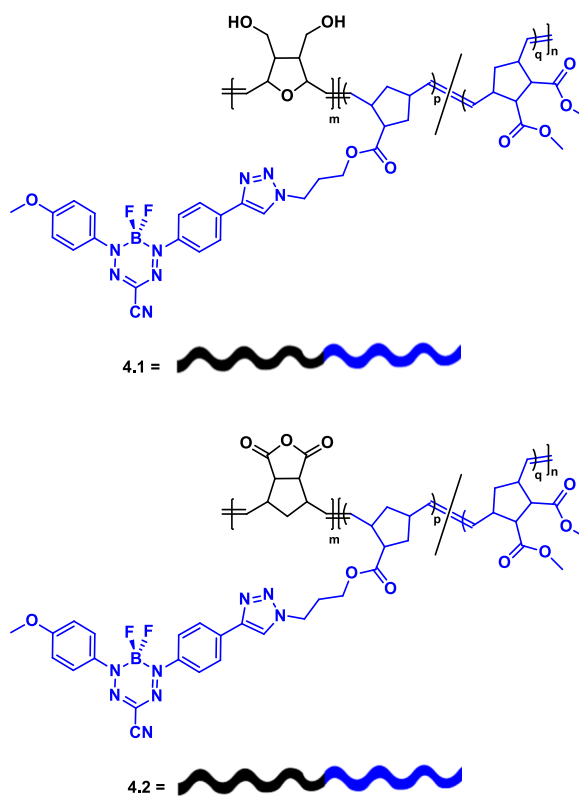


Figure 4.3. Block copolymers **4.1** and **4.2**. The cartoon is a representation of the block copolymer where the blue represents the first block (BF₂ containing random copolymer) and the black represents the non-fluorescent organic block.

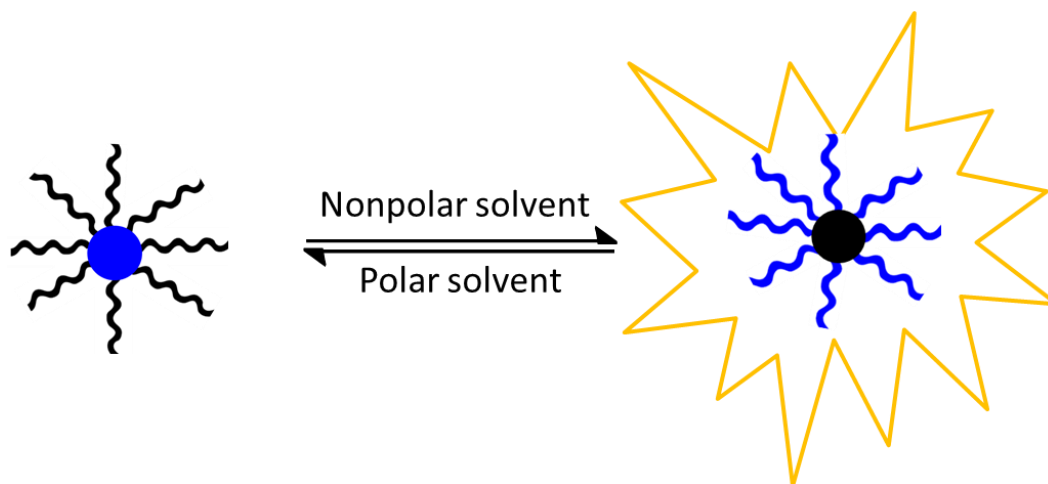


Figure 4.4. Visual representation of micelle formation of block copolymers **4.1** and **4.2**. Yellow cartoon around the micelle on the right represents fluorescence.

4.3 References

1. Buchmeiser, M. R.; Atzl, N.; Bonn, G. K., *J. Am. Chem. Soc.* **1997**, *119*, 9166–9174.
2. Lu, S.-Y.; Amass, J. M.; Majid, N.; Glennon, D.; Byerley, A.; Heatley, F.; Quayle, P.; Booth, C.; Yeates, S. G.; Padget, J. C., *Macromol. Chem. Phys.* **1994**, *195*, 1273–1288.

Appendices

Appendix 1 - Supporting Information for Chapter 2

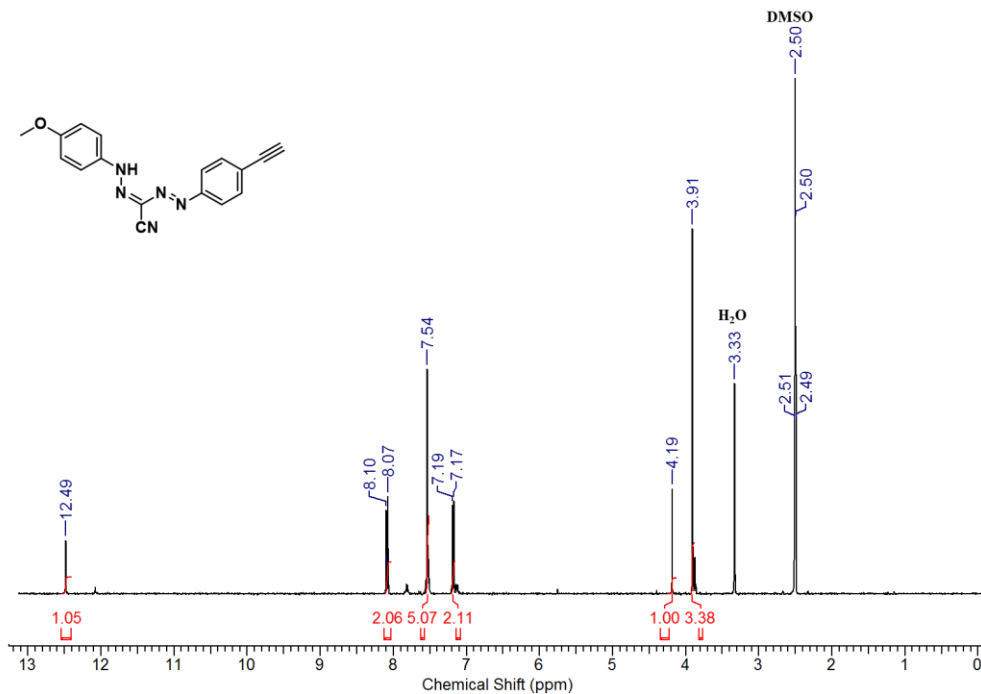


Figure A2.1. ^1H NMR spectrum of formazan **2.12** in $\text{DMSO-}d_6$.

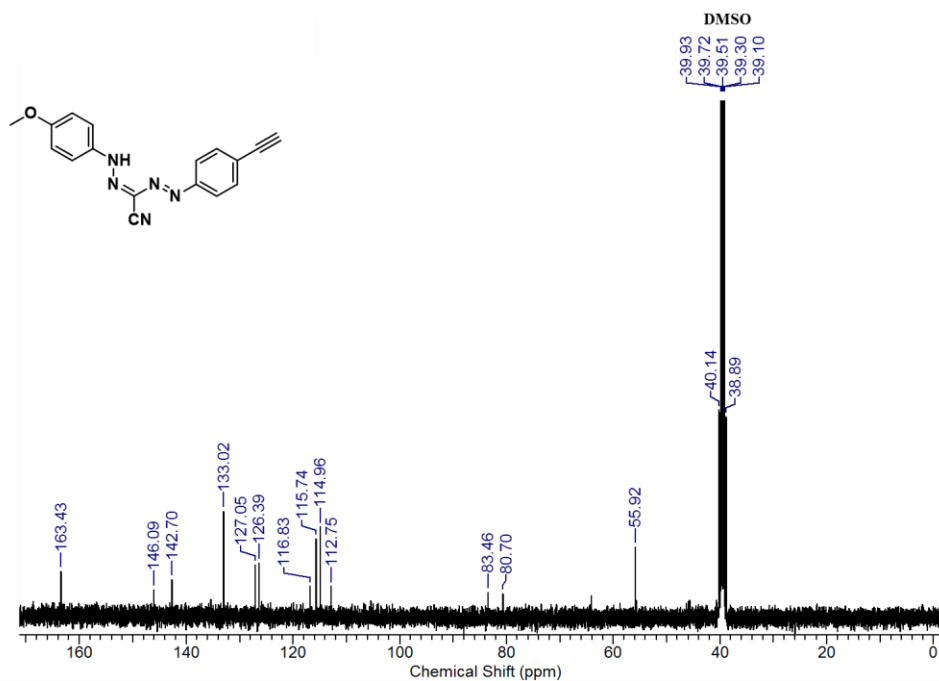
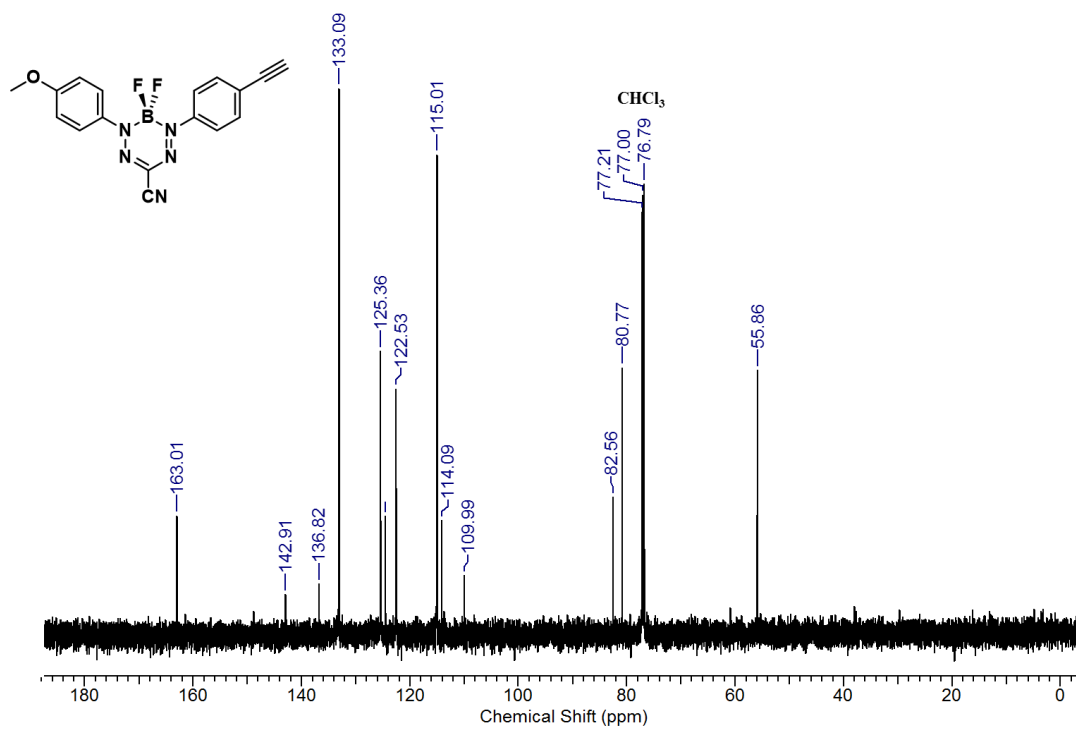
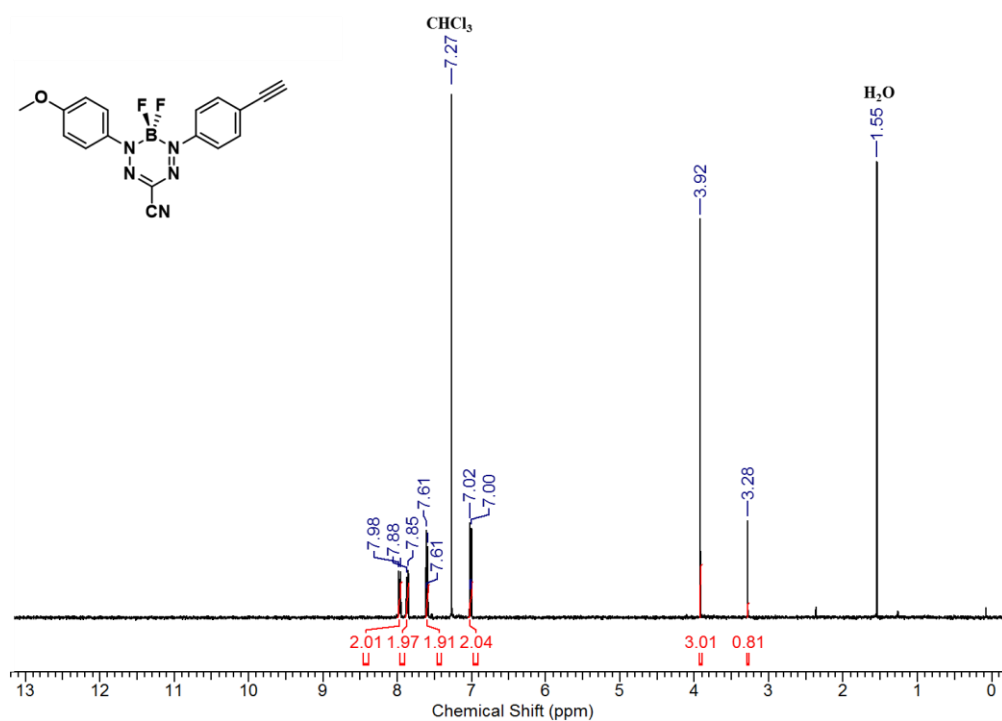


Figure A2.2. $^{13}\text{C}\{^1\text{H}\}$ NMR spectrum of **2.12** in $\text{DMSO-}d_6$. The asterisk denotes solvent signals.



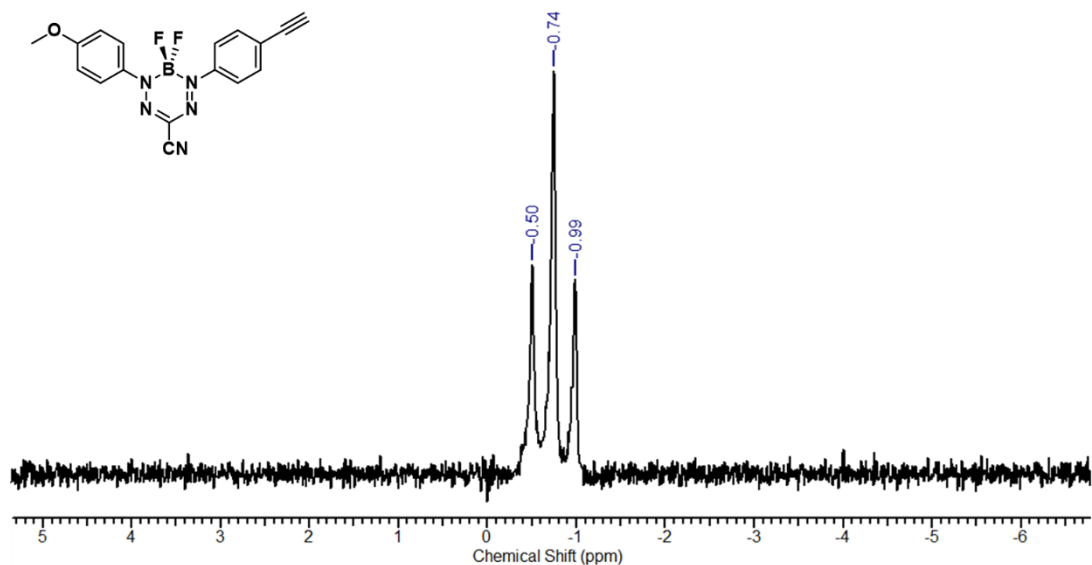


Figure A2.5. ¹¹B NMR spectrum of BF₂ complex **2.13** in CDCl₃.

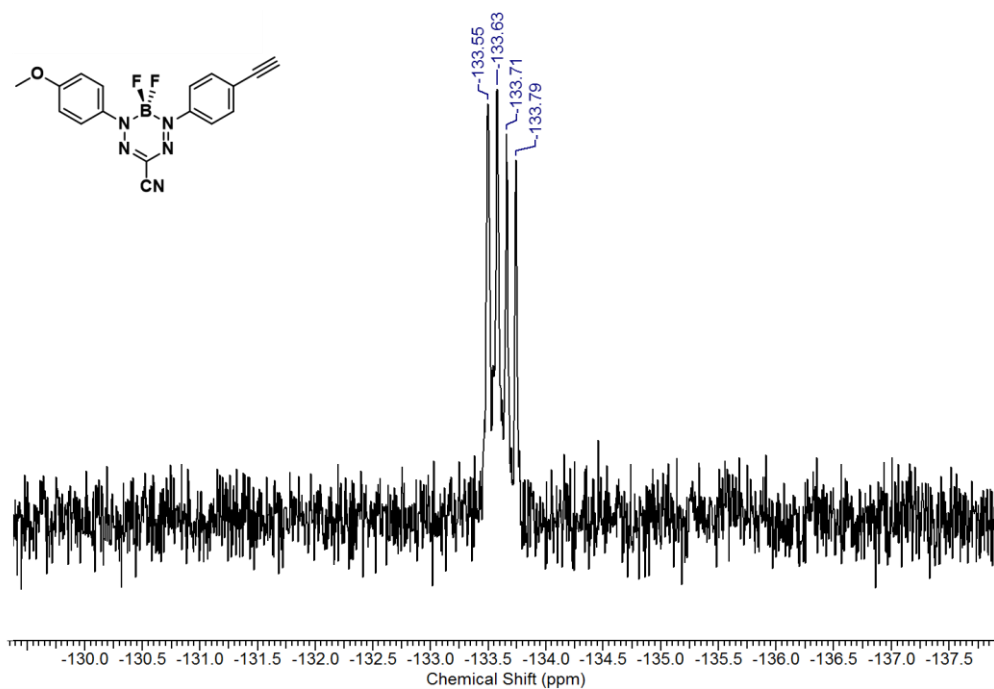


Figure A2.6. ¹⁹F NMR spectrum of BF₂ complex **2.13** in CDCl₃.

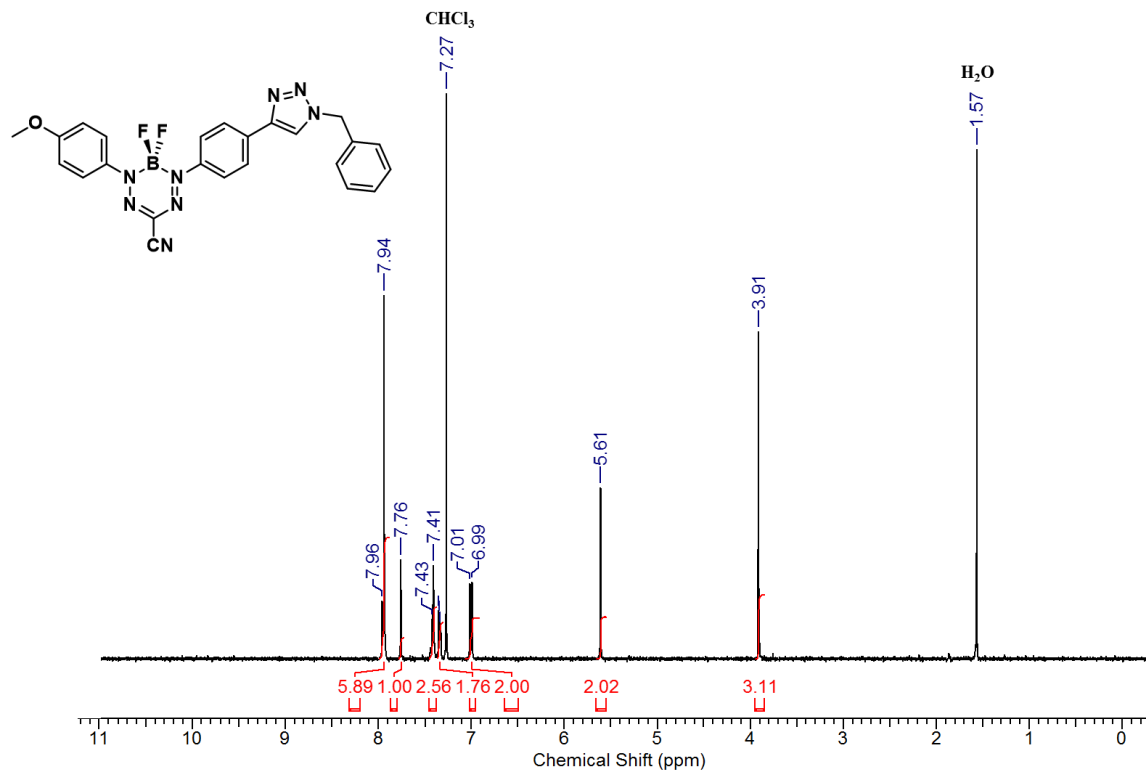


Figure A2.7. ^1H NMR spectrum of benzyl-substituted BF_2 complex **2.14** in CDCl_3 .

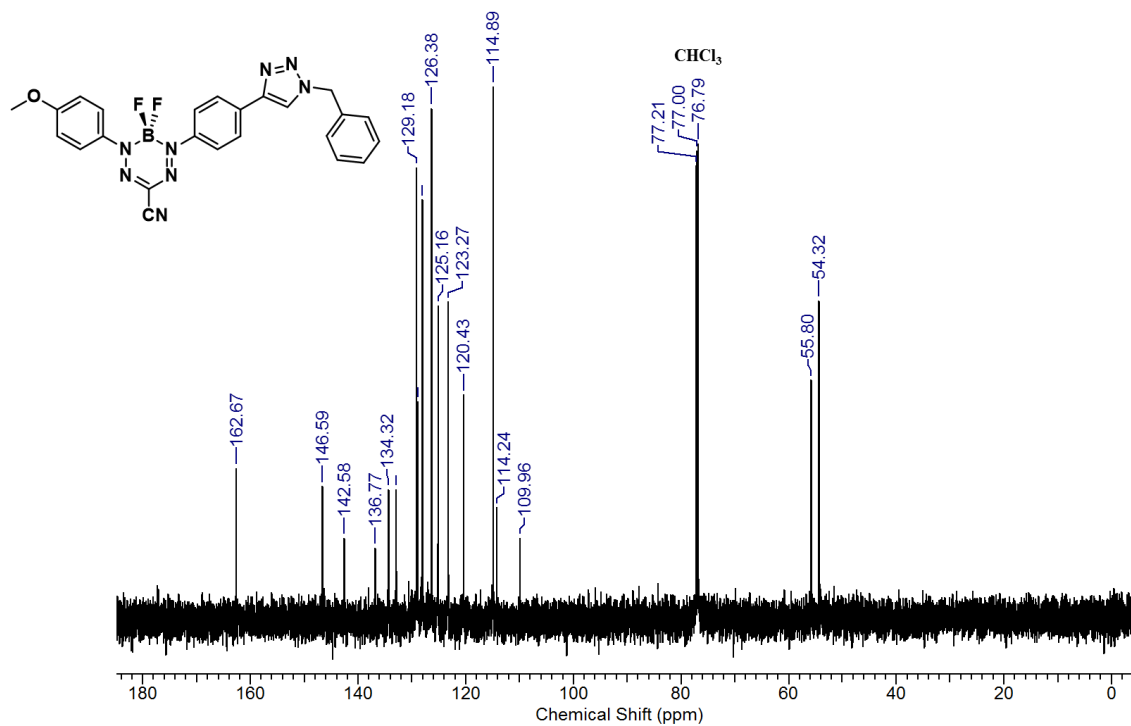


Figure A2.8. $^{13}\text{C}\{^1\text{H}\}$ NMR spectrum of benzyl-substituted BF_2 complex **2.14** in CDCl_3 .

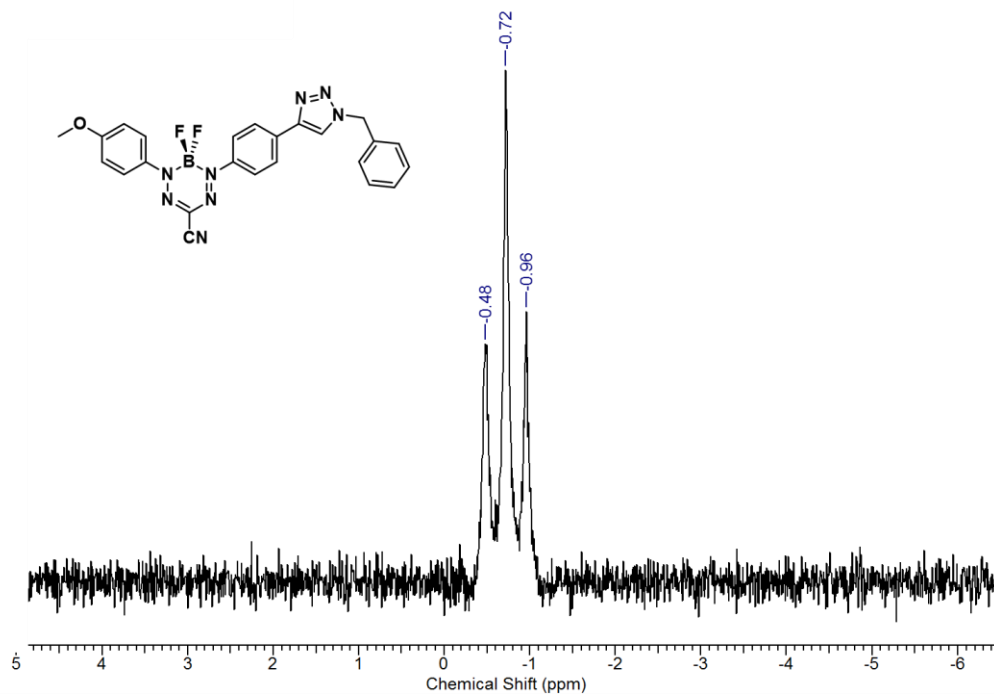


Figure A2.9. ^{11}B NMR spectrum of benzyl-substituted BF_2 complex **2.14** in CDCl_3 .

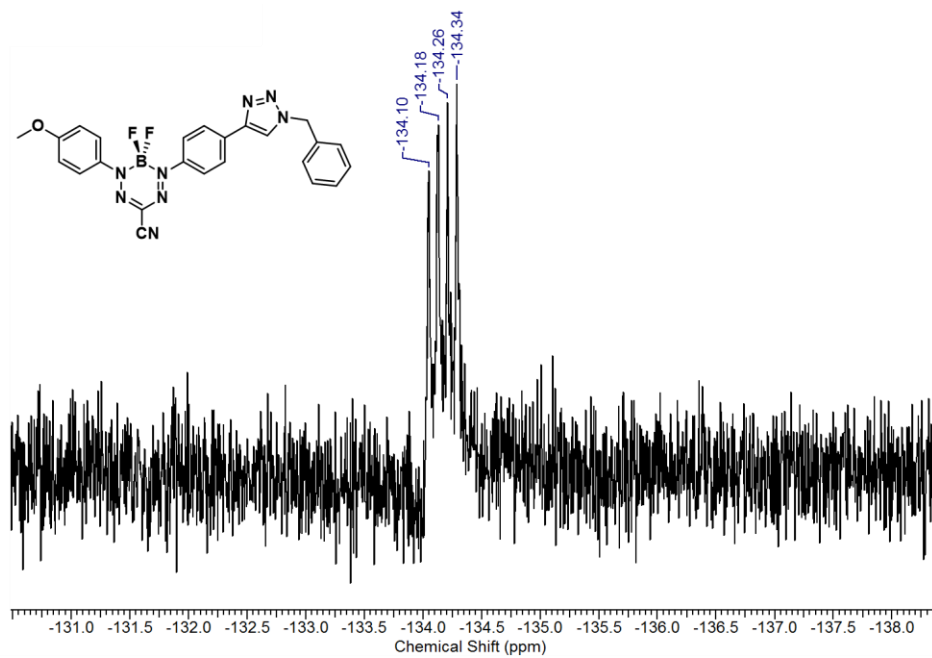


Figure A2.10. ^{19}F NMR spectrum of benzyl-substituted BF_2 complex **2.14** in CDCl_3 .

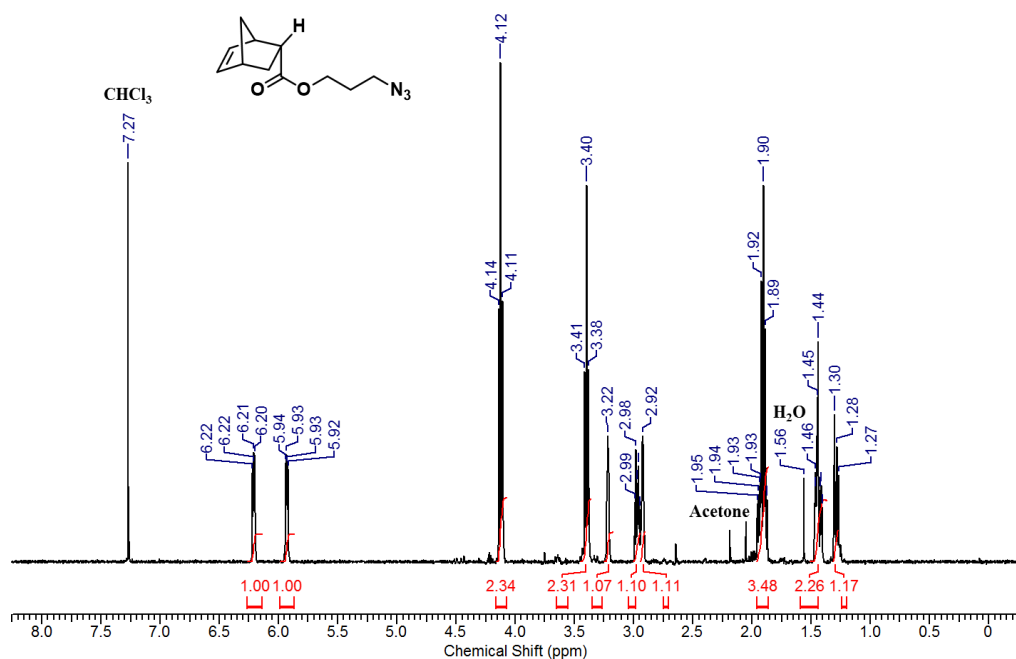


Figure A2.11. ^1H NMR spectrum of azide-substituted norbornene **2.16** in CDCl₃.

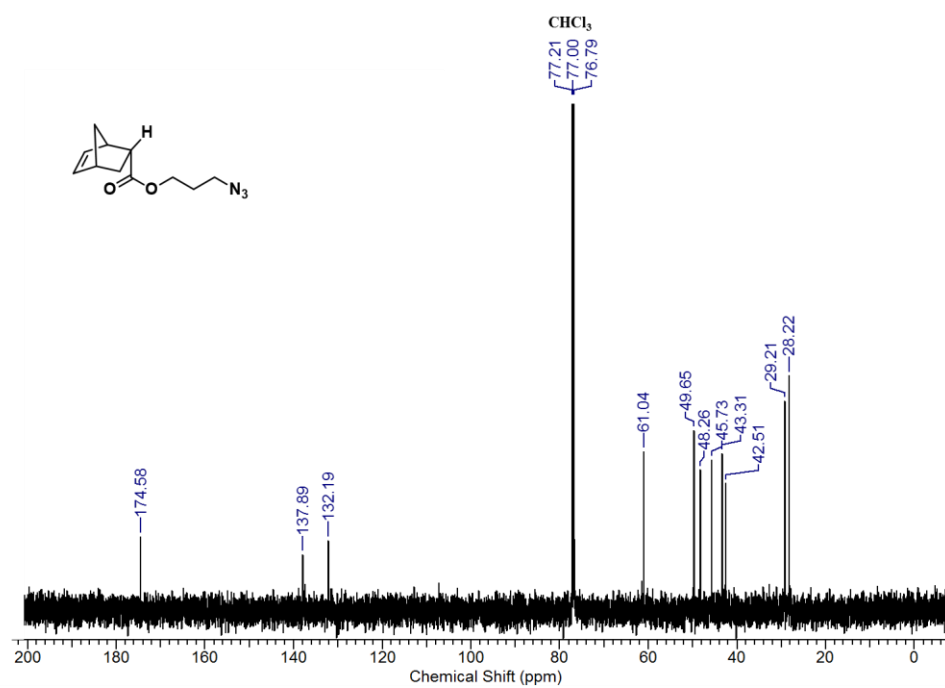


Figure A2.12. $^{13}\text{C}\{^1\text{H}\}$ NMR spectrum of azide-substituted norbornene **2.16** in CDCl₃.

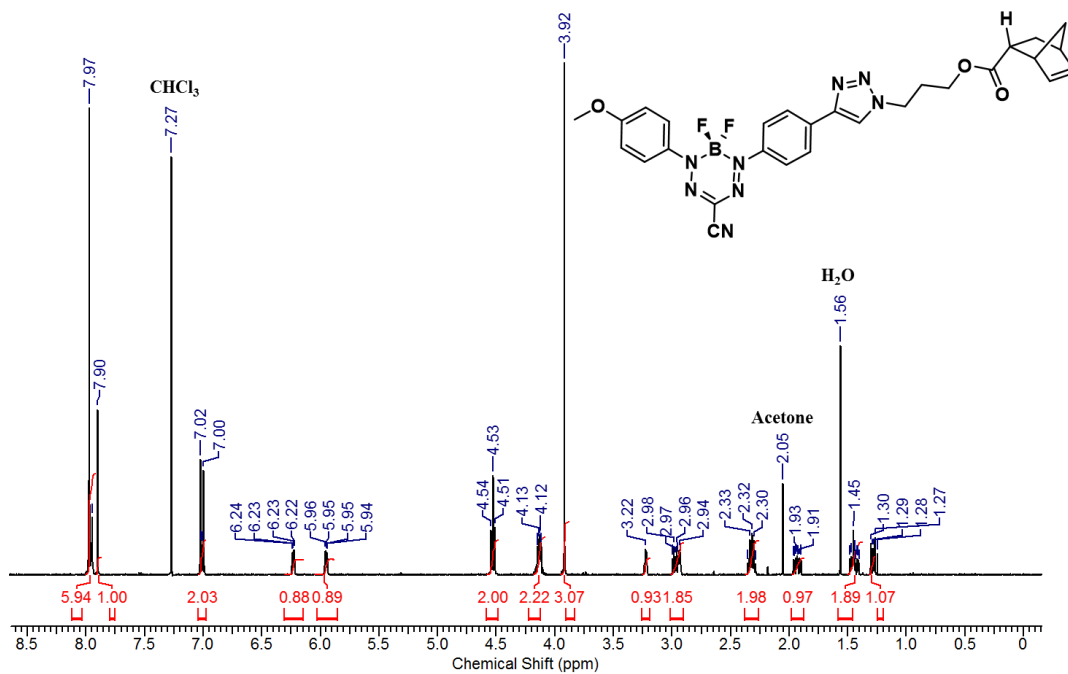


Figure A2.13. ^1H NMR spectrum of monomer **2.17** in CDCl_3 .

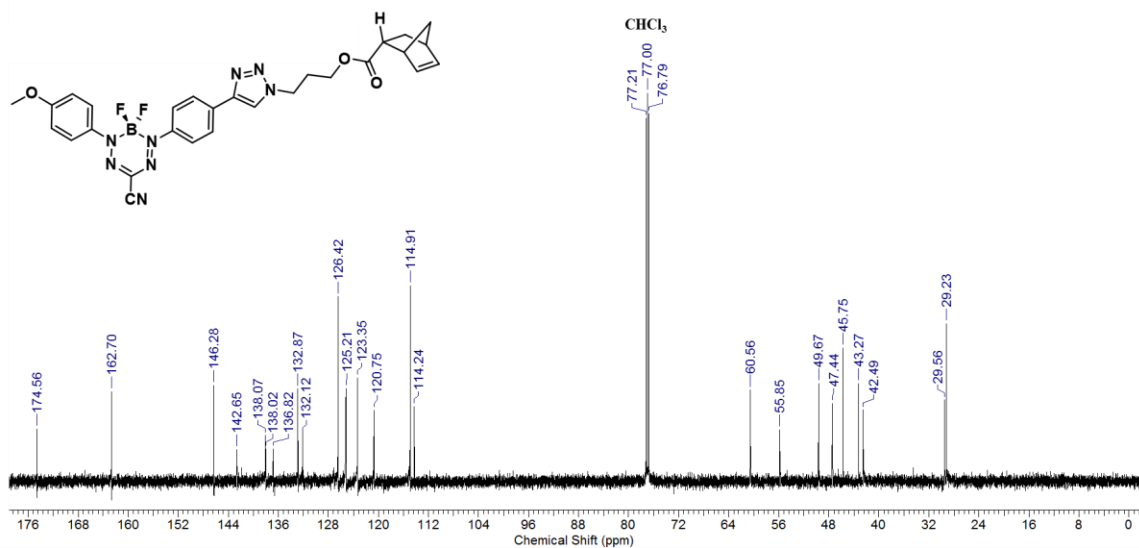


Figure A2.14. $^{13}\text{C}\{^1\text{H}\}$ NMR spectrum of monomer **2.17** in CDCl_3 .

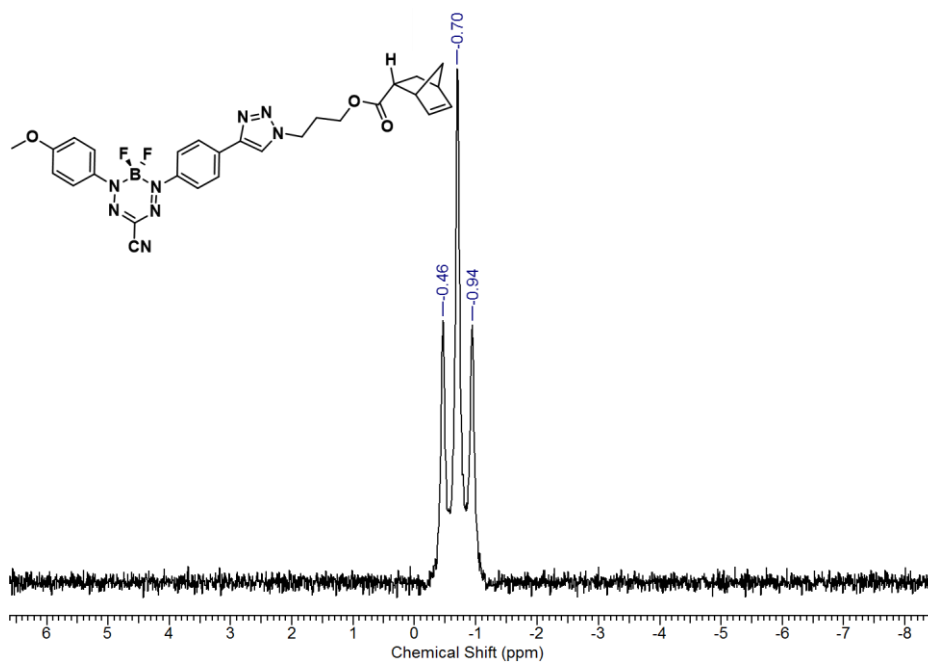


Figure A2.15. ^{11}B NMR spectrum of monomer **2.17** in CDCl_3 .

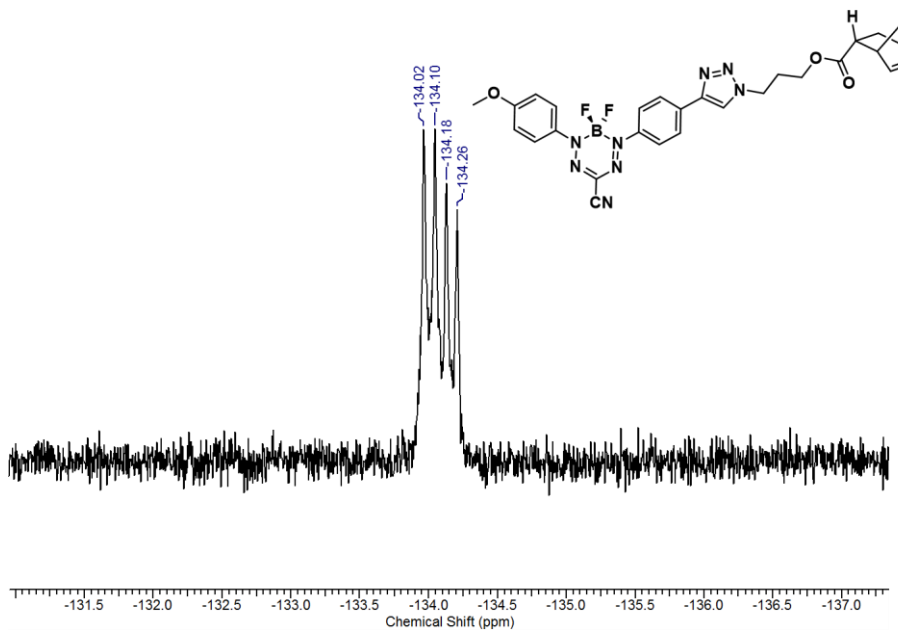


Figure A2.16. ^{19}F NMR spectrum of monomer **2.17** in CDCl_3 .

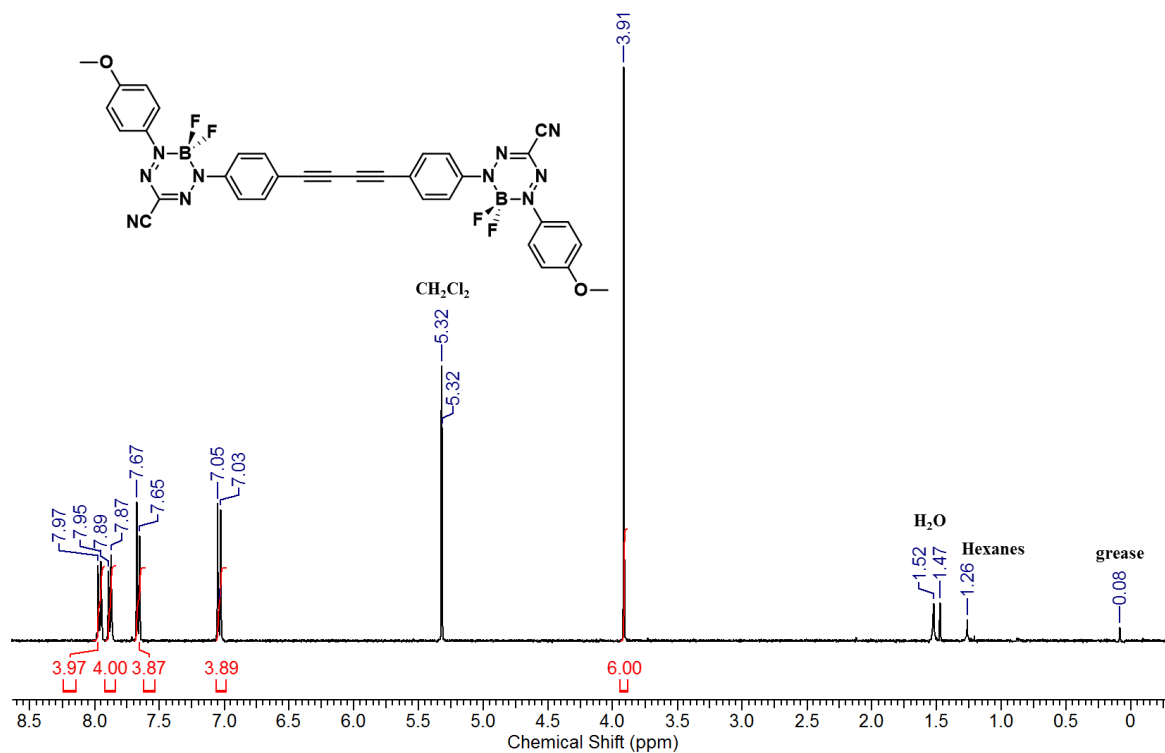


Figure A2.17. ^1H NMR spectrum of dimer **2.18** in CD_2Cl_2 .

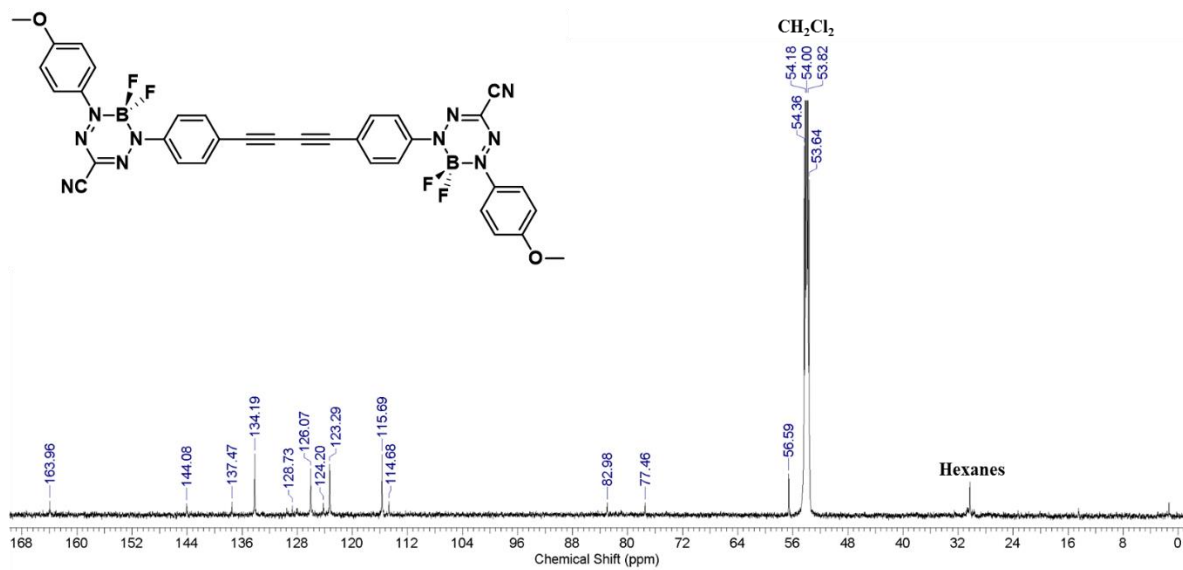


Figure A2.18. ^{13}C NMR spectrum of dimer **2.18** in CD_2Cl_2 .

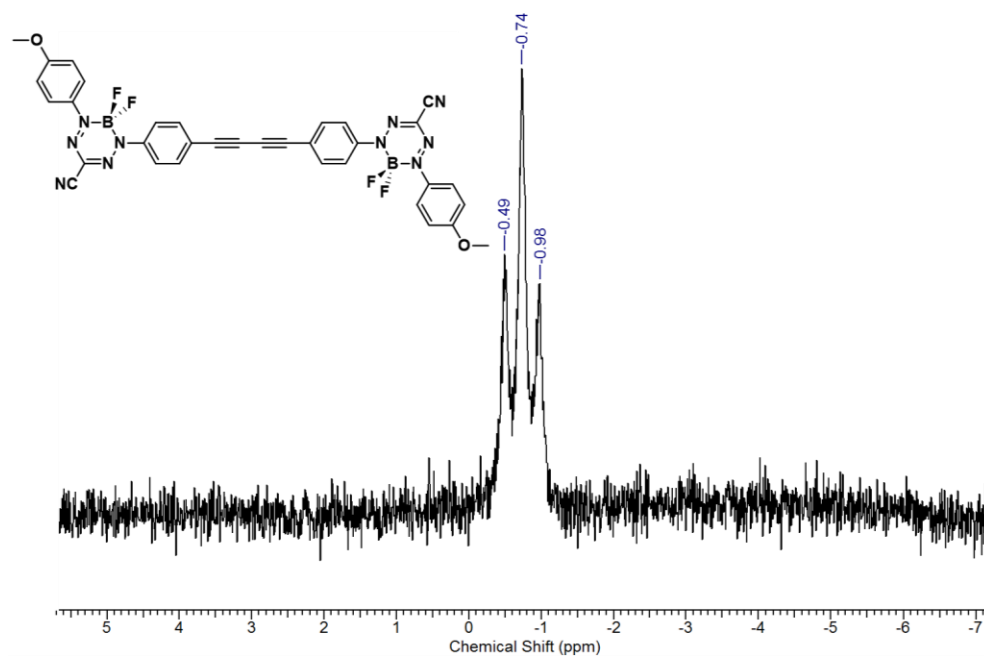


Figure A2.19. ^{11}B NMR spectrum of dimer **2.18** in CD_2Cl_2 .

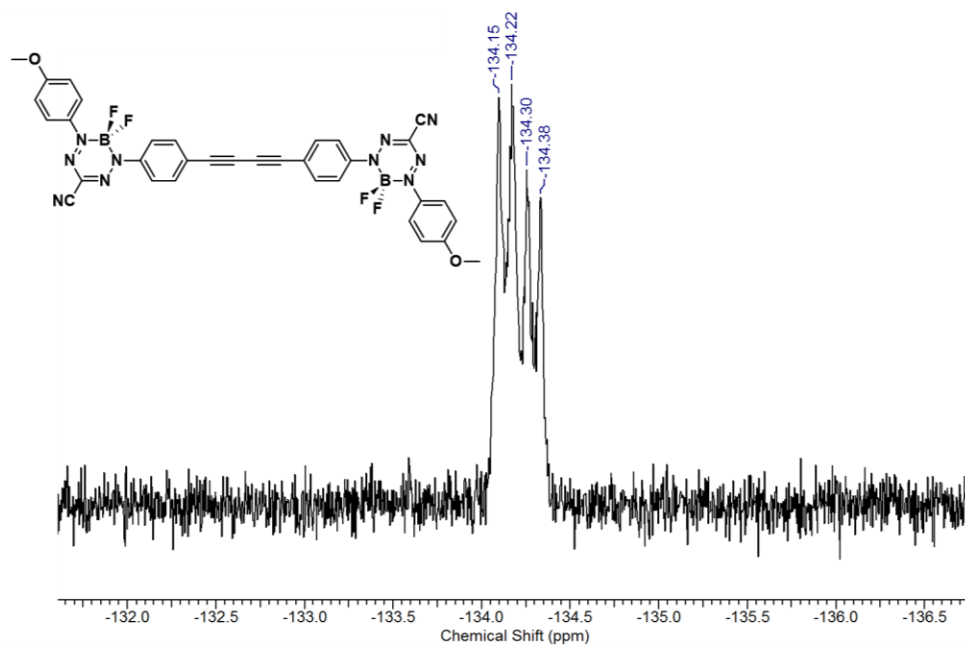


Figure A2.20. ^{19}F NMR spectrum of dimer **2.18** in CD_2Cl_2 .

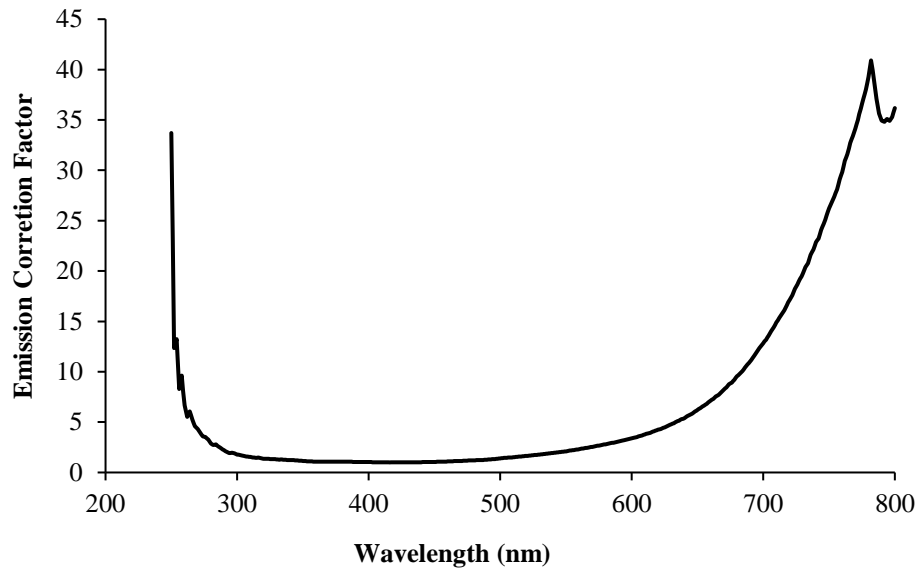
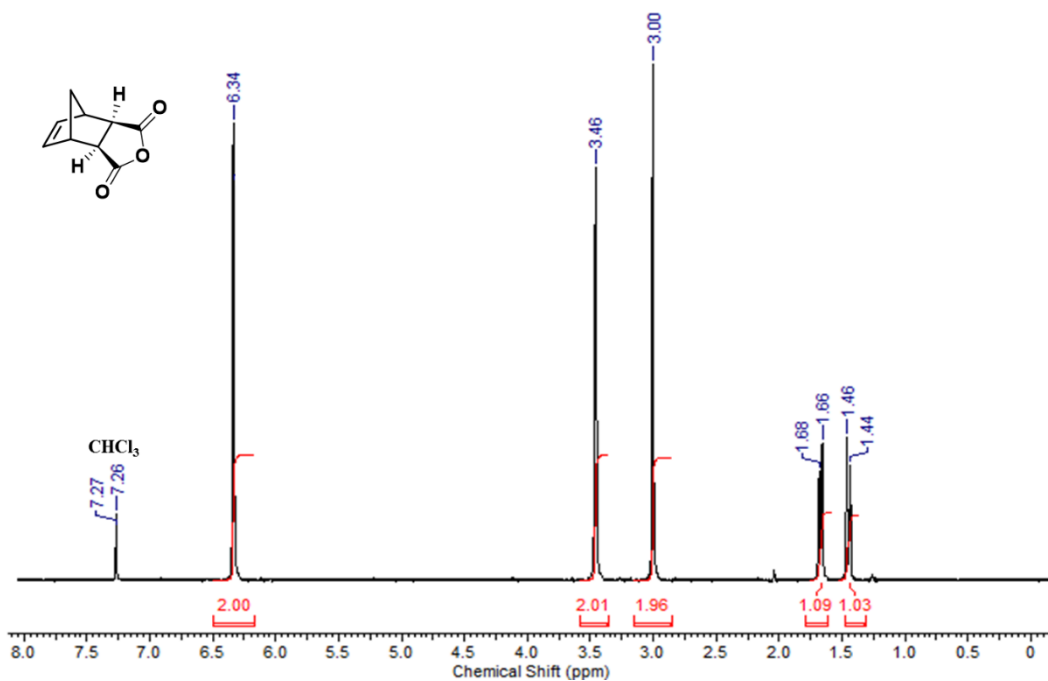
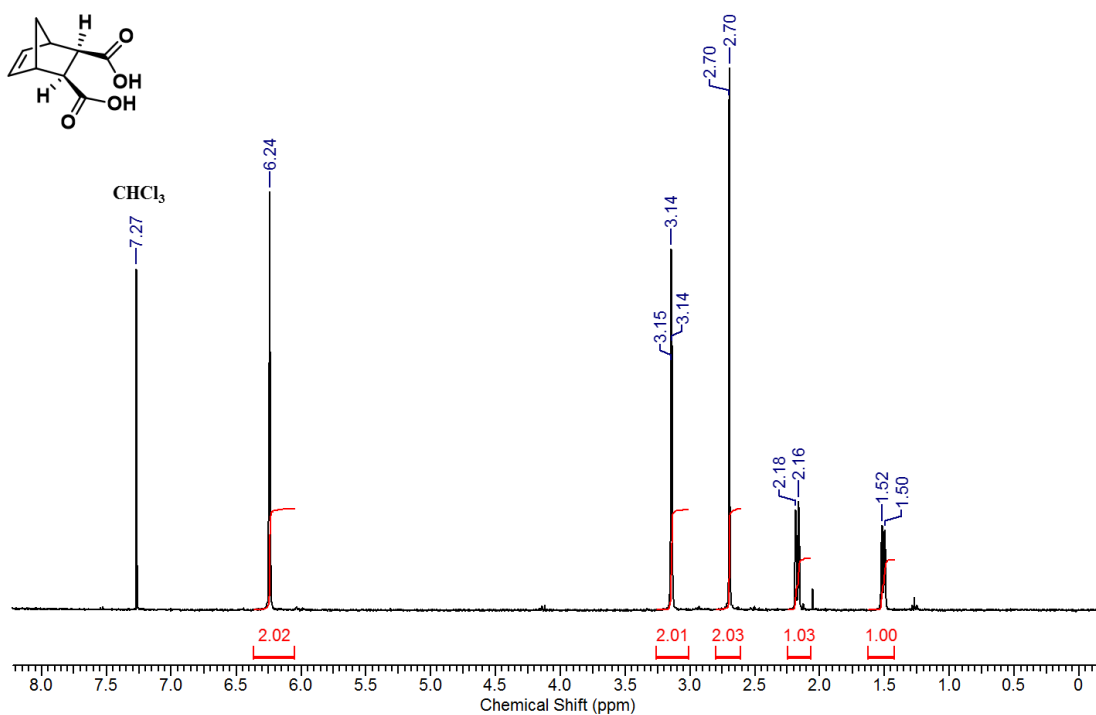


Figure A2.21. Wavelength-dependent emission correction provided by Photon Technology International.

Appendix 2 - Supporting Information for Chapter 3

Figure A3.1. ¹H NMR spectrum of *exo*-NDCAn in CDCl₃.Figure A3.2. ¹H NMR spectrum of *exo*-NDCA in CDCl₃.

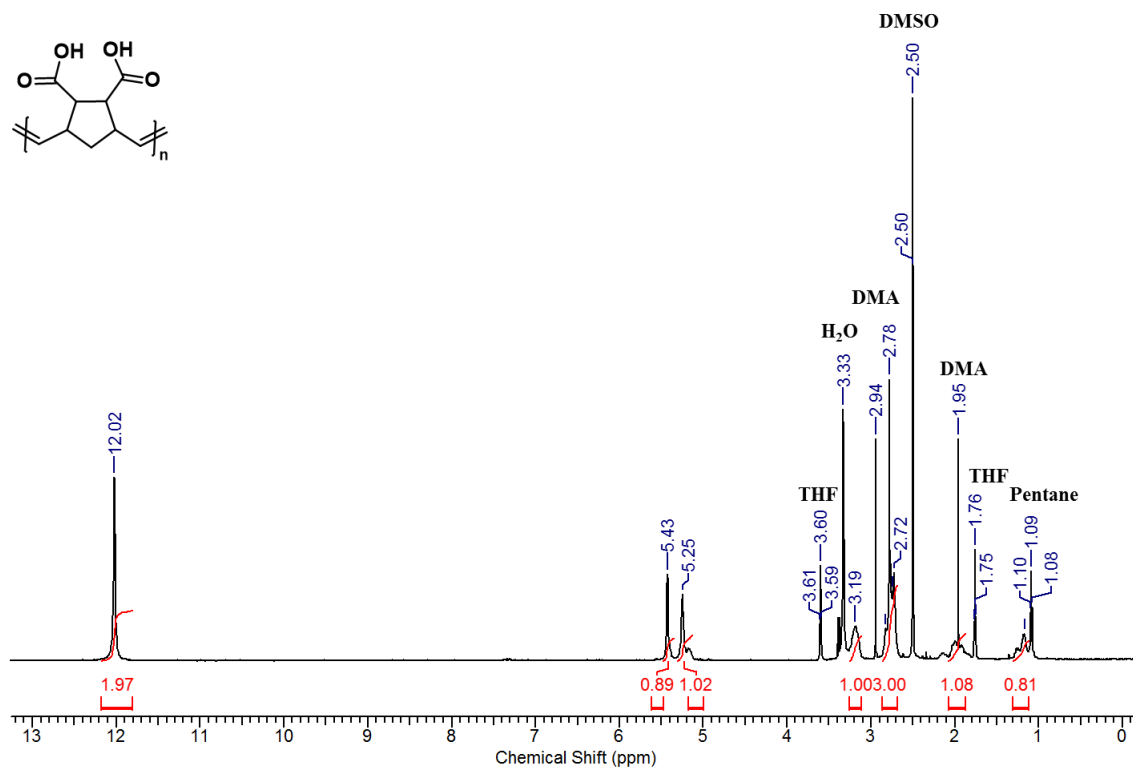


Figure A3.3. ^1H NMR spectrum of **P-*exo*-NDCA** in $\text{DMSO-}d_6$.

Table A3.1. Summary of molecular weight data determined by GPC for **P-*exo*-NDCA**.

Time (min)	M_n	M_w	\mathcal{D}
1	26,740	23,710	1.13
2	46,300	33,480	1.38
3	49,830	43,430	1.15
4	57,120	53,170	1.07
5	61,590	53,690	1.15
6	63,970	59,010	1.08

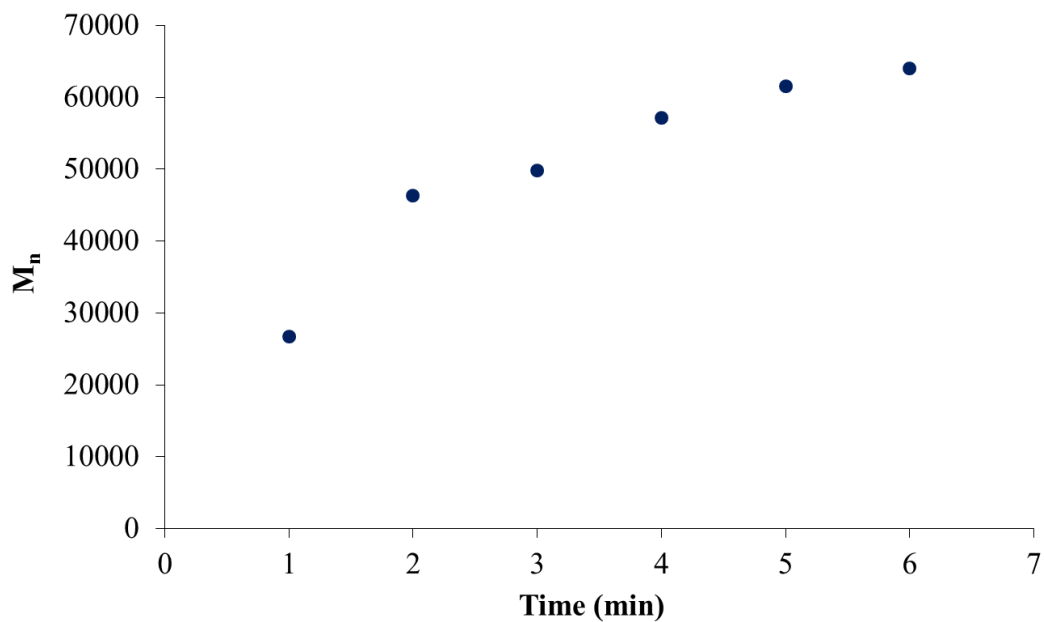


Figure A3.4. Relationship between number average molecular weight (M_n) of *P-exo-NDCA* as a function of time (min).

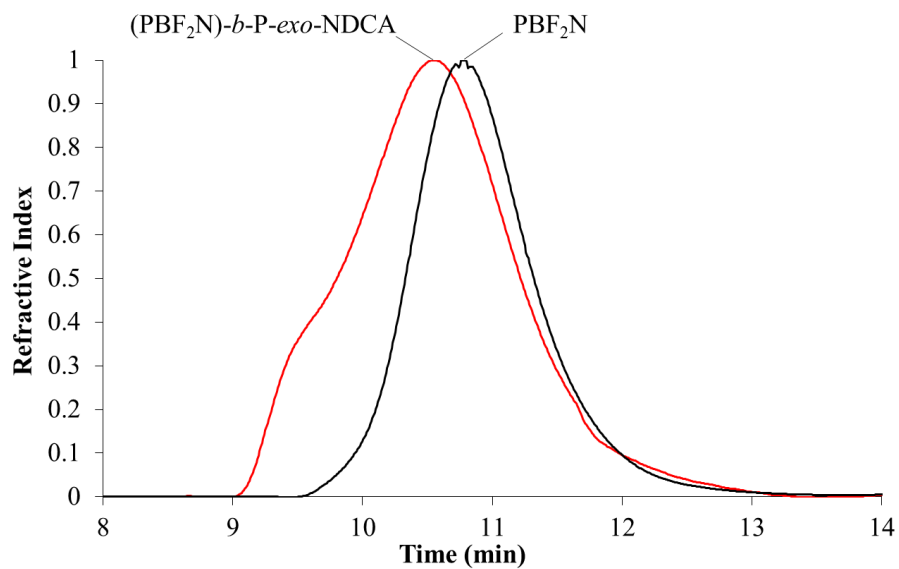


Figure A3.5. Corresponding GPC traces for *PBF₂N* and *(PBF₂N)-b-(P-exo-NDCA)*.

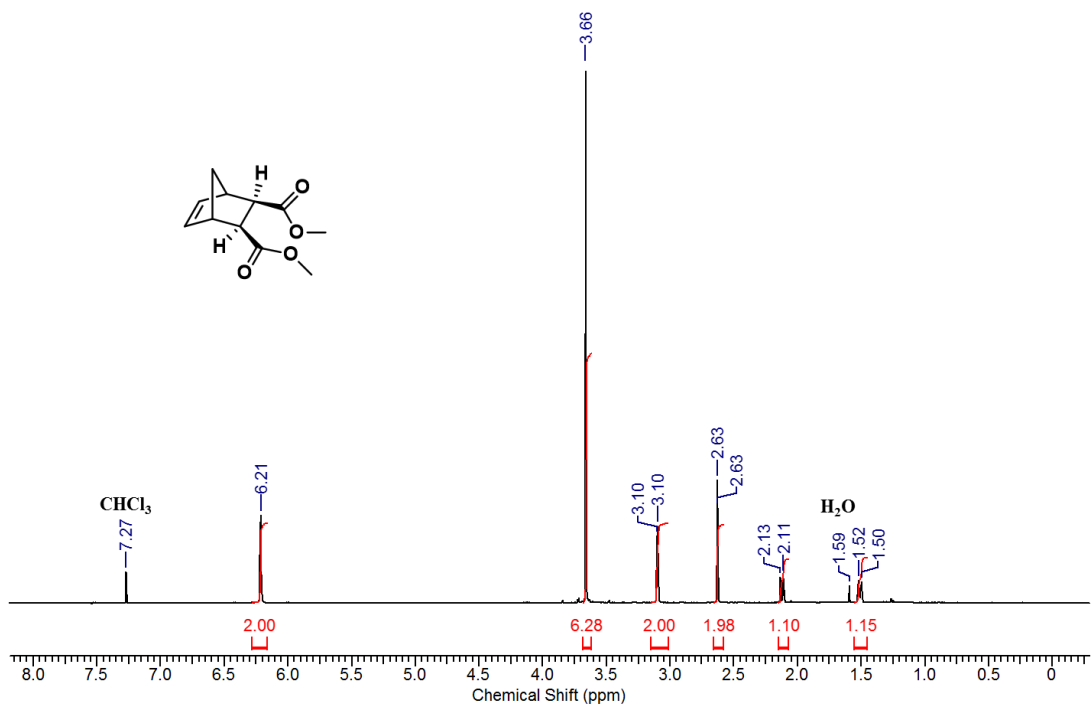


Figure A3.6. ^1H NMR spectrum of DND in CDCl_3 .

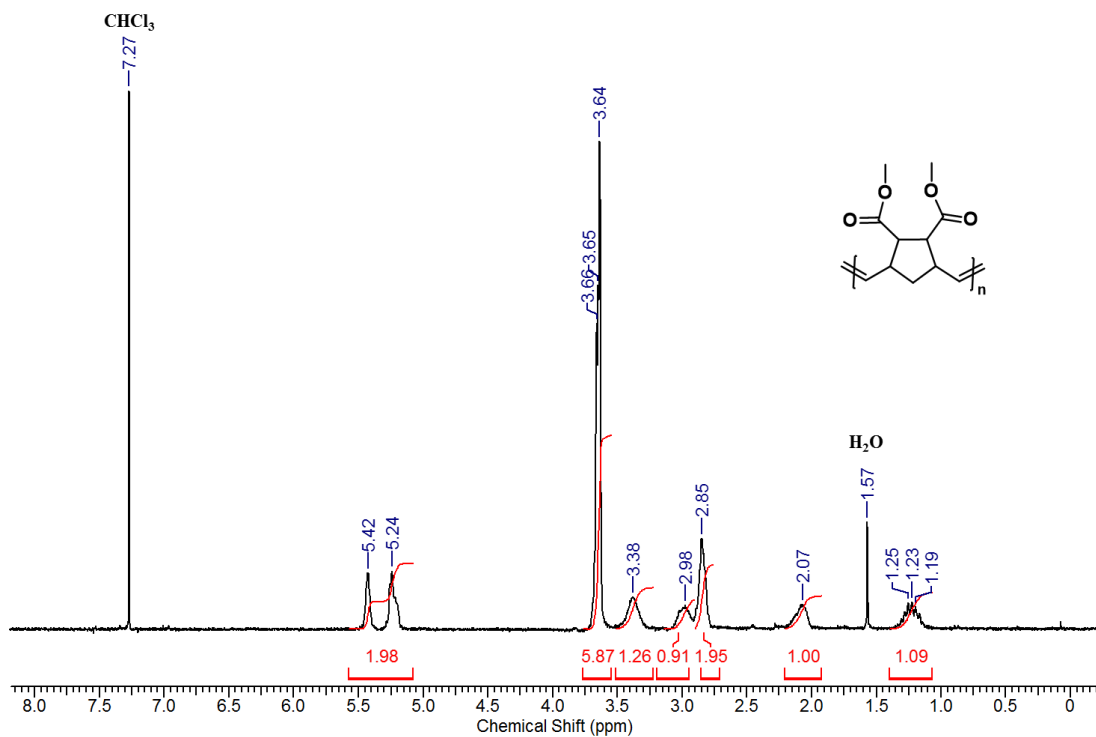


Figure A3.7. ^1H NMR spectrum of PDND in CDCl_3 .

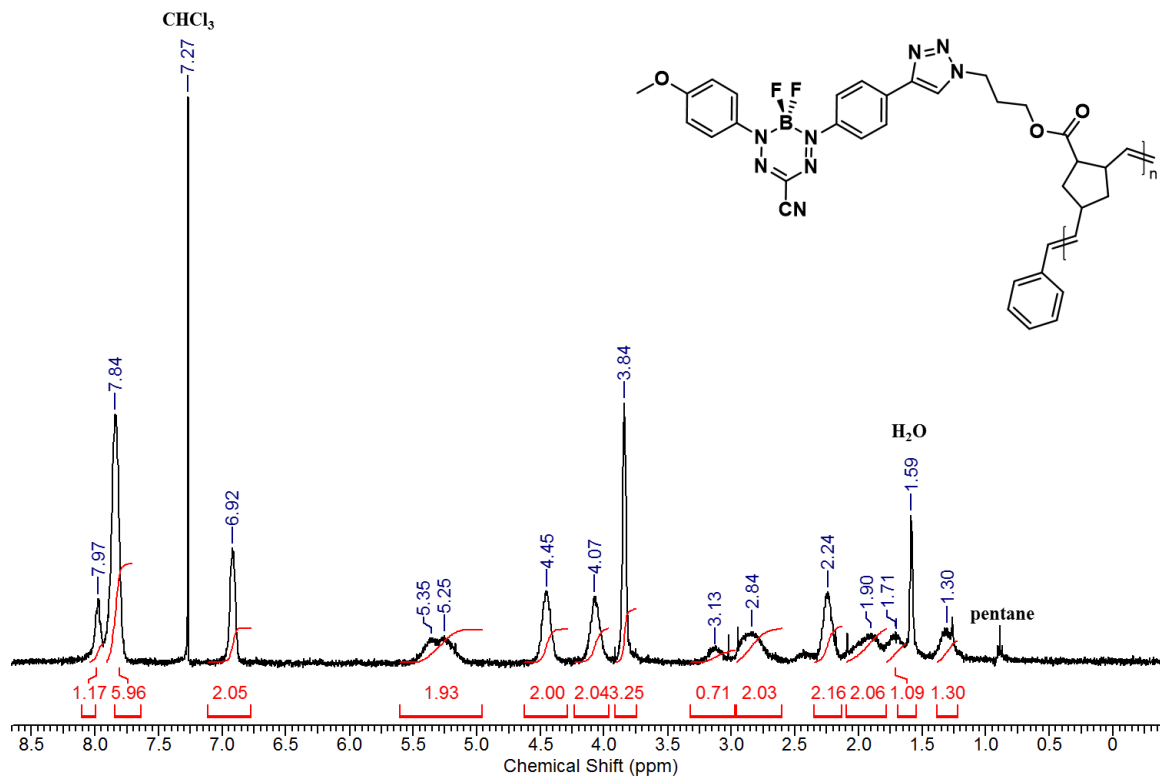


Figure A3.8. ¹H NMR spectrum of **PBF₂N** in CDCl₃.

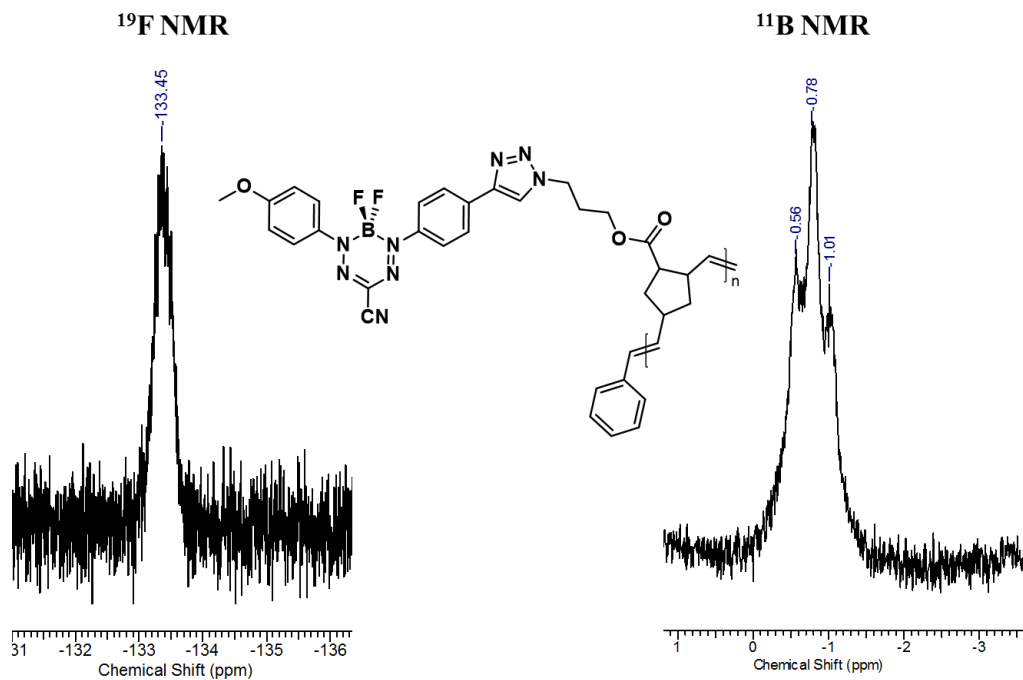


Figure A3.9. ¹⁹F NMR (left) spectrum and ¹¹B NMR (right) of **PBF₂N** in CDCl₃.

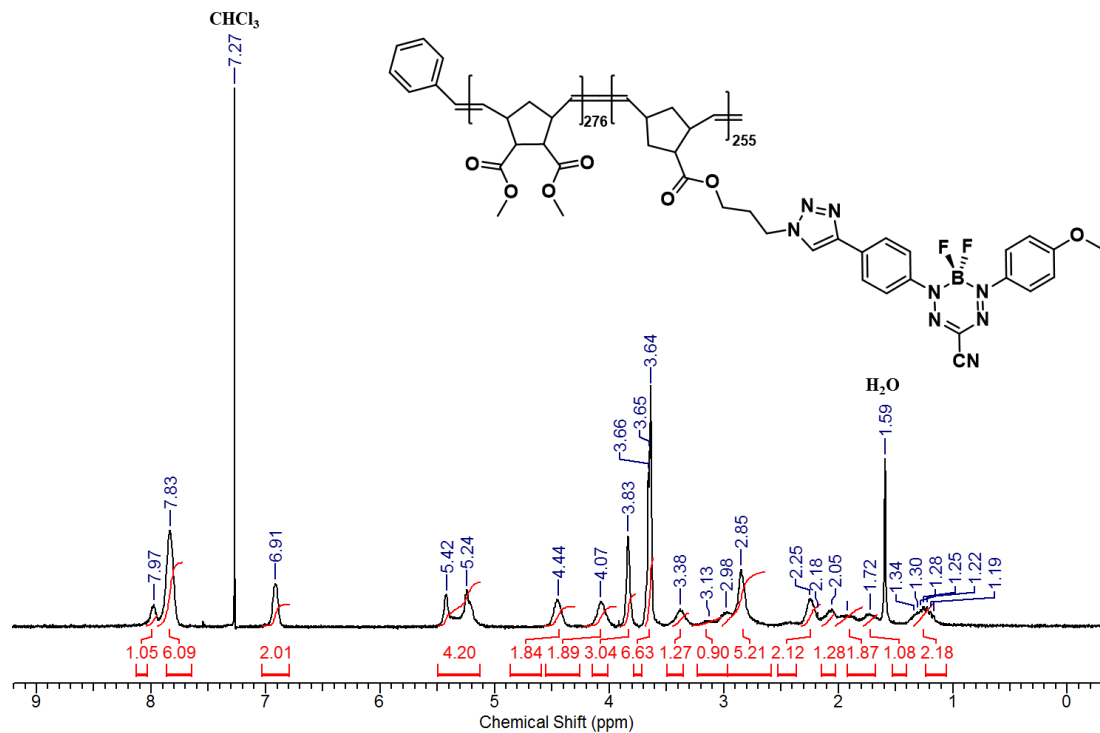


Figure A3.10. ^1H NMR spectrum of $(\text{PDND})_{276}\text{-}b\text{-}(\text{PBF}_2\text{N})_{255}$ ($f_{\text{BF}_2} = 0.48$) in CDCl_3 .

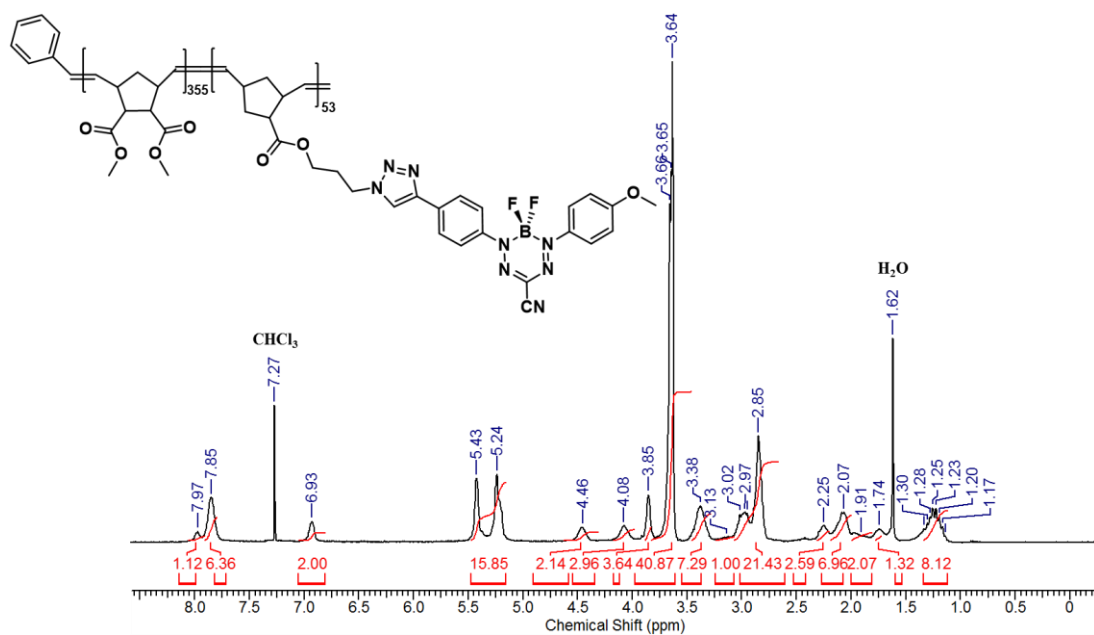


Figure A3.11. ^1H NMR spectrum of $(\text{PDND})_{355}\text{-}b\text{-}(\text{PBF}_2\text{N})_{53}$ ($f_{\text{BF}_2} = 0.13$) in CDCl_3 .

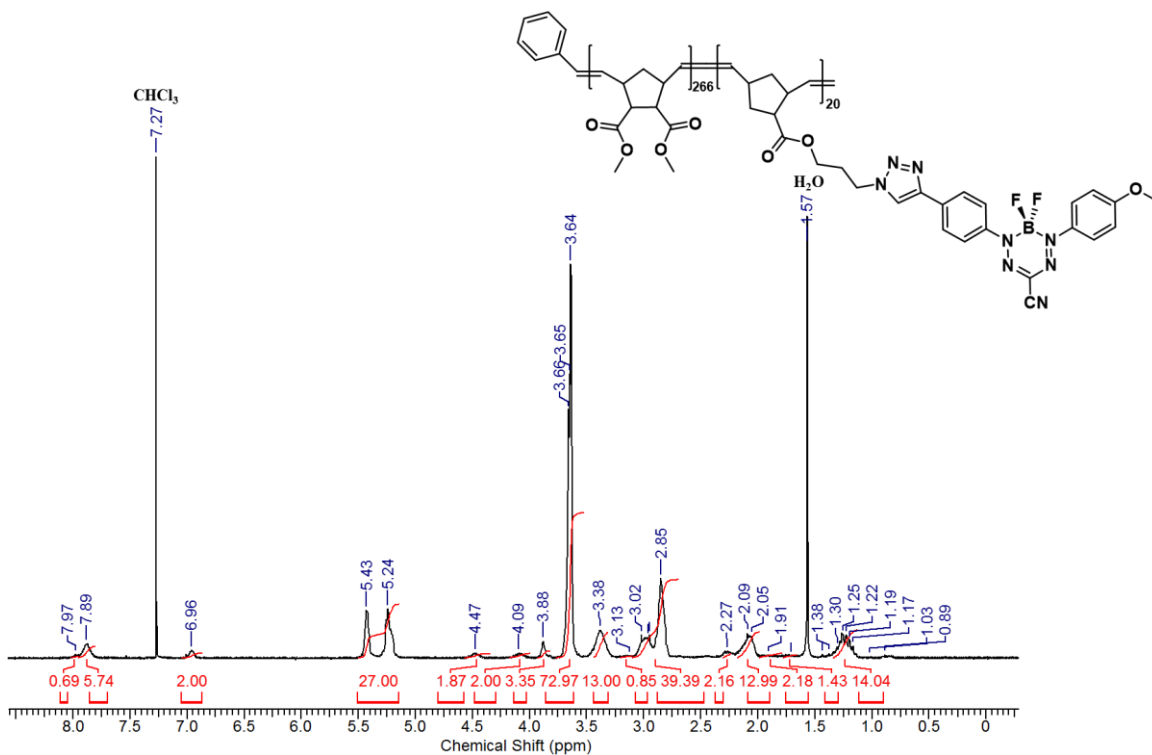


Figure A3.12. ^1H NMR spectrum of $(\text{PDND})_{266}\text{-}b\text{-(PBF}_2\text{N)}_{20}$ ($f_{\text{BF}_2} = 0.07$) in CDCl_3 .

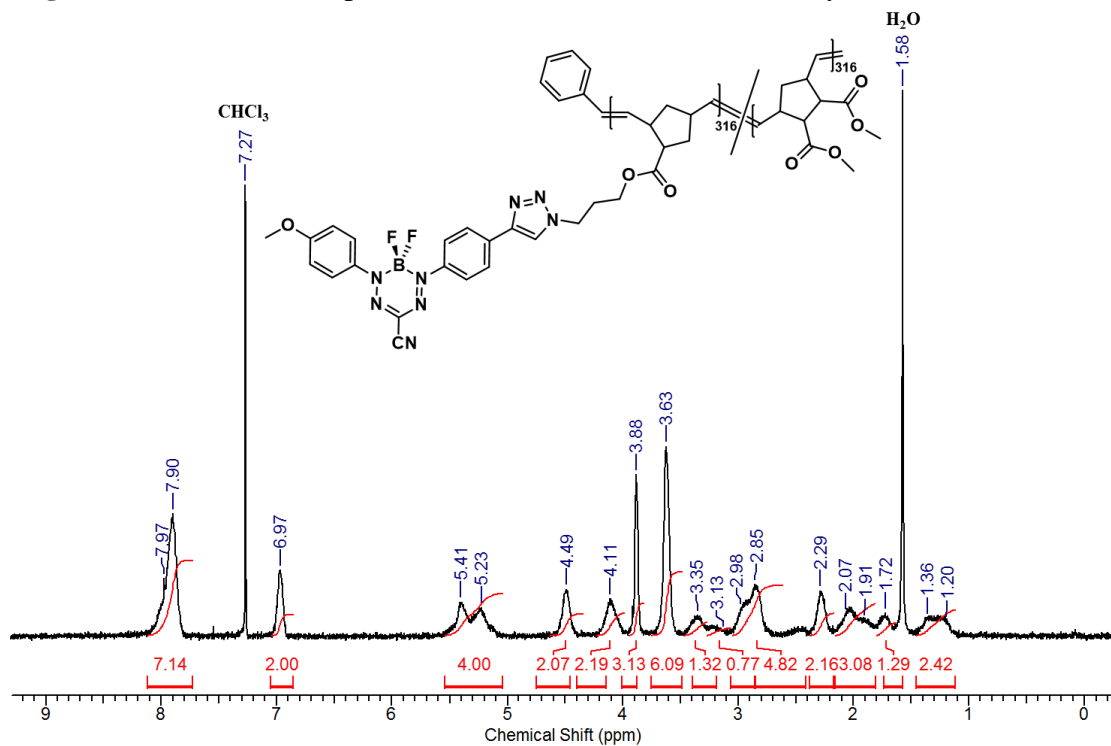


Figure A3.13. ^1H NMR spectrum of $(\text{PDND})_{316}\text{-}r\text{-(PBF}_2\text{N)}_{316}$ ($f_{\text{BF}_2} = 0.50$) in CDCl_3 .

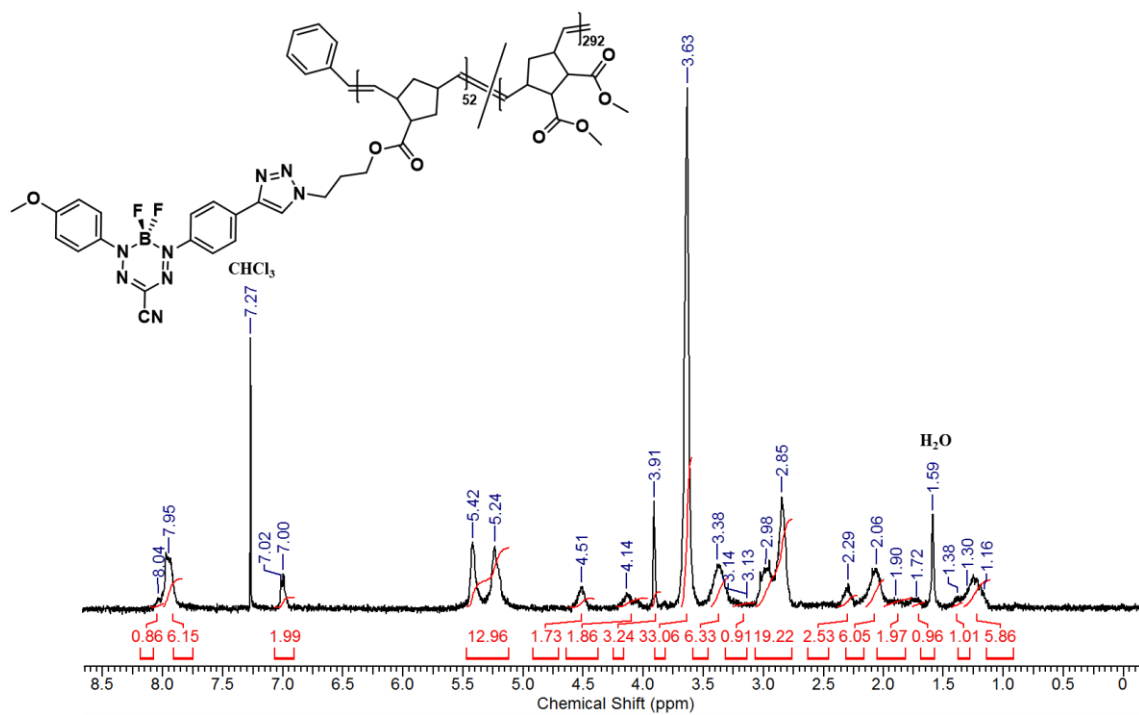


Figure A3.14. ^1H NMR spectrum of $(\text{PDND})_{292}\text{-}r\text{-}(\text{PBF}_2\text{N})_{52}$ ($f_{\text{BF}_2} = 0.15$) in CDCl_3 .

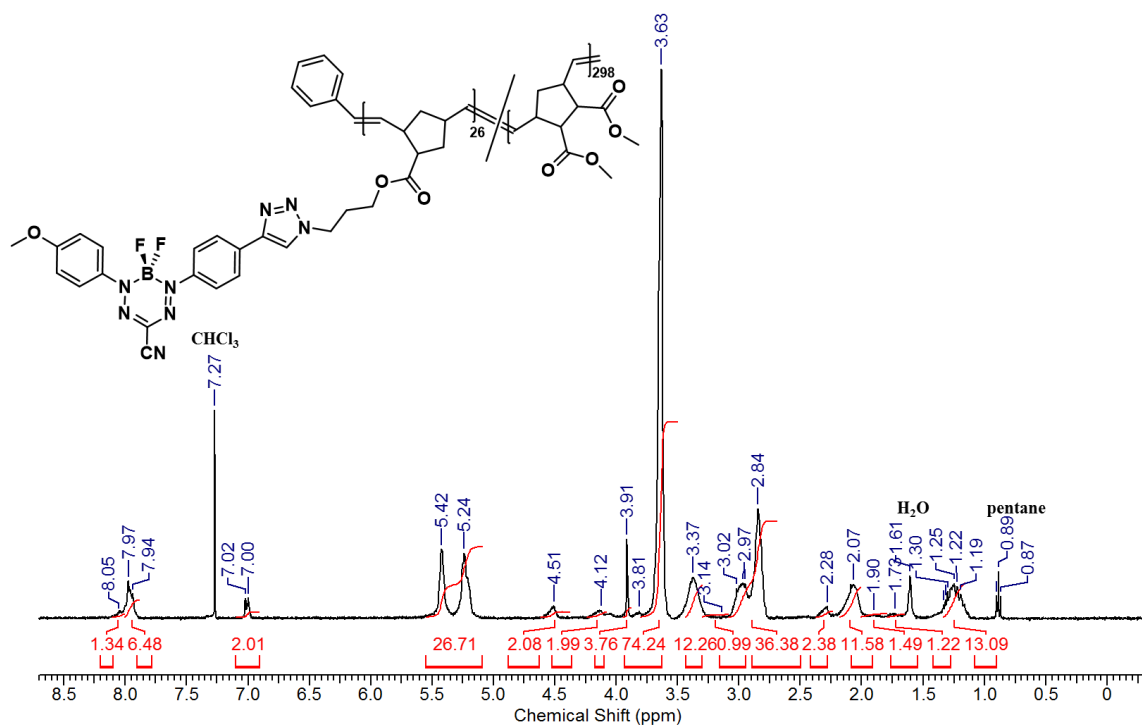


Figure A3.15. ^1H NMR spectrum of $(\text{PDND})_{298}\text{-}r\text{-}(\text{PBF}_2\text{N})_{26}$ ($f_{\text{BF}_2} = 0.08$) in CDCl_3 .

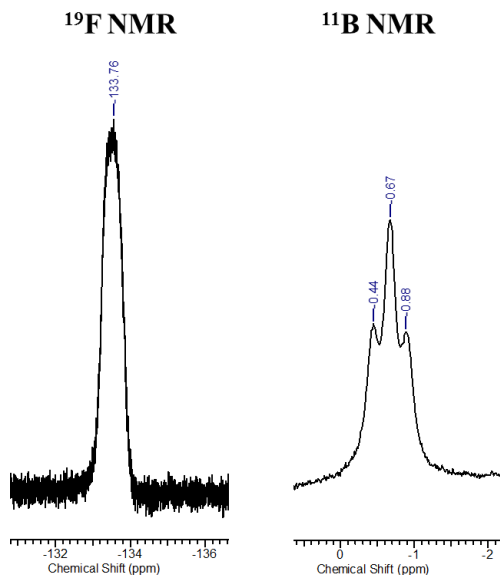


Figure A3.16. Representative ^{11}B NMR and ^{19}F NMR for block and random copolymers in CDCl_3 .

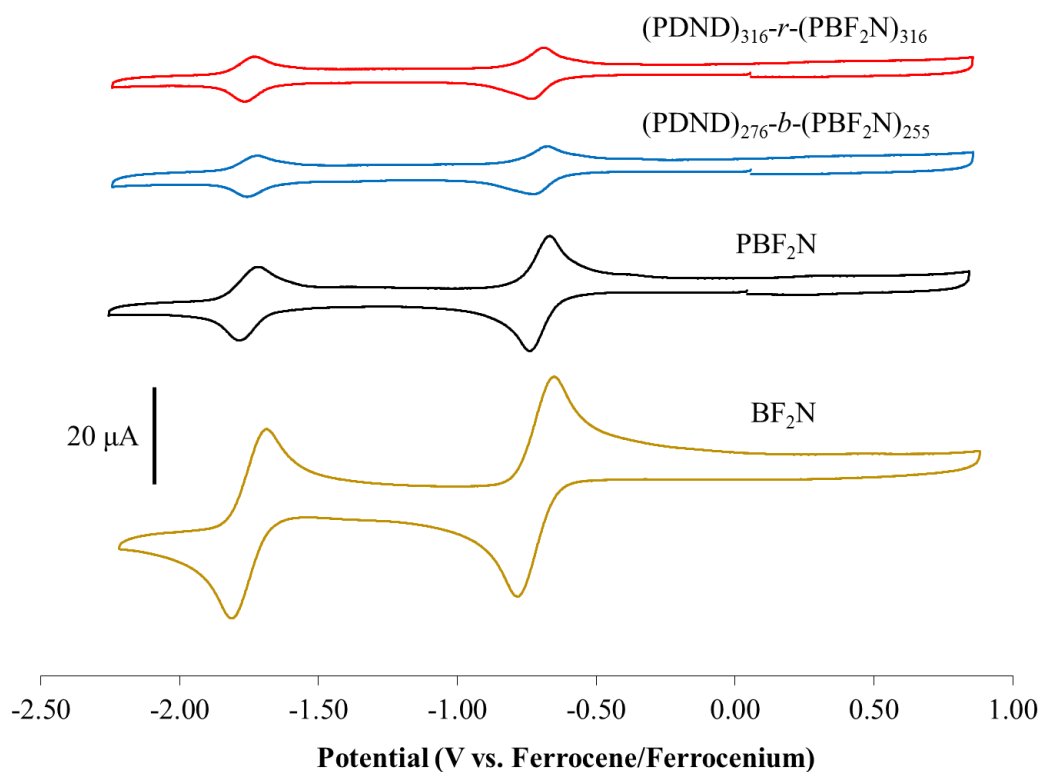


Figure A3.17. Cyclic voltammograms for BF_2N (dark yellow), PBF_2N (black), $(\text{PDND})_{276}\text{-}b\text{-(PBF}_2\text{N})_{255}$ (blue), and $(\text{PDND})_{316}\text{-}r\text{-(PBF}_2\text{N})_{316}$ (red), were recorded at a scan rate of 250 mV s^{-1} for 1 mM analyte solutions (calculated using an average molar mass for blocks and random copolymers from f_{BF_2} in each) in CH_2Cl_2 containing 0.1 M $[\text{nBu}_4\text{N}][\text{PF}_6]$ as the supporting electrolyte. Voltammograms were referenced internally against the ferrocene/ferrocenium redox couple.

Curriculum Vitae

Name: Samantha Novoa

Post-secondary Education and Degrees: The University of Western Ontario
London, Ontario, Canada
2010-2015 B. Sc.

The University of Western Ontario
London, Ontario, Canada
2015-2017 M. Sc.

Honours and Awards: Ontario Graduate Scholarship (OGS)
2016–2017 \$15,000

Canada Graduate Scholarship – Master’s Program (CGS-M)
2015–2016 \$17,500

Ontario Graduate Scholarship (OGS)
2015–2016 (declined) \$15,000

2nd Place Poster Prize
Inorganic Discussion Weekend 2016 \$50

Related Work Experience Teaching Assistant – CH2271
The University of Western Ontario
2015–2017

Teaching Assistant – CH1302
The University of Western Ontario
2015–2017

Publications:

3. “Copper-assisted azide–alkyne cycloaddition chemistry as a tool for the production of emissive boron difluoride 3-cyanoformazanates” S. M. Barbon, S. Novoa, D. Bender, H. Groom, L. G. Luyt, J. B. Gilroy, *Org. Chem. Front.*, **2017**, *4*, 178–190.

2. “Side-Chain Boron Difluoride Formazanate Polymers via Ring-Opening Metathesis Polymerization.” S. Novoa, J. A. Paquette, S. M. Barbon, R. R. Maar, J. B. Gilroy, *J. Mater. Chem. C*, **2016**, *4*, 3987–3994.

1. “Interfacial strain-promoted alkyne-azide cycloaddition (I-SPAAC) for the synthesis of nanomaterial hybrids.” P. Gobbo, S. Novoa, M. C. Biesinger and M. S. Workentin, *Chem. Commun.* **2013**, *49*, 3982–3984.

Conferences:

3. **Samantha Novoa**, Stephanie M. Barbon, Joseph A. Paquette, Ryan R. Maar, Joe B. Gilroy*. Poster Presentation. “*Synthesis and Characterization of Side- and Main-Chain Boron Difluoride Formazanate Polymers*”, Inorganic Discussion Weekend 2016, Hamilton, ON, Nov 11–13, 2016.
2. **Samantha Novoa**, Stephanie M. Barbon, Joseph A. Paquette, Ryan R. Maar, Joe B. Gilroy*. Poster Presentation. “*Synthesis and Characterization of Side- and Main-Chain Boron Difluoride Formazanate Polymers*” Boron in the Americas 2016 – BORAM XV, Kingston, ON, June 25–28, 2016.
1. **Samantha Novoa**, Stephanie M. Barbon, Joseph A. Paquette, Ryan R. Maar, Joe B. Gilroy*. Oral Presentation. “*Synthesis and Characterization of Side-Chain Boron Difluoride Formazanate Polymers*”, 49th Annual Inorganic Discussion Weekend Conference, Kingston ON, 2015/12.

Training Programs/Volunteer Work:**Teacher Assistant Training Program**

The University of Western Ontario, 2015/9

Let’s Talk Science Outreach Program

The University of Western Ontario, 2015–present

Western Chemistry Outreach Program

The University of Western Ontario, 2012/6–present

Fall Preview Day and March Break Open House

The University of Western Ontario, 2011/11–present

National Chemistry Awareness Week

The University of Western Ontario, 2011/10–present